A finite element mesh optimization method incorporating geologic features for stress analysis of underground excavations

Bahareh Vazhbakht

A Thesis

in

The Department

of

Building, Civil and Environmental Engineering

Presented in Partial Fulfillment of the Requirements
For the Degree of Master of Applied Science (Civil engineering) at
Concordia University
Montreal, Quebec, Canada

August 2011

© Bahareh Vazhbakht, 2011

CONCORDIA UNIVERSITY

School of Graduate Studies

This is to certify that the thesis prepared

By: Bahareh Vazhbakht

Entitled: A finite element mesh optimization method incorporating geologic

features for stress analysis of underground excavations

and submitted in partial fulfillment of the requirements of the degree of

Master of Applied Science (Civil Engineering)

complies with the regulations of the University and meets the accepted standards with respect to originality and quality.

Signed by the final examining committee:

Dr. Adel M. Hanna	Chair
Dr. Lan Lin	Examiner
Dr. Ali Dolatabadi	Examiner
Dr. Attila M. Zsaki	Supervisor

Approved by   Dr. Mohammed Zaheeruddin
                     Chair of Department or Graduate Program Director

                     Dr. Robin Drew
                     Dean of Faculty

Date   12 - 09 – 2011

Abstract

A finite element mesh optimization method incorporating geologic features for stress analysis of underground excavations

Bahareh Vazhbakht

Application of numerical modeling in civil and mining engineering projects not only increases the effectiveness of analysis but also improves the results of the analysis. However, due to complexity of model generation and analysis, it still is a time consuming process. The finite element method requires a discretization, or a mesh, to solve the partial differential equations representing the problem. The finer and denser is the mesh, the more time and computer memory consuming is the analysis. Therefore, one of possible solutions is to simplify the analysis by reducing the mesh density while maintaining the quality of solution. Previously, with help of a cost function, a framework was introduced for mesh optimization considering the geometries of excavations only. From the current research, the optimization strategy is improved by including the effect of geologic features represented by rock properties. Among different rock properties, Young's modulus (E) and Poisson's ratio (μ) were considered. The effect of each of these properties on the mesh optimization was investigated and it was concluded that the E has the most significant effect on the results of stress analysis of dissimilar rocks. Subsequently, an expanded cost function incorporating E was formulated. Finally, an application of expanded cost function was demonstrated using a few representation case studies.

Acknowledgements

Foremost, I would like to express my gratitude to my supervisor Dr. Attila Zsaki for his patience and continuous support. I appreciate his contributions of time and idea to the present thesis. Without him this thesis would not have been completed.

I would like to thank my committee members: Dr. Hanna, Dr. Lin, and Dr. Dolatabadi for their suggestions and insightful comments.

I have been extremely fortunate to have the support of very special friends to whom I am truly grateful: Maryam Lolo, Shaghayegh Lolo, Azam Heydari, Bahareh Khatibi, Sanam Mirzaei, Golpira Elmi, Mohammad Jabbari, and my friends outside Canada, Maryam Amir, Shaghayegh Saeidi, and Azadeh Najafi. Their support helped me overcome setbacks and stay focused on my graduate study.

My deepest gratitude goes to my family for all their love and encouragement; my parents Tahereh Hozhabri and Faramarz Vazhbakht for their constant love, concern and support all these years, and my sister Ghazaleh for her confidence in me for sharing very special moments, long and interesting conversations. I would like to dedicate this thesis to my dear grandmother and to the memory of my beloved grandparents.

Table of Contents

List of Figures

List of Tables

List of symbols

EDZ   Excavation Damage Zone

σ_1 Major Principal Stress

σ_3 Minor Principal Stress

U   Total displacement

μ   Poisson's Ratio

E   Young's Modulus

E_R Young's modulus of rock mass

E_F Young's modulus of fault zone

μ_R Poisson's ratio of rock mass

μ_F Poisson's ratio of fault zone

ROI   Region of interest

C_{ym} Cost of removing a vertex regarding Young's Modulus

W_{Ym} Relative importance of Young's modulus

E_1 Maximum E between the E's around the vertex

E_2 Minimum E between the E's around the vertex

E_{max} The maximum E of the whole area of study

E_{min} The minimum E of the whole area of study

C_g Cost of removing a vertex regarding geometry

W_g Relative importance of geometry

l Distance between the chord and the vertex

L Chord length between two vertices adjacent to the selected vertex

C_P Cost of removing a vertex regarding its distance to ROI

W_P Relative importance of proximity

d Distance between the vertex and the ROI

d_{max} Distance between the furthest vertex to the ROI

d_{min} Distance between the nearest vertex to the ROI

C_V Cost of removing a vertex regarding its visibility

W_V Relative importance of visibility

α Angle between averaged normal at the vertex and the vector pointing from the vertex to the ROI

α_{max} Largest angle between averaged normal at the vertex and the vector pointing from the vertex to the ROI

α_{min} Smallest angle between averaged normal at the vertex and the vector pointing from the vertex to the ROI

C_U Cost of removing a vertex regarding mesh uniformity

W_U Relative importance of uniformity

a For uniform mesh = Uniformity constant, For graded mesh = Uniformity variable

D_1 Element edge length

D_2 Element edge length

D_{max} Maximum Element edge length

D_{min} Minimum Element edge length

INTRODUCTION

Stability estimations for underground excavations consist of variety of analysis and design among which, stress analysis is an essential procedure. Identifying and determining different types of stress, factors which causes stress changes over time, and the consequences of stress redistribution, are important subjects that should be considered in stress analysis. There are different factors to stress redistribution one of which is geological inclusions (Martin & Chandler, 1993; Rebaï, Philip, & Taboada, 1992; Zhang, Dusseault, & Yassir, 1994). Excavations can create stress perturbation and redistribution (Eberhardt, 2001; Martin, Kaiser, & Christiansson, 2003). The coincidence of a geological discontinuity and an excavation makes the stress analysis even more complicated. As mining and tunneling progresses, excavation reaches deeper. The problem with depth is the higher risk of instability. Therefore, the presence of faults, fracture zones, microckracks, or in general, heterogeneity of the rock mass cannot be avoided. Location, direction and properties of the geological structures are the factors which control the effect of them on the stability of tunnels.

To understand and estimate the behavior of a medium, differential equations representing stresses and displacement should be solved. The introduction of numerical modeling to civil and mining engineering made it considerably simpler for engineers to solve these equations; however there are still many problems to achieve the best result in the less time and computer memory consumption. Depending on the numerical method which is being used, different procedures should be established to solve an equation. One of the generally used numerical methods is the finite elements method, which has a broad use in civil and mining engineering simulations. The method uses a mesh to solve differential

equations. To get the best results from the method, mesh generation should be adequate, not very coarse and not very dense. Despite the popularity of the method, it still is time and memory consuming, specially when used for simulations of multiple excavation, different materials (existence of geological discontinuities and inclusions), and multiple staging procedures.

Mesh simplification is a possible way to achieve the best result for these types of complicated processes. Zsaki and Curran (2005) introduced a method to simplify the mesh by removing unnecessary vertices. The method focused on the excavations geometry with respect to a region of interest (ROI). By assigning a cost value to each vertex (which is depended on the location and distance of the vertex to the ROI) the less effective vertices on the analysis will be recognized and removed. The method worked properly and accurately, even for the multiple stage mining simulations.

The aim of this research is to introduce a method to improve the finite element analysis by simplifying the mesh generation for the complicated models with a variety of materials. For that purpose the method used by Zsaki and Curran (2005) will be completed by considering material properties as well as excavations geometries.

In the first chapter, the problem will be explained by considering previous researches and studies. Then in the next chapter the effect of material properties on the stresses and displacements analysis will be studied; also the relationship between mesh density and material properties will be determined. Finally, an expanded cost function will be introduced at the third chapter and its application will be discussed.

CHAPTER ONE

1. LITERATURE REVIEW

Engineering projects related to soils and rocks are always full of uncertainties; there is always a parameter or a condition that it is not considered in planning, analysis, or design. Underground excavations, including tunnels and mining shafts, are one of the most problematic structures since they need accurate predictions of earth (soil and rock) behavior. It is very important to consider all the parameters which affect the stability of a tunnel, often from a very limited amount of available data.

Studies showed (Hoek & Brown, 1994) that there are different parameters which affect stress state around an excavation; type of rocks, existence of fractures and joints, faults near excavation and generally geological structures are the most problematic phenomena. Each of these geological features, like faults and fractures, affects stress states near an excavation in different ways; either they change the stress direction or change the magnitude of stress in particular area.

A finite area of influence can be expected for each of these geological features; outside of which their effect can be neglected. Perhaps the most important step is to find parameters which affect stresses near an excavation and to understand the effect of geological features on such excavations.

1.1 Stresses in a rock mass

Generally, stresses within the ground consist of normal stresses and shear stresses. The principal normal stresses, near the ground surface, are divided into vertical and horizontal stresses, which are orthogonal to each other. However, the stress direction varies with depth and it might not be vertical or horizontal after a certain depth. The vertical stress is also called gravitational stress and it exists due to the weight of the overburden or gravity force. It is a function of density, gravitational acceleration, and height of overburden

or depth at which it is calculated. Meanwhile, horizontal stresses are caused by tectonic forces. Thus, their origin leads changes of stress orientation and magnitude with time. Presence of these forces or stresses and their changes with time makes the rock mass, in general, a complex, heterogeneous material.

The best way to measure stress in a specific area is using *in-situ* stress measurement; however this is an expensive way to estimate stress orientation and magnitude (Fairhurst, 2003) . By avoiding those methods and to better understanding the tectonic forces and their effect on stress distribution, the Stress World Map was prepared by co-operation of a group of researchers (Fuchs & Müller, 2001; Zoback & Magee, 1991).

Previously, only a local stress distribution was studied and the effect of tectonic activities on stress distribution was not considered. Due to preparation of the Stress World Map (Figure 1-1) the relationship between tectonic activities and stress distribution and deviation has been confirmed.

The World Stress Maps is a new perspective on stress deviation and heterogeneities due to faults or mountain belts. The effect of these geological features in large scale and the effect of joints, fractures, in small scale will be discussed in the following sections.

Stress direction and magnitude is affected by not only the geological features but also by built structures or activities such as underground excavations, boreholes, oil and gas development and so on.
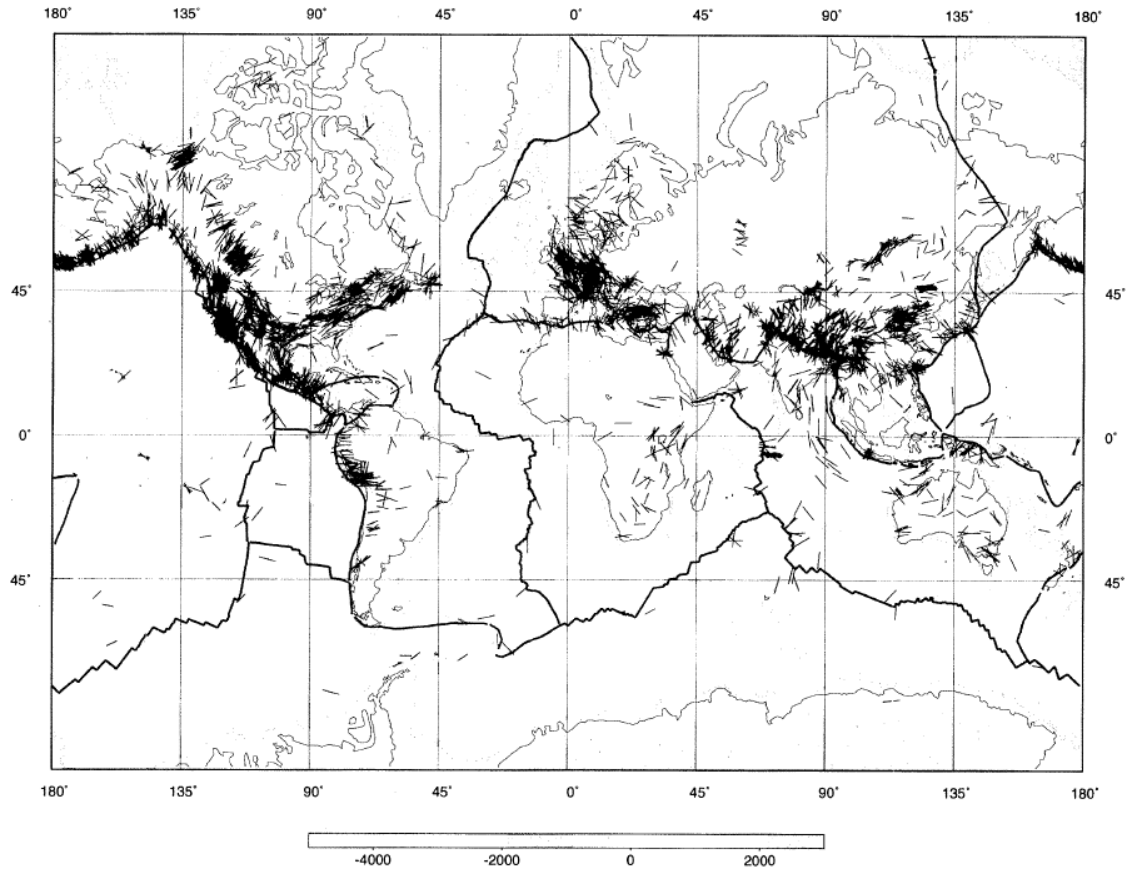
Figure 1-1 World Stress Map (Zoback & Magee, 1991)

1.2 Stress around an excavation

Considering the disturbance in the state of stress around local features, such as excavations, Hoek and Brown (1994) discussed that the extent of disturbance could lead to failure in the rock mass adjacent to the excavation. Consequently, this concept is the basis of all tunneling and excavation design currently in use today.

Figure 1-2 shows stress trajectories around a cavern located in Norway (Martin et al., 2003) . It is a good example to illustrate how an excavation could change the local stress distribution. If it was assumed that 25 m from the cavern, the stress direction is the *in-situ*

stress trajectory of the local surroundings, changes in stress direction and stress concentration near roof, side walls, and bottom edges of the cavern is illustrated in Figure 1-2. Near the side walls stress direction rotates almost 90° in relation to the *in-situ* states. Stress density has its highest value near the crown of the cavern and the bottom edges. Farther from the cavern, the stress direction changes back to its original orientation and its distribution changes as well to the *in-situ* one.
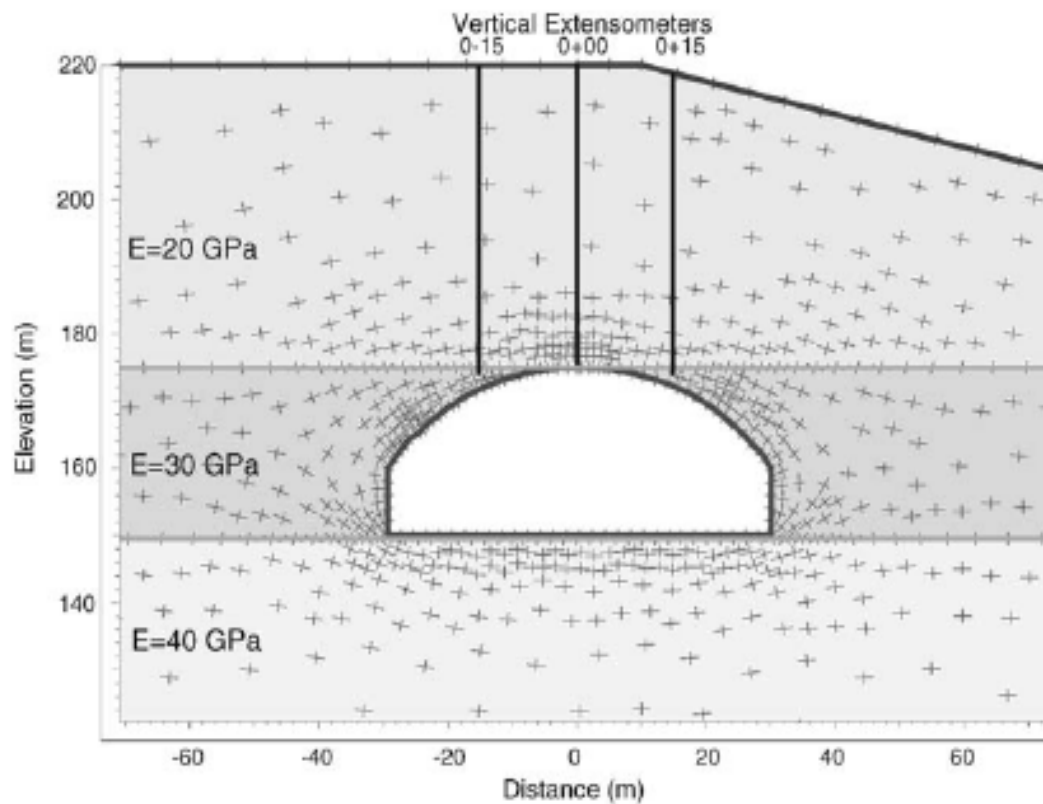
Figure 1-2 Stress perturbation due to an excavation of a cavern in Norway (Martin et al., 2003)

Generally, the normal stresses present in rock mass changes due to a decrease or increase in the magnitude of the overburden load. This will help to better understand that how tunneling or opening an excavation may cause redistribution of stresses. Since construction of an underground structure is equal to removing a considerable mass of rock

or soil and creating a hollow cavity, it will result in stress change. Constructing a tunnel or a

cavern not only means elimination of rocks and soils but also it creates a new free surface

(Fuchs & Müller, 2001) . Thus, the combined effect of these, results in stress perturbation.
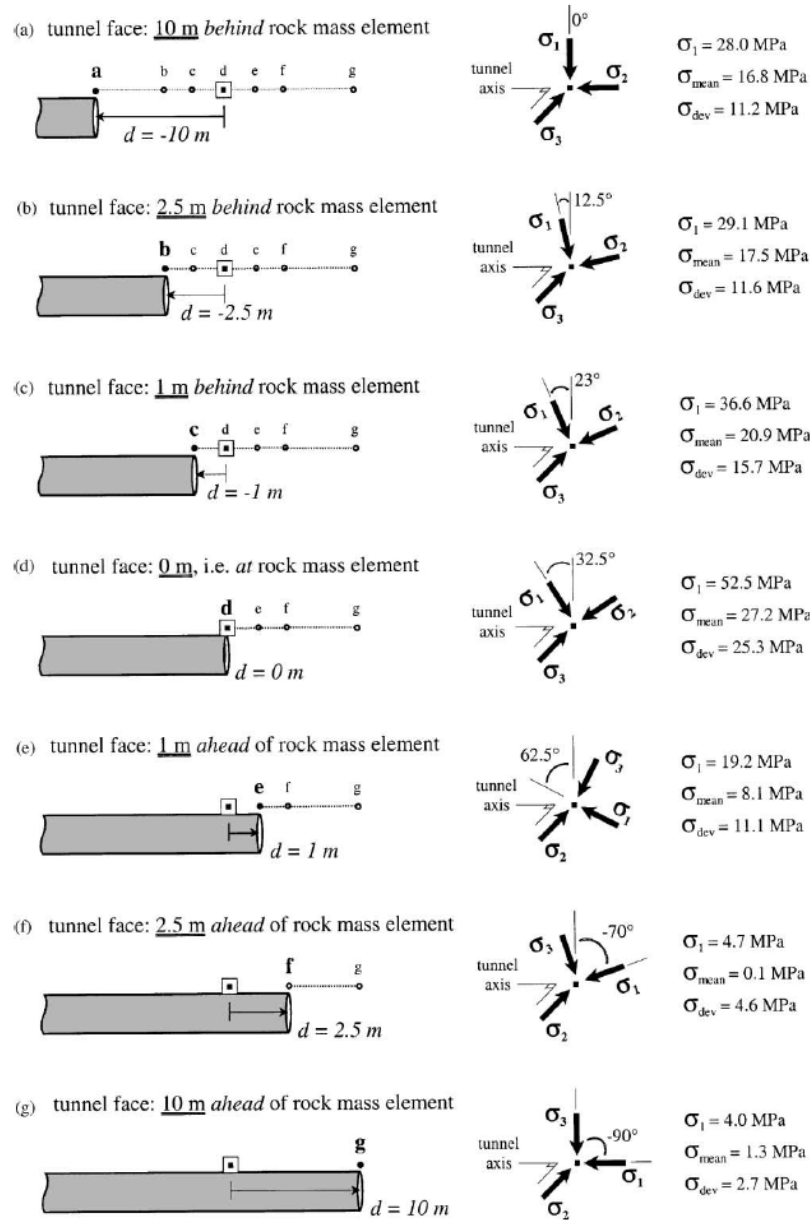
Figure 1-3 Stress orientation rotation and stress magnitude changes as tunnel approaches and passes the rock mass (Eberhardt, 2001)

Stress redistribution and deviation from the *in-situ* values near an underground excavation consists both changes in magnitude and rotation of orientation of stress. Far from the excavation, the stress state reaches its *in-situ* local or regional direction and magnitude.

As Eberhardt (2001) demonstrated that for a given volume of rock, as the tunnel advances through the rock mass, the stress orientation will rotate almost 90° and the magnitude of stress may increase or decrease as the tunnel passes through the rock. Figure 1-3 illustrates different states of tunneling advancement and changes in stress direction and magnitude in these different states.
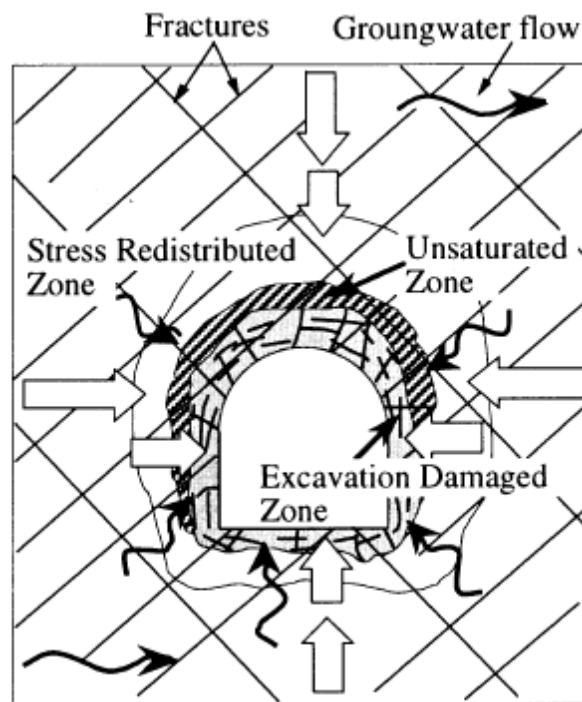
Figure 1-4 Conceptual model of the EDZ (Sato, Kikuchi, & Sugihara, 2000)

Stress redistribution, and in general, rock mass disturbance due to excavation results in the existence of a zone, which is called excavation damage zone (EDZ). As it has

been noted by Sato et al. (2000) , rock properties and conditions such as, fractures, permeability, and stress state, are expected to be different in this zone due to excavation (Figure 1-4). Presence of EDZ is the reason of instability of underground openings and it has been proven that it is strongly depends on the excavation method itself (Cai et al., 2004) .

1.3 The effect of geological structures on stress state

The effect of geological structures on stress distribution should be discussed considering different parameters. Depending on the scale of structures, changes in stress orientations and magnitudes are different; however this does not mean that the effect of the microcracks is negligible. To understand the point, it can be said that the effect of large scale structures like tectonic structures due to for instance, continental collision is used to prepare stress maps whereas the effect of the fractures and joints cannot be included in maps since they are much more localized. However, when discussing engineering cases these types of geological structures may be considered as more important, due to smaller, local scales.

Any geological structure within the rock mass such as joints, faults and any other type of discontinuities, regardless of their size and geometry, significantly influence the stress orientation and magnitude throughout the rock mass. Martin and Chandler (1993) in a research done using stress measurement from URL (Underground Research Laboratory) concluded that stress magnitude varies significantly near a geological structure over a short distance, and also they found that stress orientation can rotate even near 90° in the presence of geological structure, similar to the advancing from in tunneling, as discussed earlier (Fairhurst, 2003; Martin & Chandler, 1993).

Figures 1-5 and 1-6 illustrate stress magnitude near a fracture zone due to a fault, and changes in stress magnitude adjacent to fracture zone at URL, respectively.
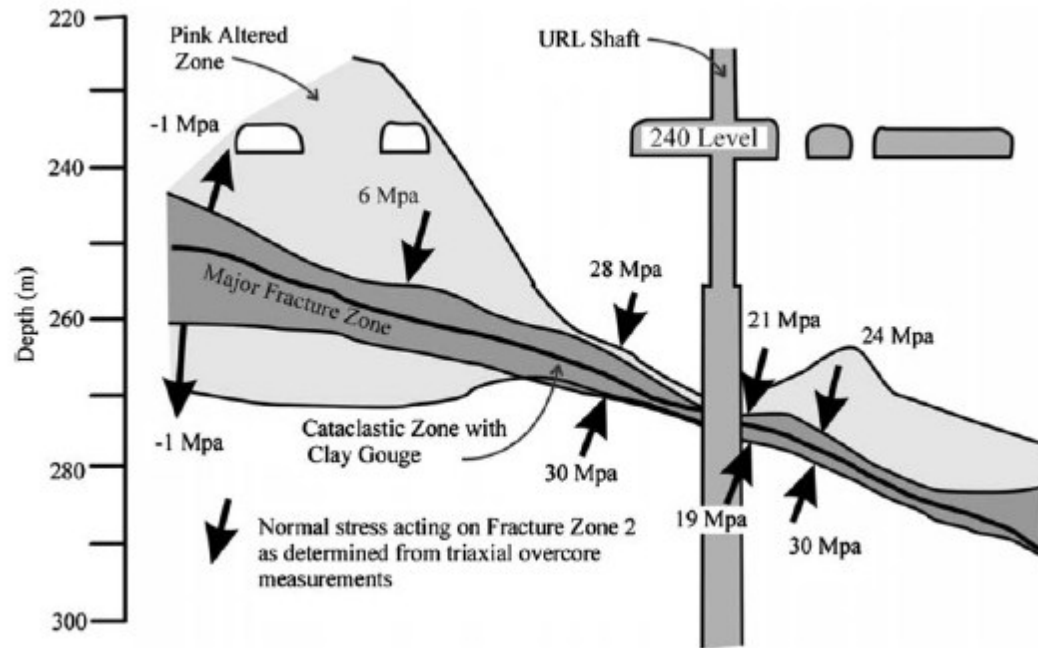
Figure 1-5 Variation of normal stress magnitude along a thrust fault at the URL, Canada. Vertical and horizontal scales are the same (Fairhurst, 2003; Martin & Chandler, 1993)

Included in their research, Martin and Chandler (1993) determined stress state for three different geological structures of varying scales; microcracks, fractures, and a thrust fault.

For microcracks the analysis showed a reduction in stress magnitude and this reduction is more significant in a borehole perpendicular to the microcracks (Martin & Chandler, 1993). In another investigation, Martin and Chandler (1993) studied the effect of fractures on stress distribution and magnitude. Results show that the orientation of the

minor principal stress (σ_3) rotates almost 90°and the stress magnitude also changes near the fracture zone (Martin & Chandler, 1993).

Similar results for stress magnitude and orientation changes were observed near large scale geological structures like faults. The stress magnitude above the fault is less than the stress magnitude below the fault (Martin & Chandler, 1993). Similarly, Zhang et al. (1994) concluded that shear stress at the sides of the fault shows a reduction in magnitude.
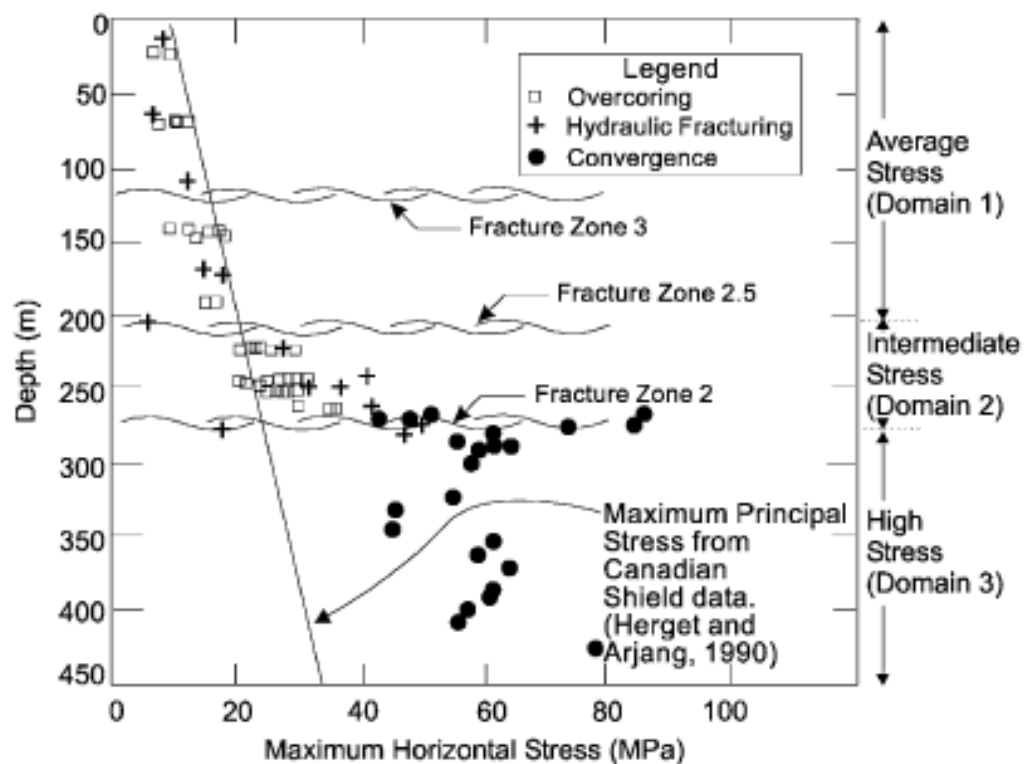
Figure 1-6 *In-situ* **stress magnitude at URL and its changes with respect to fracture zone (Martino & Chandler, 2004)**

In general, not only the existence of geological structures but also presence of any kind of inclusion affects stress distribution. The effect can occur as a decrease or an increase in the magnitude of stress or as a change in stress orientation or both together.
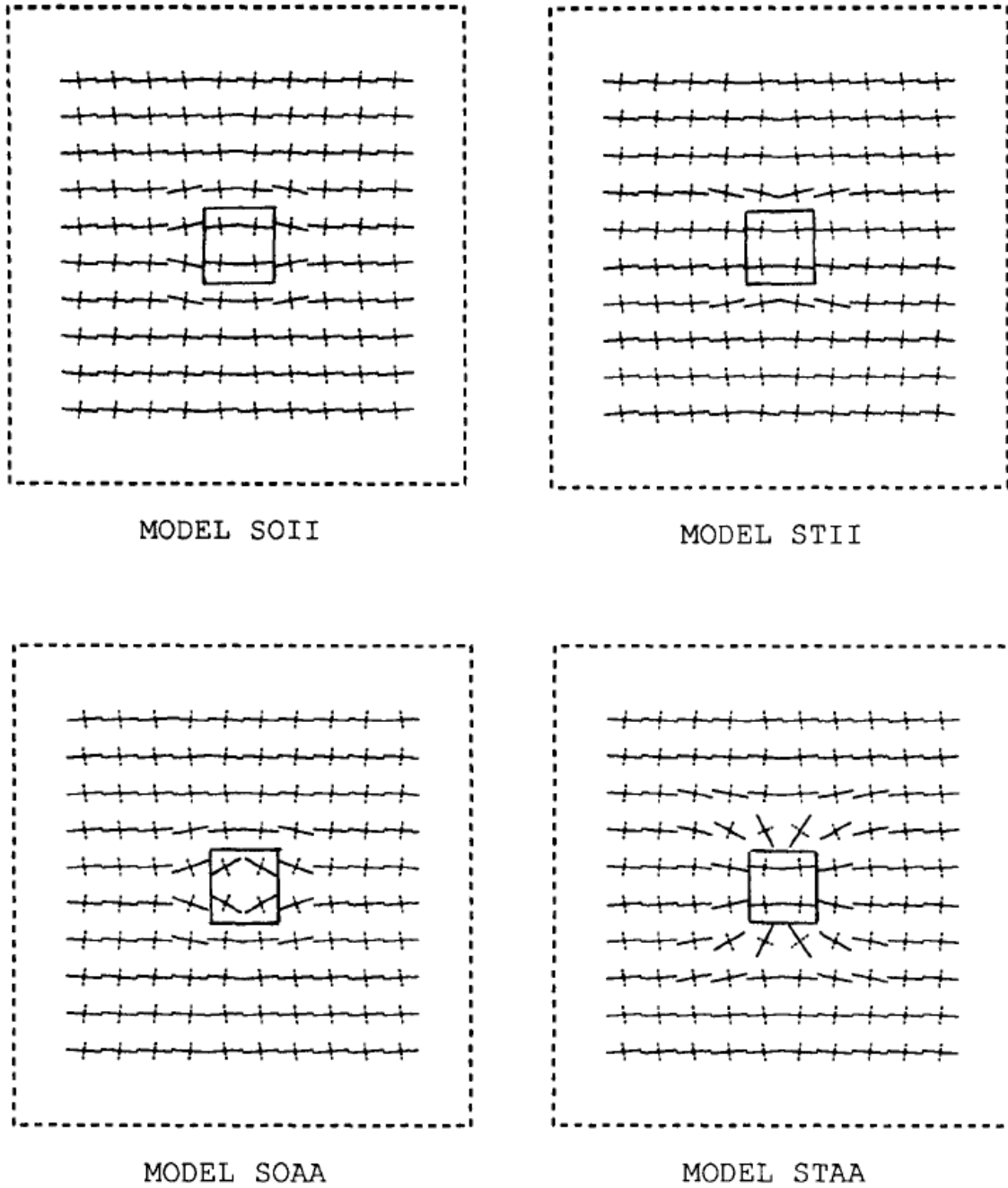
Figure 1-7 Effect of inclusions on horizontal stress orientations in soft and stiff, isotropic and anisotropic inclusion and materials. The square represents inclusion (Zhang et al., 1994)

Zhang et al. (1994), by testing four cases of isotropic and anisotropic inclusions and host material explained that no matter what kind of inclusion (isotropic or anisotropic), its

presence will affect the stress distribution; however the intensity of the effect will vary from one case to another, which can be seen in figure 1-7. In this figure, the effect of inclusion on stress orientation is illustrated and it is understandable that the intensity of this effect is much higher when an anisotropic inclusion exists in an anisotropic material (Zhang et al., 1994). The same result achieved from studying the effect of inclusions on stress magnitude. Once again, changes in stress magnitude from anisotropic inclusion in anisotropic material were the most significant (Zhang et al., 1994).

Although the effect of geological inclusions on stress distribution including stress magnitude and stress direction has been proven, changes may not necessarily occur in both stress magnitude and orientation simultaneously. Research done in a copper mine in central Chile shows that, despite the fact that the stress orientation in a mine area (which is located in a shear zone of a fault) is completely different from the regional stress orientation, the magnitude of the stress shows no significant changes due to presence of the fault (McKinnon & Garrido de la Barra, I., 2003).

The stress concentration in porphyroclasts is an example of small scale inclusions and their effect on stress distribution. Kenkmann and Dresen (1998) showed that the interface of a porphyroclasts and its surrounding matrix is a suitable place for stress concentration. This phenomenon can be due to dislocation density and its relation to the applied stress (De Bresser, J. H. P., 1996). As stresses concentrate in the porphyroclasts-matrix interface, their magnitude increases in all directions (Kenkmann & Dresen, 1998).

Therefore, it can be concluded that stress distribution (regardless of the given scale) strongly depends on discontinuities and their activities (Rebaï et al., 1992).

1.4 Underground excavation in the vicinity of geological structures

The vicinity of an excavation and a geological inclusion, like faults, requires careful analysis and excavation design. Concentration of stresses near geological inclusions is a detail that makes stability analysis more and more essential for underground structures. Existence of geological structures like faults or fractures is one of the most important reasons of underground failures. This is because of the lack of knowledge about the behavior of geological discontinuities or heterogeneities. By assuming a potential fault negligible, the stability estimation may be inaccurate. Several case studies have been done to give a better perspective of these kinds of scenarios; however there still remain too many questions and problems to solve.

In summary, the effect of geological structures on an underground excavation depends on different factors. These factors may be classified as type of the inclusion, distance between an inclusion and the excavation, the geometry of the inclusion, roughness or softness of the geological structure, etc (Everitt & Lajtai, 2004; Hao & Azzam, 2005; Singh, Singh, Singh, & Jethwa, 1994; Suorineni, Tannant, & Kaiser, 1999).

As it has been mentioned, problems related to excavation stability are considered with respect to the concept of EDZ. This means that the effect of heterogeneity should be estimated on excavation damage zone. Nevertheless, a plastic zone may be preferred by some scientist instead of EDZ to explain this particular area, which surrounds an underground opening (Golshani, Oda, Okui, Takemura, & Munkhtogoo, 2007).

Lei et al. (1995) illustrated the effect of fault near an excavation by using numerical modeling (Figure 1-8). An underground tunnel and the stress trajectory around the tunnel

has been modeled and then by adding two faults, stress perturbation has been studied (Lei et al., 1995).
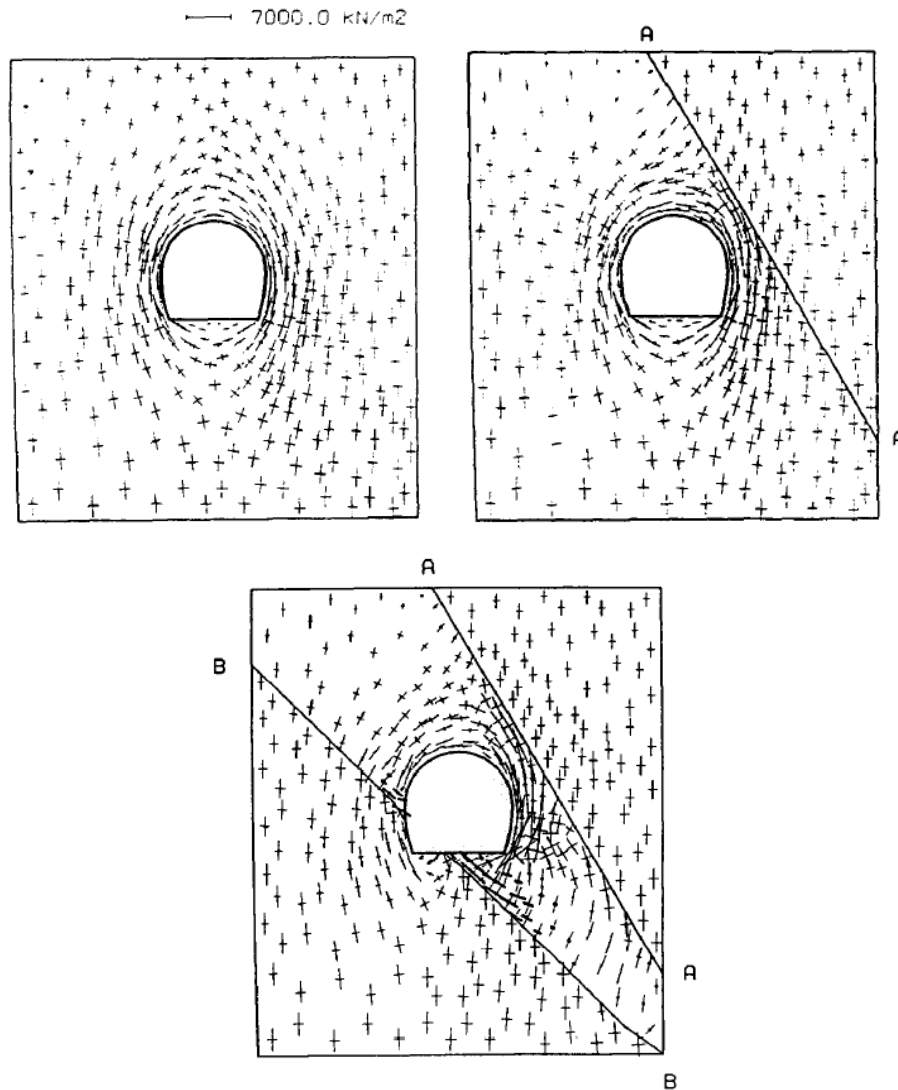
Figure 1-8 Principal stress distribution due to an underground excavation and presence of faults (Lei et al., 1995)

Later Hao & Azzam (2005), in a study of fault parameters' effect on displacement near an excavation, indicated changes of horizontal stress near a fault and its effect on plastic zone near an excavation and the fault. It was concluded that augmentation of

horizontal stress causes an increase in plastic zone (Hao & Azzam, 2005). This can be clearly seen in the figure 1-9; however there are other parameters which play a significant role like fault dip and location. Also changes in horizontal stress not only results in increase of plastic zone, but also it causes redistribution of the plastic zone (Hao & Azzam, 2005).
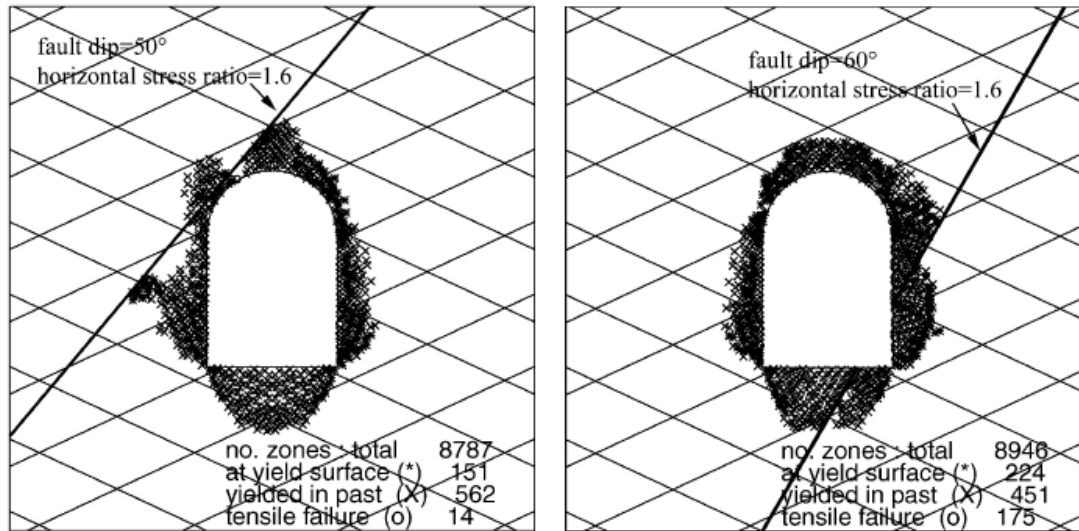
Figure 1-9 The effect of horizontal stress state on plastic zone distribution affected by fault in two different locations (Hao & Azzam, 2005)

In addition, the effect of the fault's location can be seen from Figure 1-9, and it can be concluded that the fault, which intersects the sidewall of excavation, is more dangerous than the fault near the roof of the excavation (Hao & Azzam, 2005).

Singh et al. (1994) with respect to Singh's equation (1991) concluded that the effect of fault on excavation stability does not only depend on fault orientation but also it is strongly depends on fault's location. Actually, effect of the fault orientation is considerable until it reaches certain degree (in Singh's study 45°) (Singh et al., 1994).

Zhu & Bruhns (2008) investigated parameters, which affect EDZ and its redistribution. Analyzing different parameters, they concluded that since stress

redistribution has the most effect on EDZ, therefore, all the parameters, which cause stress deviation, should be considered as the most effective parameters on EDZ redistribution (Zhu & Bruhns, 2008). As it had been demonstrated, geological inclusion or generally rock heterogeneity results in stress perturbation. Accordingly, Zhu and Bruhns (2008) studied rock heterogeneity and the consequence of its existence on EDZ near a circular opening. They found out that it is not the homogeneity index, which controls disturbance of damage zone; the EDZ is in fact controlled by the ratio of the boundary stress (Zhu & Bruhns, 2008).

To emphasize heterogeneity, the effect of two faults near an excavation was investigated and crack initiation due to fault presence and stress concentration near faults was considered (Zhu & Bruhns, 2008). The results are the same as the result achieved by Lei et al. (1995). Similarly to Lei et al. (1995), Zhu and Bruhns (2008) concluded that the effect of faults is strongly depends on the fault's location and direction. They also discussed that *in-situ* stress magnitude is the other parameter that, together with stress concentration around fault, may drastically change the shape and effective area of the EDZ (Zhu & Bruhns, 2008).

As it has been discussed, generally all kind of inclusions will lead to stress changes, the question is whether they will all change or accelerate the changes in EDZ? Everitt and Lajtai (2004) studied the effect of rock fabric and texture and also the effect of rock heterogeneity and anisotropy on excavation failures. From their work it can be concluded that by being familiar with the fabric of host rock (near tunnel) even the fracture distribution by excavating can be predicted (Everitt & Lajtai, 2004). Also as it has been expected the rock fabric as like as faults, joints, and fractures controls EDZ (Everitt & Lajtai, 2004). Their report also indicates that even batholiths, which seem homogenous and isotropic, have a complicated interior texture (Everitt & Lajtai, 2004). The effect of these

types of anisotropy and heterogeneity specially depends on the location and direction of the excavation with respect to these inclusions.

In general, existence of any kind of heterogeneity or inclusion in rock mass, even existence of variability of rock fabric and texture will make an underground opening to be subjected to different kind of failures. Excavating an underground opening around a geological structure will increase EDZ. This increase strongly depends on additional parameters like properties of inclusion (such as friction, density, permeability), and its direction and location from excavation.

1.5 Numerical modeling

Expensive and time consuming *in-situ* testing in conjunction with the rapid progress of numerical computation lead to application of numerical modeling to solve geological, geotechnical, and rock mechanics problems. Although, highly accurate modeling of complex geotechnical situations is not achievable at this time due to the data-limited nature of the field, numerical modeling finds its place in geo-science and it is now applied in variety of research projects; however the accuracy of the result still needs to be considered (Wiles, 2006). Additionally, it also has its disadvantages. One of the most important problems with numerical modeling is the memory and speed of the computations (Zsáki & Curran, 2005). Generally, the more complex is the problem, the more time consuming is the process of simulation.

Numerical modeling is now used to compute stress state in a particular area, stress magnitude and orientation around geological structures, development of EDZ, stress perturbation due to mining or tunneling, and stability of underground openings.

Based on different numerical models, various computer simulation programs are available. Depending on the assumptions and implementation of numerical model used in these programs, the results will be different. Therefore, not all of these programs are suitable to solve all kinds of geo-science problems.

The finite element method, boundary element method, elasto-static and elasto-dynamic boundary element method, the discrete element method and variations and combinations of these methods are some, which are applied to solve the models. Siebrits and Crouch (1993), and Fotoohi and Mitri (1996) successfully applied the boundary element method to simulate geological structure and stress distribution around them, and the effect of fault near an excavation, respectively.

FLAC (Itsaca International Inc., 2000), UDEC (Itasca International Inc., 2000), and Phase^2 (Rocscience Inc., 2008), are some of the simulation programs, which are widely applied for analyzing geotechnical and rock mechanics models. For instance, Hao & Azzam (2005) claim that for simulating the effect of fault around an excavation in a block rock mass the most appropriate numerical tool is UDEC (Itasca International Inc., 2000). UDEC (Itasca International Inc., 2000), based on distinct element method, has been proven by other researchers (Hart, 2003; Jiang, Li, & Yamashita, 2009) as a better numerical simulation program to illustrate discontinuity in rocks; however Hart (2003) indicated that to simulate geological structures it is better to use 3DEC (Itasca International Inc., 1998) instead of UDEC (Itasca International Inc., 2000), for the true three-dimensional geologic structures.

Cai (2008) made a comparison between two simulation programs, FLAC (Itsaca International Inc., 2000) and Phase^2 (version 5.0) (Rocscience Inc., 2008) to illustrate that the result of these two programs can be different, and the similarity of the result depends

on excavation method and properties of host rock. FLAC (Itsaca International Inc., 2000) is based on explicit finite difference method and Phase² (Rocscience Inc., 2008) is based on implicit finite element method (Cai, 2008). Table 1-1 compares some properties and capabilities of these two programs.

Table 1-1 Comparison between FLAC and Phase² (Cai, 2008)

	FLAC	Phase²
Solution scheme	Explicit	Implicit
Computer memory requirement	Low	High
Non-linear problem handling	No iteration necessary Computationally stable	Iteration required Diverge may occur
Physical process	Always follow the physics if the timestep criterion is guaranteed	Need to be demonstrated that it follows the physical process
Excavation method	Delete or assign null element	Excavation(assign very low modulus)
Structural elements	Yes	Yes
Discontinuity model	Yes (interface element)	Yes (joint element)
User interface	Good	Excellent
First release	1986	1990

The results from two simulation programs differ in some cases, and it is a consequence of different applied numerical modeling. Cai (2008) concluded that although these simulation tools seem easy-to-use, the users can only gain an accurate result if they had considerable knowledge about numerical modeling. He also indicated that the result of the research is not a key to find that which of these tools are more accurate or powerful, the result just simply illustrates that each of these numerical methods are compatible with a specific area of geo-science.

The application of numerical methods is extremely wide that in every research area, one or two numerical methods are used and discussed; however this vast application did not eliminate usage of physical methods. Most of the time physical methods are still employed and the final decision is based on comparison between the results of these two methods (Cavendish, Field, & Frey, 1985). Some attempts have been done to combine these two methods together to achieve the most reliable results (Li, Liu, Dai, & Su, 2005). Li et al. (2005) combined the two methods, and with benefits of both numerical and physical modeling demonstrates more accurate results. They also successfully applied the combined method to solve the problem of a large underground hydropower project.

As it has been indicated by Cai (2008) it is not wise to compare different numerical methods to find the best one. They can only be compared in their ability to solve the same problem.

1.5.1 Mesh Generation

As it was discussed in previous section, numerical modeling is more and more employed to solve geological problems. In order to apply numerical modeling to a problem, first a mathematical method should be selected to solve the partial differential equations via a discretization or mesh of the problem domain, like in the finite element, finite difference or boundary element method. These methods work in conjunction with a mesh generator, which can be done automatically or manually. Giving inaccurate results and being time consuming are two main disadvantages of manual meshing. Therefore many efforts have been done to automate mesh generation (Cavendish et al., 1985; Denayer, 1978).

Ho-Le (1988) presented almost the first classification of mesh generation methods (Figure 1-10). This classification has been done according to the temporal order of the creation of nodes and elements (Ho-Le, 1988).
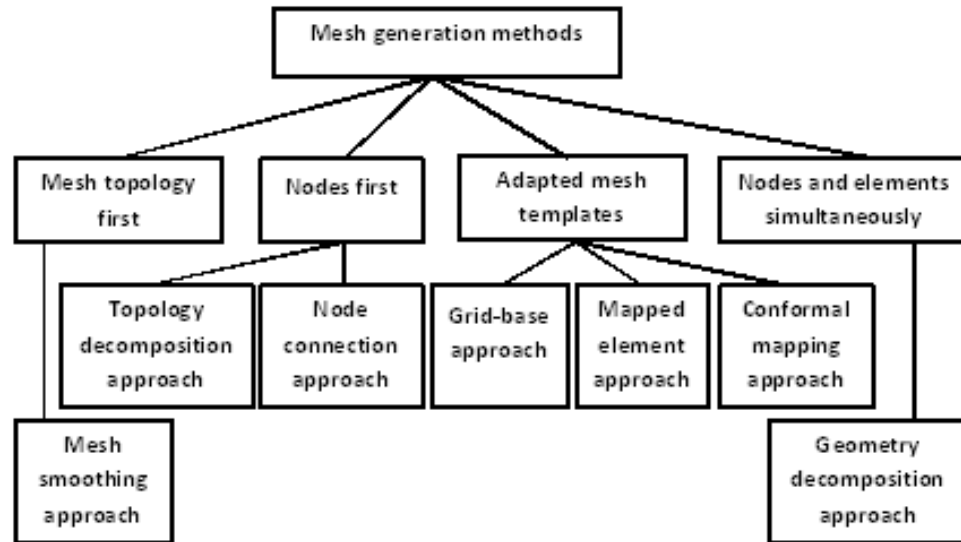
Figure 1-10 Classification scheme for mesh generation methods (Ho-Le, 1988)

Different methods have their own merits and demerits. As an example, a comparison of four automatic methods is summarized in Table 1-2; however this comparison is not very accurate and up to date.

Although most of these methods generate triangular meshes, few of them can produce quadrilateral meshes in 2D (table 1-2). Not all of these methods can be used for 3D mesh generation; however in this thesis only 2D mesh generation will be considered (table 1-2).

Table 1-2 Comparison of the mesh generation approaches (Ho-Le, 1988)

Approach	Quadri-lateral	Brick	Element shape	Mesh density control	Time efficiency
Topological decomposition	No	No	Poor	No	$O(N^2)$
Node connection	Yes	No	2D good 3D fair	Yes	$O(N)$
Grid-based	Yes	Relatively easy	Interior elements excellent	Yes	$O(N)$
Geometric decomposition	Yes	No	2D good 3D unknown	Yes	Unknown

(N = number of nodes in the mesh)

The latest mesh classifications are determined based on mesh connectivity or element's geometry. Connectivity-based classification included Cartesian, structured, unstructured, hybrid and gridless (Soni, 2000). Cartesian grids consist of a network of grid lines with constant spacing which are located in a 2D rectangle or 3D rectangular box (Soni, 2000). Structured mesh generation is based on regular connectivity. A logical rectangular or hexahedral pattern is expected for structured mesh generation (Soni, Shih, & Ito, 2010); whereas unstructured mesh generation is based on irregular connectivity, and it does not follow a logical connections of adjacent points (Soni et al., 2010). Unstructured 2D grids are usually in form of triangles and 3D unstructured grids are mostly tetrahedrons (Soni, 2000). Compared with unstructured mesh generation, structured meshes are simpler to use, they need less computer memory and it is easier to control their shapes and sizes; however since they are not flexible enough to adapt to an irregular geometry of geologic structures, thus it is more preferable to use unstructured meshes (Bern & Eppstein, 1992). Hybrid or

generalized grids included polygonal shapes with unlimited numbers of sides (Soni, 2000). In gridless method explicit connectivity between nodes is unnecessary (Soni, 2000).

From the first application of mesh generations until now, this field of mathematics, relevant to meshing, has made a considerable progress. The history of different mesh generation methods and their future is shown in figure 1-11.
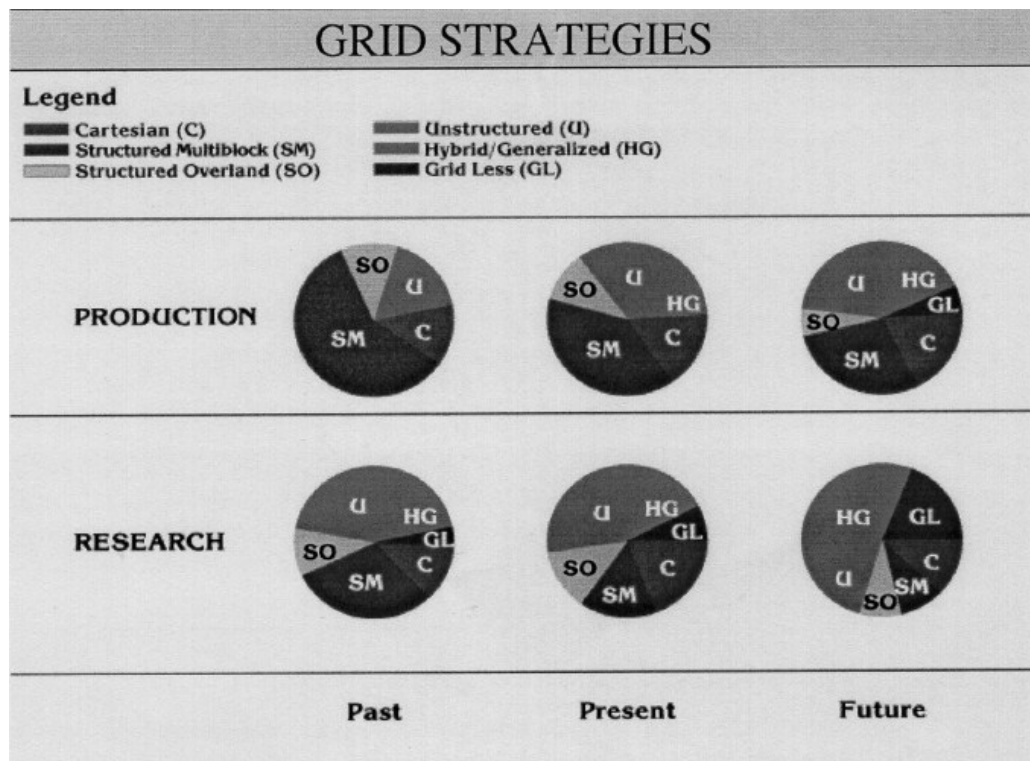
Figure 1-11 History of grid generation application (Soni, 2000)

As it can be seen from figure 1-11, unstructured mesh generation and hybrid meshes will be used mostly in the future, which is due to their high flexibility. Among all the shapes, triangular and tetrahedral forms of unstructured mesh generation are the most common.

There are three different methods that can be used to generate mesh in these two forms: Octree, Delaunay, and Advancing Front (Owen, 1998). Delaunay criterion (Figure 1-12) is the most popular method, which can be achieved in two ways; by point insertion or by boundary constrained triangulation (Owen, 1998).
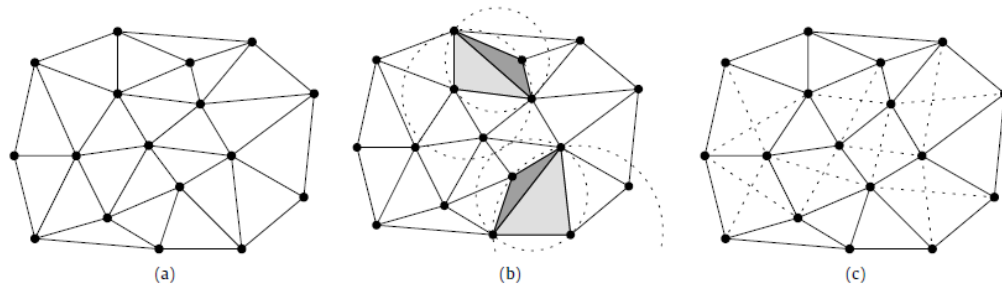
Figure 1-12 Delaunay criterion (van Kreveld, Löffler, & Silveira, 2010)

All these methods and criterions just generate meshes. However, these meshes, with some post-processing improvements, will reach the required quality for numerical modeling.

1.5.2 Smoothing and clean-up

Smoothing and Clean-up are two main categories of mesh improvements (Owen, 1998). Smoothing is a procedure in which, by repositioning individual nodes, the quality of the elements is improved (Owen, 1998). All the smoothing techniques can be classified in four groups: averaging, optimization-based, physically-based, and mid-nodes placement methods (Owen, 1998). Smoothing is done using different kinds of algorithms that the simplest one is Laplacian which can be classified in averaging methods group (Owen, 1998).

Clean-up will improve mesh quality by changing the elements' connectivity while improving shape or topology (Owen, 1998).

1.5.3   Refinement

One of the most commonly used post-processing procedures that are applied on meshes is mesh refinement. This operation will reduce the element size by increasing the number of elements in a region. Refinement can be done several times in succession to achieve the desired element size. Different methods and algorithms can be used for mesh refinement operation. One method is to regenerate the meshes with desired element size and distribution; however this method is computationally expensive and complicated (De Cougny & Shephard, 1999). Other methods and algorithms can be classified depending on meshes; whether meshes are triangular, tetrahedral, quadrilateral, or hexahedral. The refinement methods will be different for each type; however some of these methods can be applied for two or more types.

Owen (1998) presented a general classification for mesh refinement depending on meshes form. According to Owen (1998), there are two base groups of refinement methods: 1) triangular/tetrahedral refinement which consists of three sub-groups; edge bisection, point insertion, and templates, and 2) quad/hex refinement.
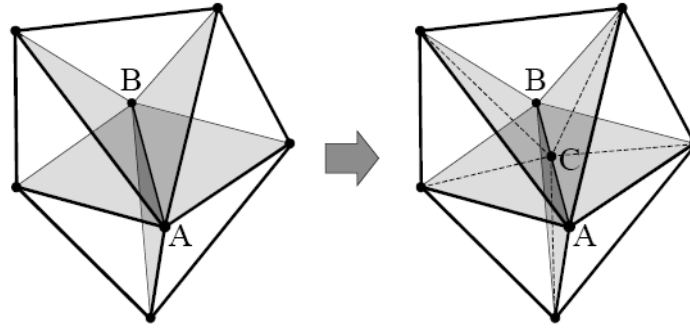
Figure 1-13 Edge bisection refinement methods (Owen, 1998)

Edge bisection splits the edges and therefore the two triangles which are adjacent the same edge will split into two. Figure 1-13 illustrates this refinement methods and the result of refinement (Ho-Le, 1988). In the figure edge A-B is split at point C and it causes the splitting of the surrounding tetrahedral (Owen, 1998).

The simplest method is point insertion, in which a single node will be inserted at the center of an element and divide it into three (for triangle) or four (for tetrahedral) new elements (Owen, 1998). A potential disadvantage of this method is the poor quality of the resulting elements (Owen, 1998). This method is equal to insertion of Delaunay criterion in another classification.

Another method is the templates method, which consist of different variations to decompose a triangle. One of these methods is shown in Figure 1-14. As it can be seen each triangle divided to four triangles by inserting 3 nodes at each of the edges of the triangle (Owen, 1998).
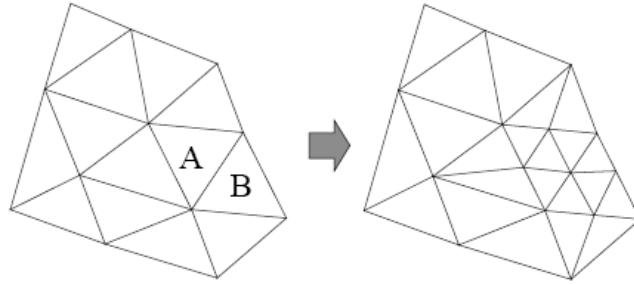
Figure 1-14 Templates refinement methods (Owen, 1998)

Quadrilateral and hexahedral meshes generated by structured mesh generation are due to their forms, not suitable for edge bisection and point insertion. Only the templates method is good for these meshes (Owen, 1998).

1.5.4 Coarsening

As it has been discussed, many post-procedures are carried out in order to reduce computation time and error in the solution. The last, but not least, operation is mesh coarsening. This is a procedure, which eliminates all unnecessary nodes and elements from a mesh (Hattangady, 1999a). The general changes due to mesh coarsening (depending on coarsening factor) are illustrated in Figure 1-15.

(a) The original mesh.   (b) Coarsening factor 2.1.   (c) Coarsening factor 4.   (d) Coarsening factor 8.
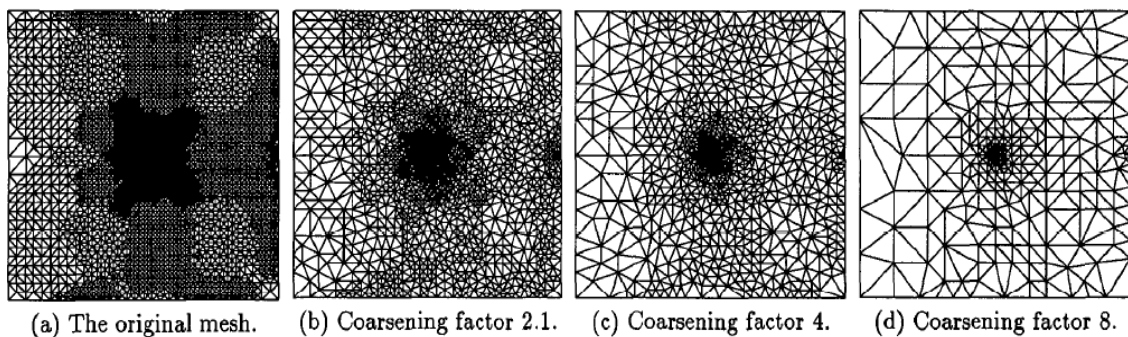
Figure 1-15 Mesh coarsening procedure (Miller, Talmor, & Teng, 1999)

Miller et al. (1999) classified coarsening methods into 3 groups of; element-nested, node-nested, and non-nested. Another classification proposed by Hattangady (1999a)which has three methods such as; edge collapsing, edge swapping, and planar smoothing. Following is a brief explanation of these methods.

Edge collapsing is a procedure, which removes all the edges that comply with the edge collapsing criteria, and all the adjacent faces connected to these edges (Hattangady, 1999a). Edge swapping is about rearranging face connectivity by decreasing the maximum angle of the triangular face (Hattangady, 1999a). Planar smoothing works with relocating nodes, for which all the faces that are connected to it are located in the same plane (Hattangady, 1999a). After planar smoothing it may be necessary to use edge collapsing (Hattangady, 1999a).

1.5.5 Influence of mesh size

Numerical modeling is applied in different fields of science and engineering. It has been determined that the finite element mesh size has a considerable effect on analysis result. Some of these supporting investigations will be discussed in this section to clarify the importance of mesh size on final results of the numerical modeling. Generally, mesh size may have an effect on the accuracy of the final result, and the time of analysis.

Choi and Kwak (1990) illustrated that when using non-linear analysis to monitor the effect of load increasing on concrete reinforced structures, the finite element mesh size plays a significant role. Their research showed that by changing the mesh sizes the errors which depend on the mesh size, will be reduced (Choi & Kwak, 1990). It can be seen from this research that the mesh size, should not be very large (Choi & Kwak, 1990). By their

proposed model the best mesh size can be achieved, which will then decrease the numerical error caused by mesh fineness (Choi & Kwak, 1990).

Another field in which numerical modeling has a wide application is metallurgic science, in particular metal forming. Fatigue crack closure is an important discussion in this field and it has been proven that to achieve the most appropriate numerical crack opening results, it is necessary to use the proper mesh sizes through different applied mesh sizes (Lee & Song, 2005). It was also considered by Park et al. (1997) that the result of the finite element analysis, which used on the most suitable mesh size, is more compatible with experimental analysis results.

Relationship between mesh size and analysis or computation time is an important aspect of mesh generation and numerical modeling. It has been proven that analyzing fine meshes needs more time than coarse meshes. Hattangady (1999b)shows that by coarsening meshes, the time spent to analyze the geometry will be significantly reduced. In simulating the metal forging process, which is a time consuming process simulation-wise, coarsening meshes will reduce CPU time almost 20.55% and the result of the analysis of coarse mesh and fine mesh are almost identical (Hattangady, 1999b). It is also considered in their research that more the mesh is uniform, the more dramatic is the reduction of CPU time (Hattangady, 1999b). Another advantage of a coarse mesh in their research is: reduction of memory usage, smaller result file, faster visualization, and faster transmission of files (Hattangady, 1999b).

All these investigations show that, as it was expected mesh size not only improved analysis accuracy, but also it will help to reduce analysis time and even the memory usage. As was mentioned in previous sections, with mesh refining and coarsening we can have a more appropriate finite element model to be solved in a shortest amount of time.

CHAPTER TWO

2. THE RELATION OF MESH OPTIMIZATION WITH YOUNG'S MODULUS AND POISSON'S RATIO

Mining and civil excavation analysis and design consists of considerable amount of input data fed into a numerical or analytical model. The amount of input is required due to the inherent uncertainty and complexity associated with geologic media, such as rocks and soils. In contrast to the limited nature of analytical models, numerical modeling not only makes the analysis simpler but also improves the result of the analysis and predictions. There are different numerical methods of stress analysis like boundary element and finite element methods. Although the finite element method simplifies stress analysis, due to complexity of model generation and analysis it still is time consuming process which also needs adequate computational resources. The finite element method requires a discretizations, or a mesh, to solve the problem. The meshes are created by mesh generation. Mesh density has a direct effect on time and memory consumption of the analysis. Therefore one of the possible solutions to simplify the analysis is to reduce the mesh density and element number while the analysis result is comparable with the original results.

There are different parameters which should be considered for estimating mesh adequacy. Stress analysis of an underground excavation depends on the excavation's geometry, its location and geological, geotechnical, and rock mechanical properties of the rock mass. Therefore mesh density and the number of mesh elements are directly dependent on these parameters as well. Zsaki and Curran (2005) introduced a framework for boundary and finite element mesh optimization with respect to excavations' geometry. With help of a cost function, they introduce an equation for simplifying a mesh depending on the geometry of the excavation. However, their method did not include the influence of geologic features on simplification.

The focus of this thesis is mesh optimization with respect to rock material properties. As discussed in the preceding chapter, the mesh optimization scheme of Zsaki and Curran (2005) only considers the optimization of geometry of excavations. This thesis expands on the optimization strategy by including rock properties. Among the many different properties of rocks Young's Modulus (E) and Poisson's Ratio (μ) are considered in this thesis. Thus different mesh generation methods are applied and the relation between rocks' properties (E and μ) with number of elements will be studied to find out which of these two properties has the most significant effect on the stress analysis as affected by the number of elements in a FEM analysis. Subsequently, a cost function for the most effective property will be formulated.

For modeling and stress analysis phase[2] (a finite element program by Rocscience) is used (Rocscience Inc., 2008). The effect of mesh density and mesh element number on a model without excavation was studied, to establish a base case, and then an excavation was added to the model and stress analysis was repeated. Models and analysis details are summarized in following sections.

For each model a set of different values for E and μ was used for evaluating their effect on mesh optimization. Estimations were carried out for 4 different E values: 10000, 20000, 40000, and 75000 MPa and for 3 different μ values: 0.1, 0.2, and 0.3. These values cover a range of representative rock properties from very weak to a fairly competent and sound rock. As a resource, Table 2-1 shows E for different type of intact rocks. Similarly, the values of μ are chosen considering Figure 2-1. Although the effect of E and μ were considered and investigated, the examination was not simultaneous; when the effect of E was studied μ was assumed to be constant and equal to 0.3, and E was considered constant and equal to 20000 MPa during the stress analysis with different values of μ.

Table 2-1 Typical values of uniaxial compressive strength and elasticity modulus of some rocks (Palmström & Singh, 2001)

Average values from tests of rock samples		Test of rocks world-wide			
Rock		σ_c MPa	E GPa	E/σ_c	Number of tests
Crystalline texture	Dolomite	86	38	443	8
	Limestone	107	47	441	81
	Marble	113	63	474	20
	Clay schist/-stone	68	38	563	2
	Micaschist	104	39	374	16
	Gneiss	130	53	406	27
	Granulite	90	41	451	4
	Amphibolite	212	101	474	7
	Greenstone	281	101	359	1
	Quartzite	209	58	276	28
	Anorthosite	228	90	395	2
	Diorite	173	64	368	6
	Granite	154	48	313	71
	Granodiorite	160	51	319	2
	Gabbro	228	106	466	5
	Norite	229	82	356	8
	Peridotite	197	55	280	1
	Monzonite	110	28	256	8
	Andosite	152	31	206	6
	Basalt	145	50	347	25
	Diabase, dolerite	229	88	384	13
Clastic	Graywacke	81	25	310	12
Texture	Sandstone	109	28	257	95
	Siltstone	89	31	350	14
Very fine-grained rocks	Hornfels	111	74	668	3
	Claystone	5	2	301	2
	Phylite	39	26	672	4
	Chalk	1	2	1606	2
	Marl, marlstone	17	2	133	9
	Mudstone	11	1	106	4
Organic rocks	Coal	30	3	107	14

There are four types of mesh generation options available in Phase^2 (Rocscience Inc., 2008): graded, uniform, radial, and "no internal nodes". Since only the uniform mesh generation creates a mesh without any consideration to geometry it was selected to serve as a base case without bias such as gradation of elements. However, the number of elements and mesh density was changed to compare the results from a coarse and fine mesh. These changes first applied to whole model and later in a selected area of the model.
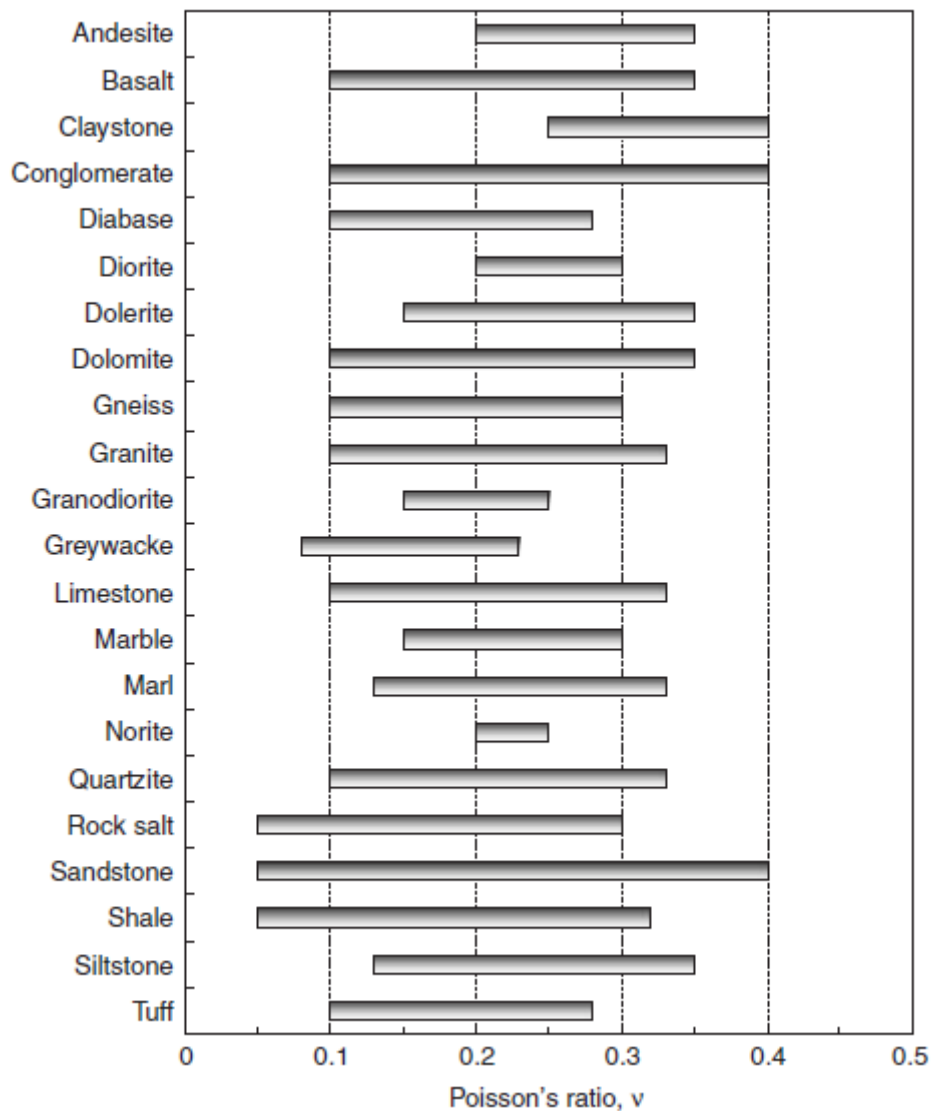
Figure 2-1 Typical ranges of values for Poisson's ratio of some rock types (Gercek, 2007)

2.1 Model without excavation

This simple model scenario, in which a fault line traverses a host rock, consists of two different types of material (different E and μ) for rock mass and fault zone. Figure 2-2 shows models geometry details.
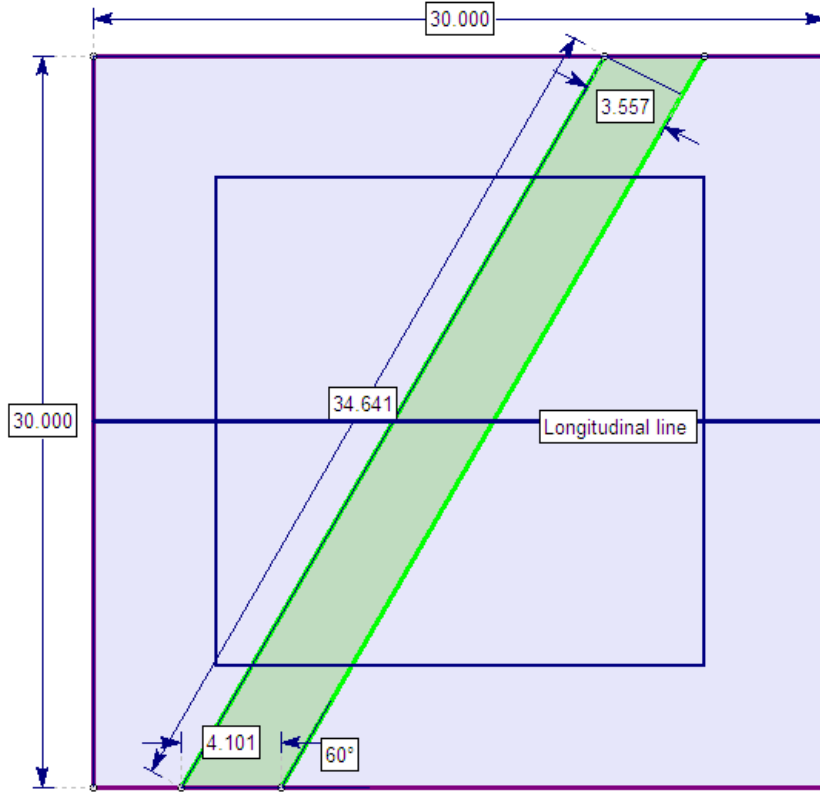
Figure 2-2 Model's geometry - without excavation (the dimensions are in meters)

Material properties when E is different and μ is constant and equal to 0.3 are summarized in Table 2-2.

For this model *in-situ* field stresses are assumed to be constant and equal to 10 MPa in all the directions (essentially a hydrostatic case). Due to the changes of E and μ of the

material in the fault zone, the resulting behavior could be softer or stiffer, or more brittle or ductile than the host rock mass.

Table 2-2 Material properties with different E and constant μ.

Material Name	Color	Initial Element Loading	Unit Weight (MN/m3)	Elastic Type	Young's Modulus (MPa)	Poisson's Ratio	Failure Criterion	Material Type	Tensile Strength (MPa)	Friction Angle (peak) (deg)	Cohesion (peak) (MPa)	Piezo Line	Ru
rock mass	☐	Field Stress and Body Force	0.027	Isotropic	5000	0.3	Mohr Coulomb	Elastic	0	35	10.5	None	0
fault zone	☐	Field Stress and Body Force	0.027	Isotropic	75000	0.3	Mohr Coulomb	Elastic	0	35	10.5	None	0

Analysis can be classified into two main categories; a.) the set of analysis in which μ is constant, and b.) in which E is constant. Each category has two sub-categories as illustrated in figure 2-3.

Figure 2-3 Classification of Young's modulus and poisson's ratio analysis

Subscripts R and F are used for Rock mass and Fault zone respectively. It should be noted that in each sub-categories just one of the parameters is changing and the other one is fixed, it means that for instance when E_R is greater than E_F, E_F will be constant and equal to 5000 MPa and E_R will change from 10000 MPa to 75000 MPa (10000, 20000, 40000, and 75000 MPa). Therefore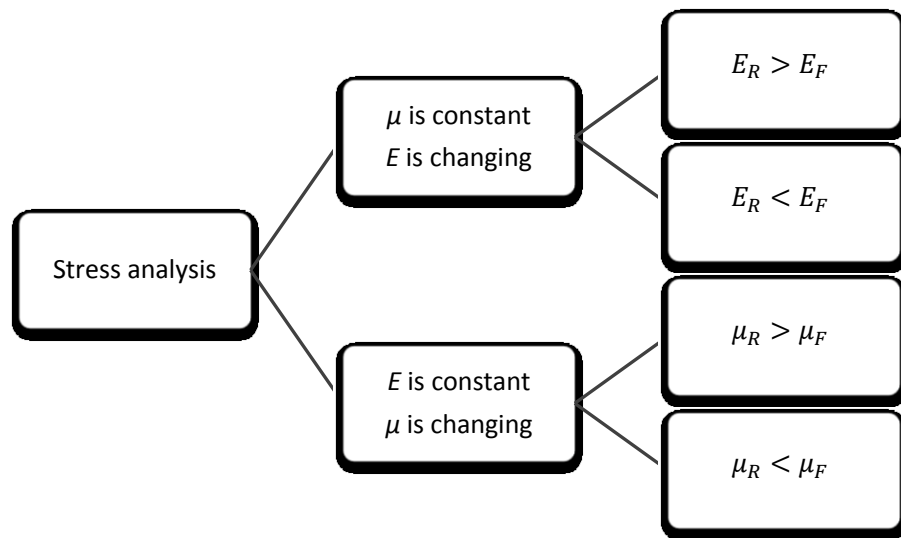 in each sub-categories of the first category the lowest value of E will be 5000 MPa whether it is for fault zone or for rock mass, and for μ the one with the greater value will be assumed to be constant and equal to 0.4.

For each modeling case the principal stresses (σ_1, σ_3) and total displacement (U) were interpreted from the result of analysis and their changes were plotted along a longitudinal line which has been showed in Figure 2-2.

Likewise, to avoid the errors caused by the closeness of boundaries and their effect, the interpretations were considering only inside a specified area (the box in figure 2-2), far from boundaries.

2.1.1 μ is constant and E is changing

a) $E_R > E_F$

As it has been said, E_F and μ are assumed to be constant and equal to 5000 MPa and 0.3, respectively. The analysis was carried out with two different methods of mesh generation; in the first method uniform mesh was applied in whole model with sets of different numbers of elements. For this method the result of five different numbers of elements including 500, 1000, 3000, 5000, and 10000 was examined and compared. These numbers cover a wide range from coarse to fine element distribution.

As it has been indicated for each analysis, the values of σ_1, σ_3, and U were plotted along a longitudinal line. This is to illustrate the changes in values along the domain analyzed. A special consideration has to be given to the issue of obtaining the most accurate and representative graph, the sampling of data should be considered. Sampling should contain enough values with the most appropriate distance between them to avoid both over and under sampling problems. To find the best number of values that should be plotted, a trial and error method was applied. Along each line 50, 200, 500 and 1000 locations were chosen to be plotted, and then the results were compared to find the most appropriate number of locations or values. The result for σ_1 analysis in a model with 500 element's number and E_R equal to 10000 MPa is illustrated in figures 2-4 to 2-7.

Figure 2-4 σ_1 stress analysis, E_R : 10000 MPa and E_F : 5000 MPa - 500 element, 50 location along a longitudinal line is sampled.

Figure 2-5 σ_1 stress analysis, E_R : 10000 MPa and E_F : 5000 MPa - 500 element, 200 location along a longitudinal line is sampled.

Figure 2-6 σ_1 stress analysis, E_R : 10000 MPa and E_F : 5000 MPa - 500 element, 500 location along a longitudinal line is sampled.

Figure 2-7 σ_1 stress analysis, E_R : 10000 MPa and E_F : 5000 MPa - 500 element, 1000 location along a longitudinal line is sampled.

In the figure with 50 values (Figure 2-4) the distance between values is not small enough to create a smooth and well-shaped graph. Although for the 500 and 1000 number of values the graph is smooth enough, as it can be seen too many values were plotted. In figure 2-6 and 2-7 the overall shape of the graph does not differ from the graph with 200 values; however 200 values seems inadequate to cover enough data's in the selected area (figure 2-5). This can be due to under sampling or lack of enough mesh elements. Since inadequacy of values in the selected area is slightly observable in figures 2-6 and 2-7 with 500 and 1000 values, respectively, it is hard to accept the under sampling as a reason. Therefore it should be due to inadequate number of finite element. To further investigate the real reason, the results of the same analysis with 10000 elements' are shown in figures 2-8 to 2-11.
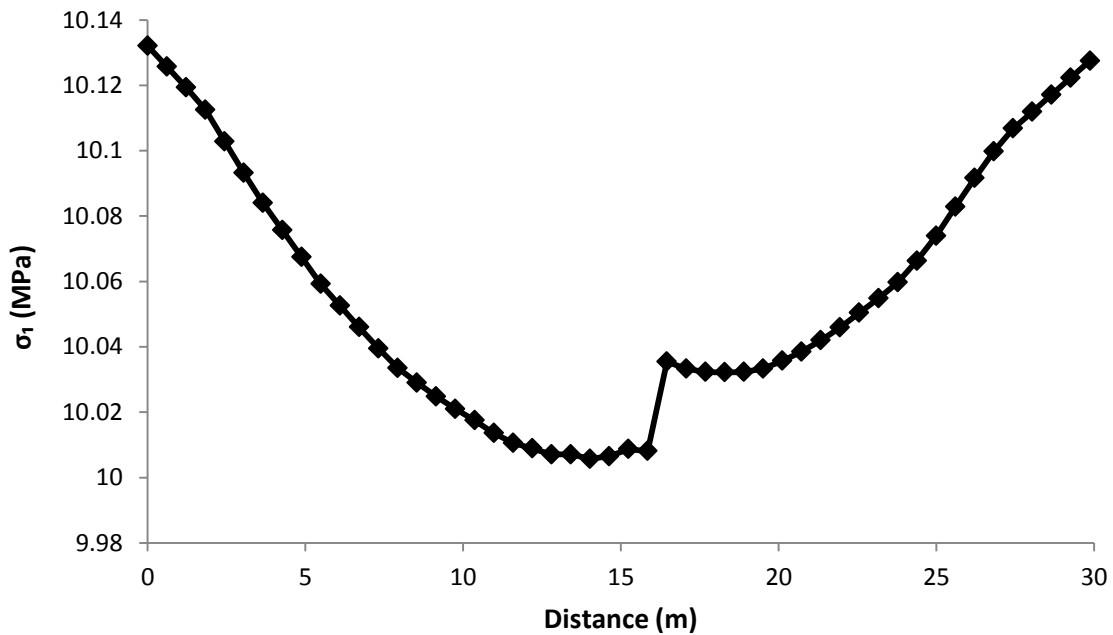
Figure 2-8 σ_1 stress analysis, E_R : 10000 MPa and E_F : 5000 MPa - 10000 element, 50 location along a longitudinal line is sampled.
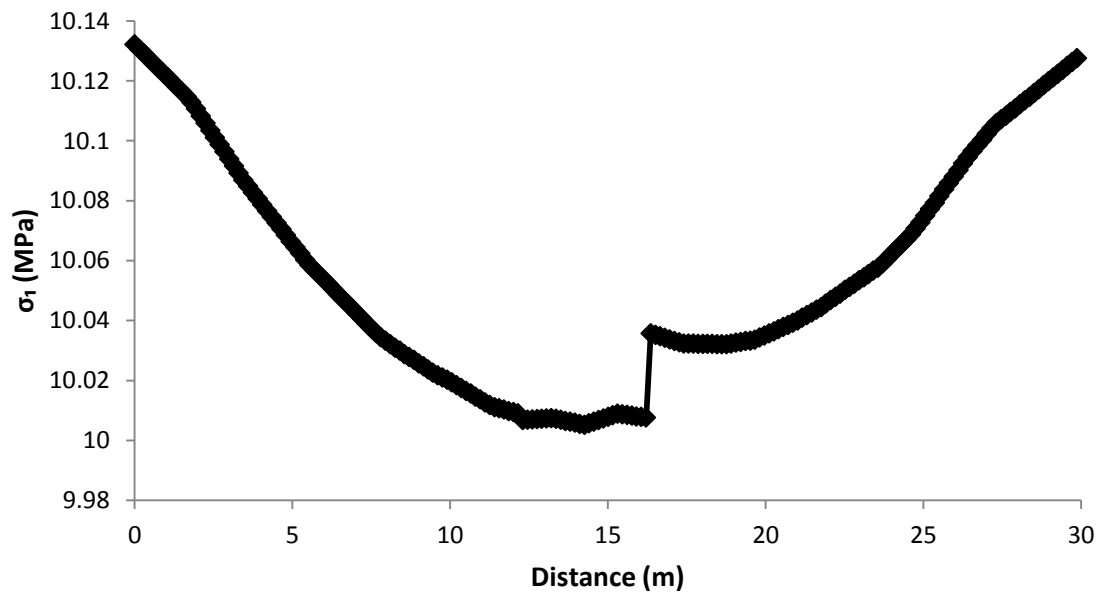
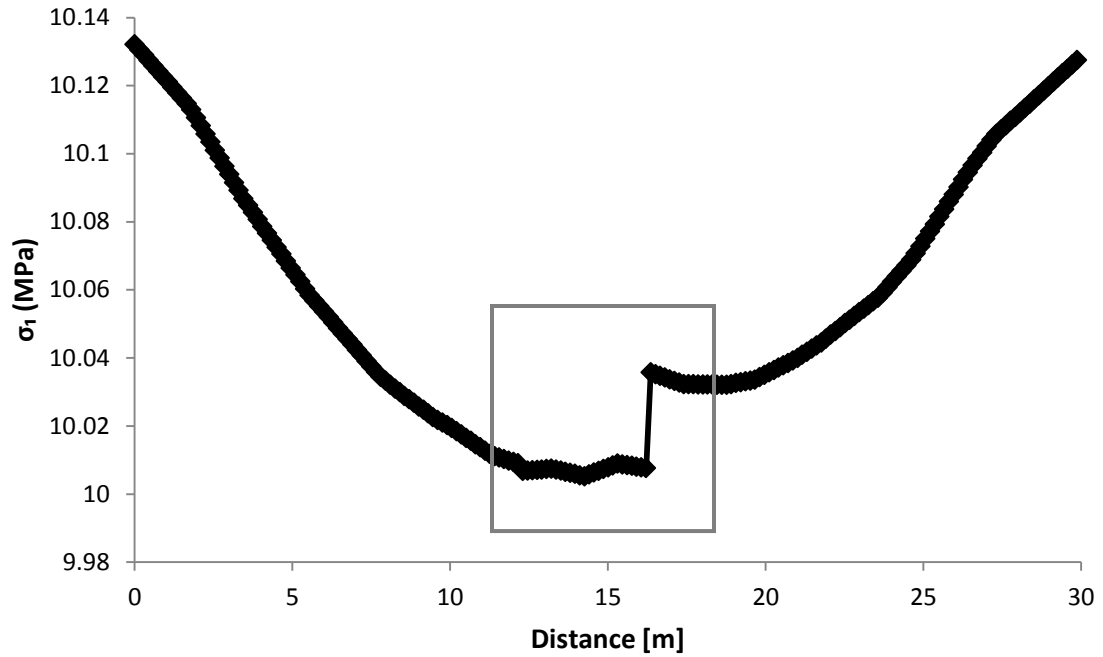**Figure 2-9** σ_1 stress analysis, E_R : 10000 MPa and E_F : 5000 MPa - 10000 element, 200 location along a longitudinal line is sampled.
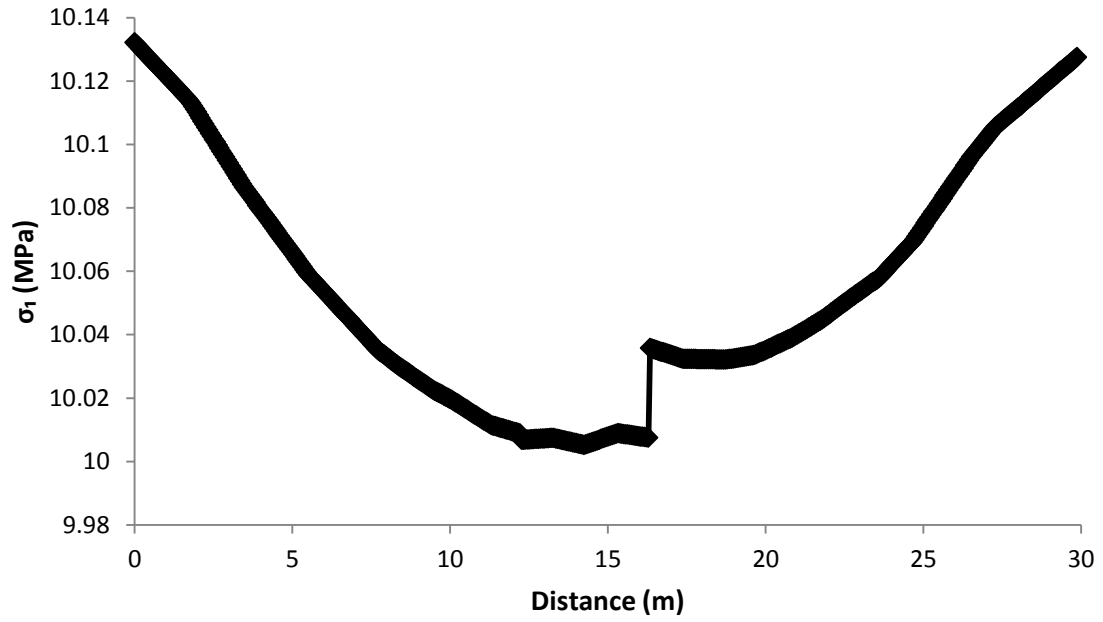
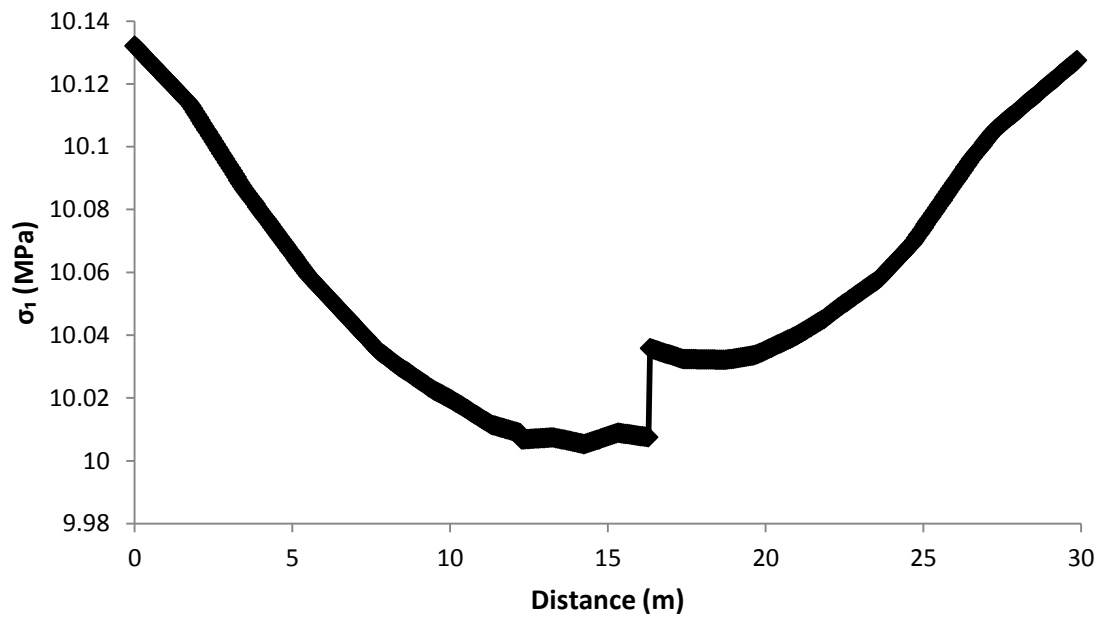**Figure 2-10** σ_1 stress analysis, E_R : 10000 MPa and E_F: 5000 MPa - 10000 element, 500 location along a longitudinal line is sampled.
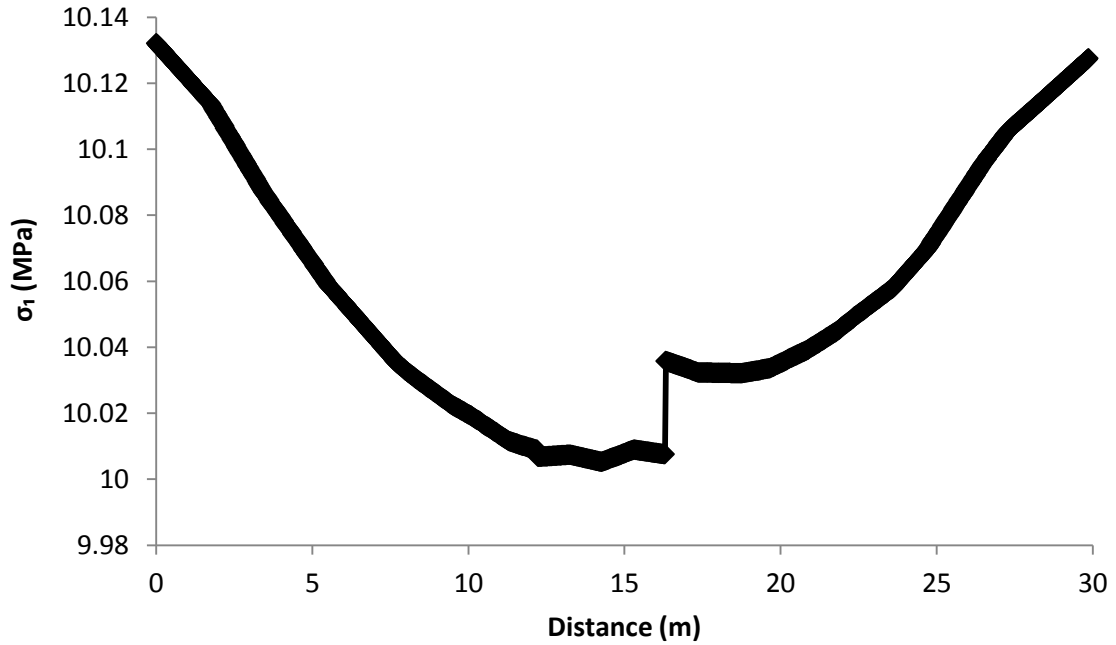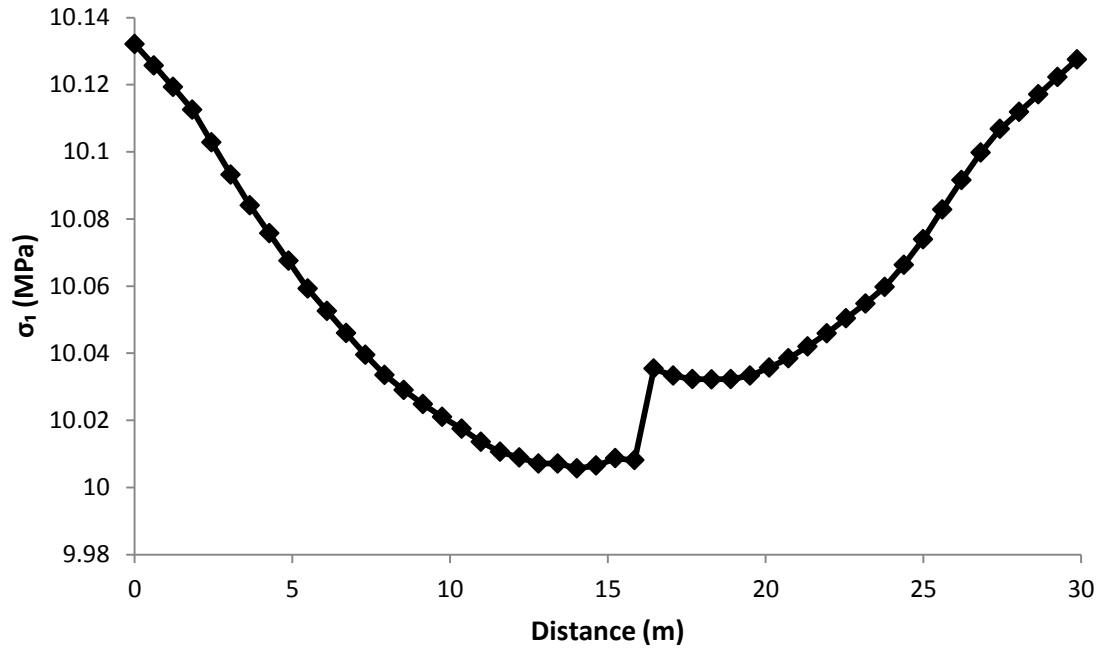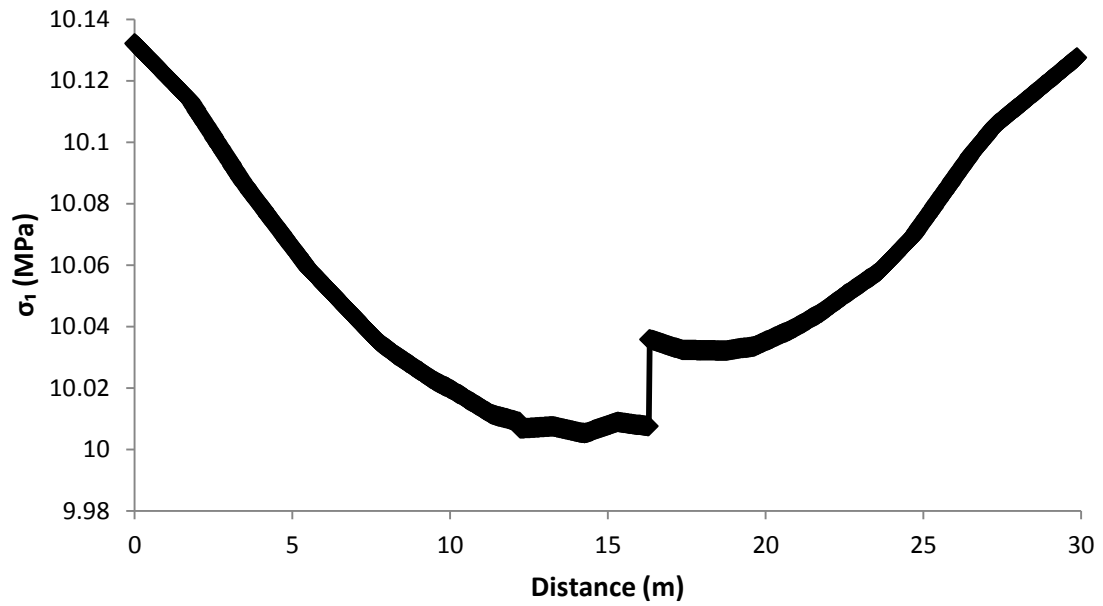

Figure 2-11 σ_1 stress analysis, E_R : 10000 MPa and E_F : 5000 MPa - 10000 element, 1000 location along a longitudinal line is sampled.

By comparing figures 2-8 - 2-11 with figures 2-4 – 2-7, it is evident that in figures 2-8 – 2-11 from figure 2-9 with 200 plotted values the shape of the graph does not change by adding more sample points; however in figures 2-4 – 2-7 as the number of sample points changes the shape of the graphs changes as well. For figures 2-8 – 2-11 it is due to more finite elements that the shape of the graphs does not change by adding more data samples. Since figure 2-9 does not significantly differ from figures 2-10 and 2-11, 200 values were assumed to be adequate number of samples to represent the graph.

Eventually, after considering the effect of number of elements on stress analysis for σ_3 and displacement analysis in which E_R is equal to 10000 MPa, It can be seen that as the number of elements increases the shape of the graphs changes into a smoother graph. This is due to adequate values along the lines which help to cover lack of values and results in smoother and well-shaped graphs.
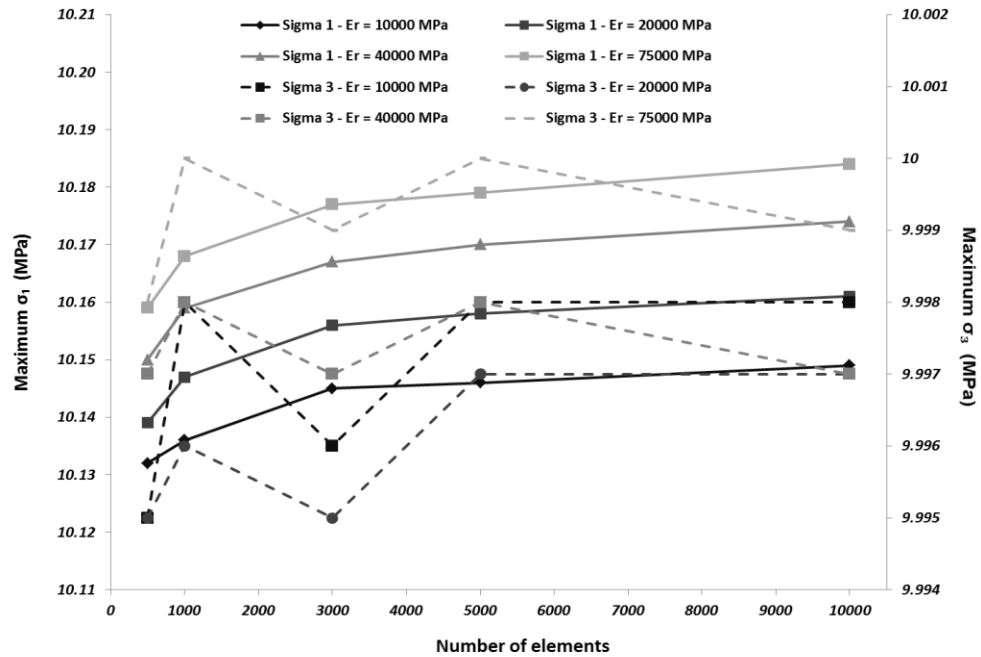
Figure 2-12 Changes in maximum σ_1 (solid line) and maximum σ_3 (dashed line) as the number of elements increases for different E_R

To estimate the effect of number of elements on the result of analysis, maximum values for σ_1, σ_3, and U were determined from a query line with 200 values (figures 2-12 and 2-13).

The graphs illustrate an increase in σ_1 by increasing the number of element (figure 2-12). Almost identical result is achieved for values of σ_3 (figure 2-12); whereas U stays constant as the number of elements increase, as seen from figure 2-13.
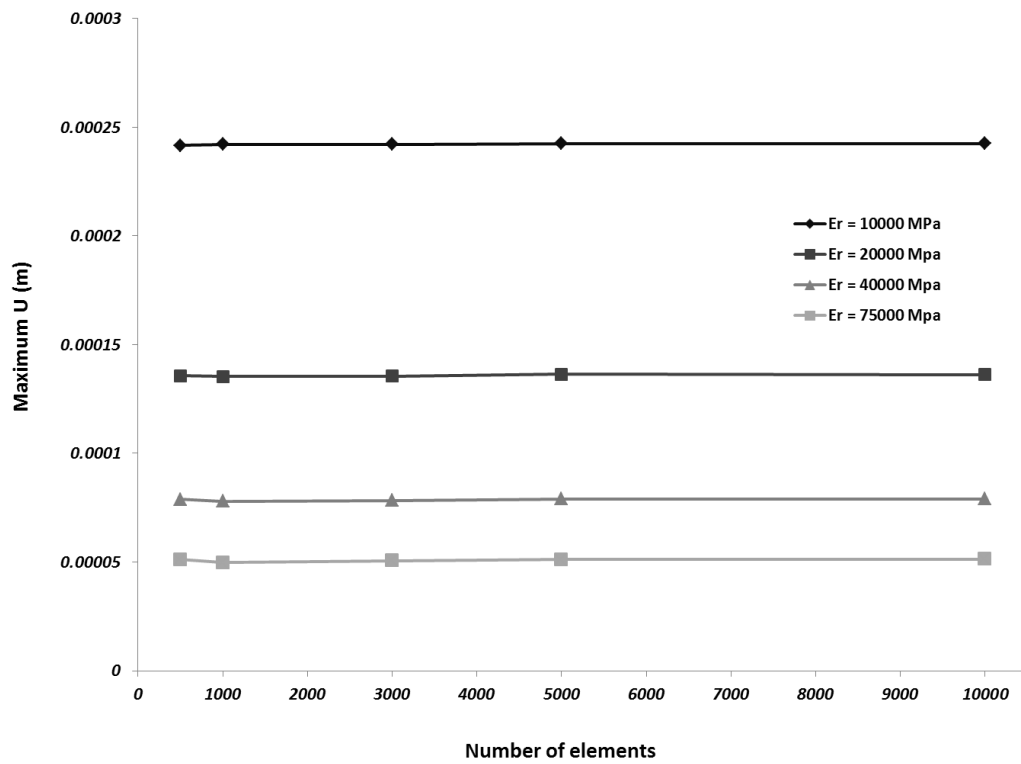
Figure 2-13 Changes in maximum U as the number of elements increases for different E_R

It is evident from figures 2-12 and 2-13 that the changes in analysis results for different E values can be estimated as well; however for each set of number of elements an average was determined for stresses and displacements to clearly show the effect of E on analysis results (figures 2-14 and 2-15).
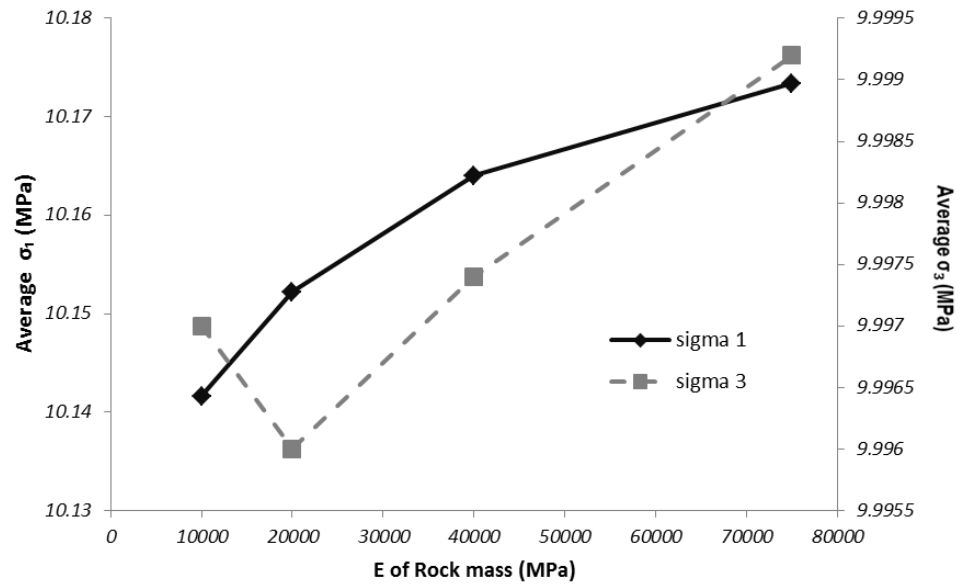
Figure 2-14 Changes in σ_1 and σ_3 with E_R (an average of maximum values of σ_1 and σ_3 for each set of element numbers were used)

Figure 2-15 Changes in U with E_R (the average of maximum values of U for each set of element numbers were used)

47

It should be noted that since E_F is constant and equal to 5000 MPa (to show that fault zone consist of a softer material), by increasing E_R the ratio of E_R to E_F (E_R/E_F) increases. The changes in σ_1 and σ_3 are in direct proportion to the changes of E_R/E_F. Thus σ_1 and σ_3 will increase by an increase of E_R/E_F; While U decreases with the increase in E_R/E_F.

The effect of number of elements and mesh density was also examined by applying a uniform coarse mesh with approximately 500 elements which was then partially refined. Refinement was applied in a specific area which can be seen in figure 2-2. To find the most appropriate mesh density, refinement was carried out once, twice and five times.
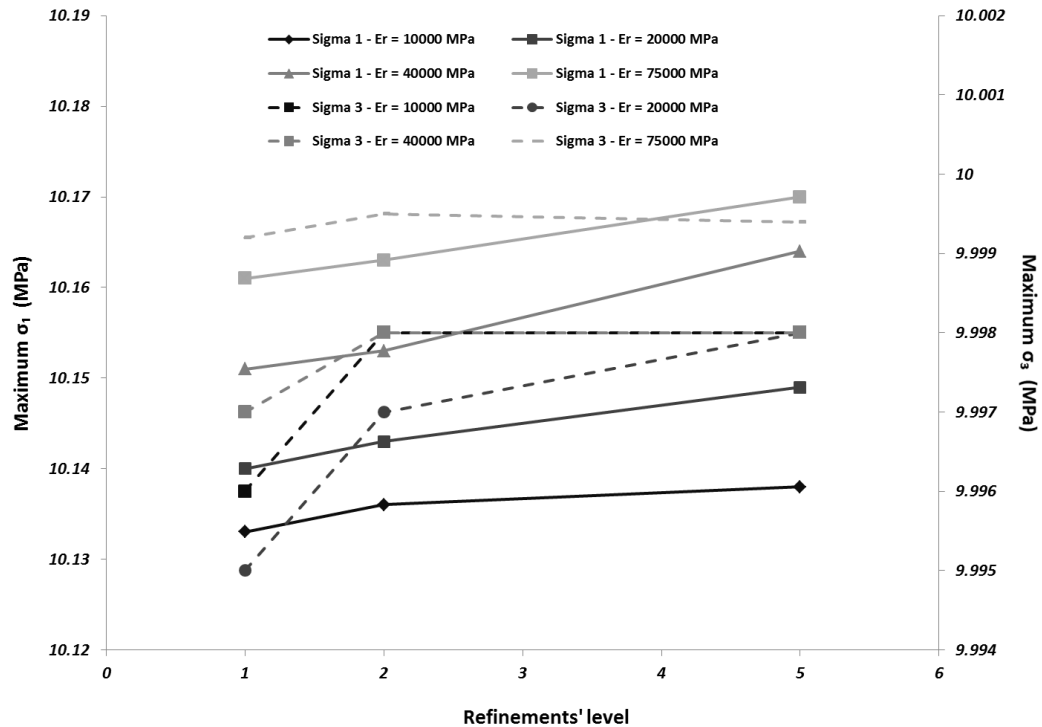
Figure 2-16 Changes of maximum σ_1 (solid lines) and σ_3 (dashed lines) with refinements' grades for different E_R

For these analyses longitudinal line was used and data sampling was accomplished by 50, 200, 500, and 1000 values. The comparison verified that again 200 values are adequate to determine the analysis result with enough sampling precision. After comparing the result of the two methods it can be concluded that the result of the both methods are substantially the same; however it is necessary to compare maximum values of stresses and displacements, and their changes with number of elements and Young's modulus as well.

Changes of maximum σ_1, σ_3, and U with mesh refinement levels can be determined from figures 2-16 and 2-17,respectively.
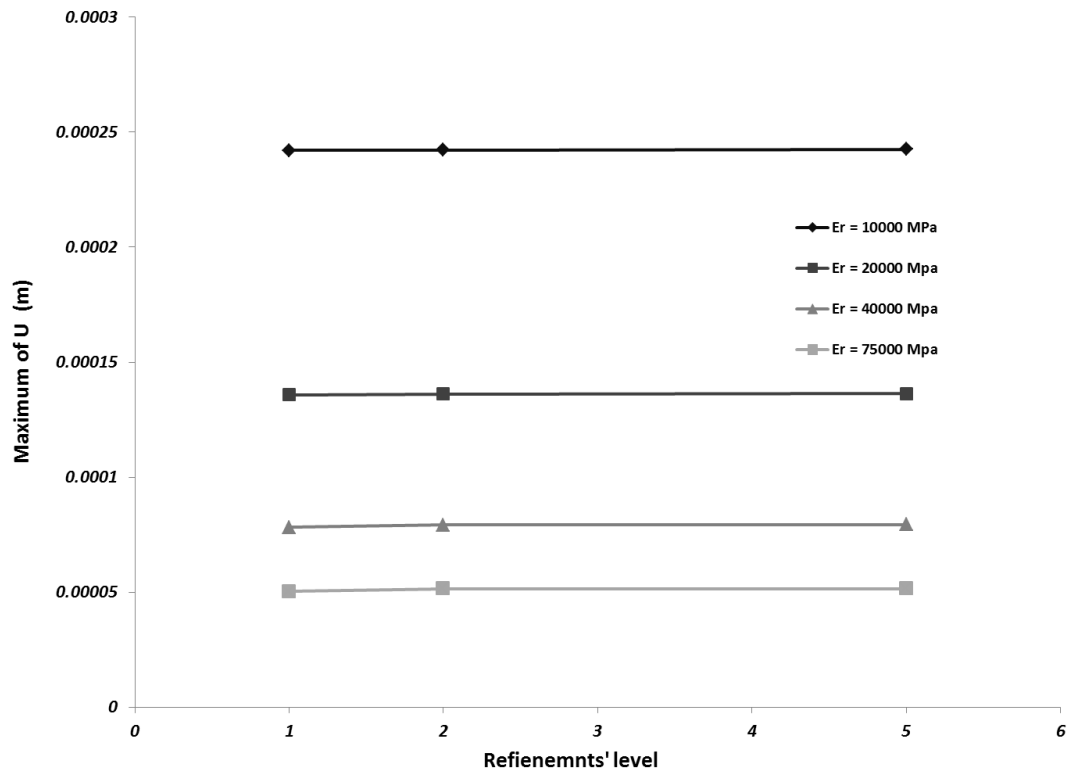
Figure 2-17 Changes of maximum displacement U with refinements' grades for different E_R

The maximum values were derived using the same method as the one which was discussed before in the previous section. Likewise, the average values of stresses and displacements were computed and the relation between changes of stresses and displacements was determined by considering figures 2-18 and 2-19.
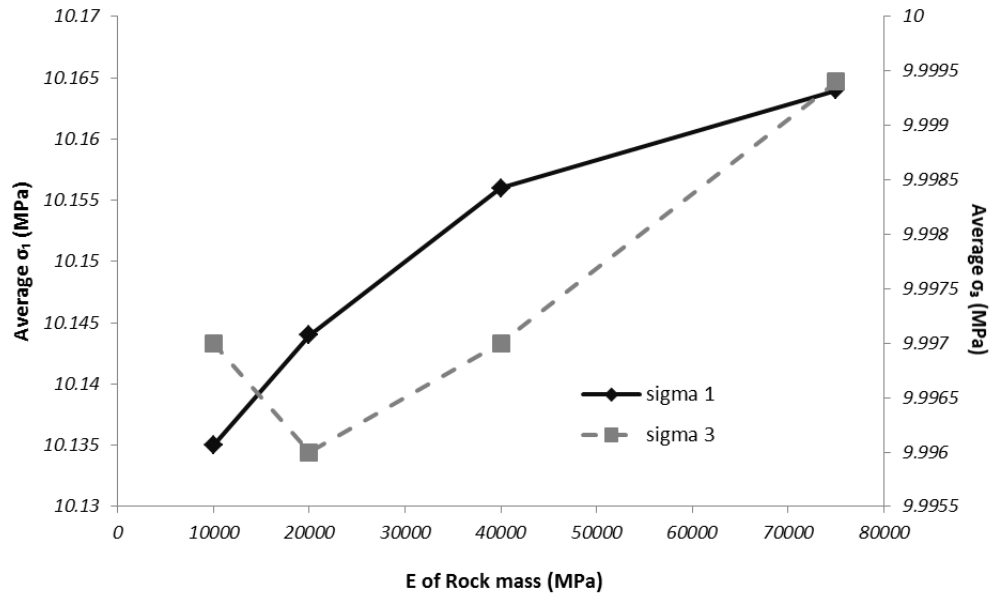
Figure 2-18 Changes in σ_1 and σ_3 with E_R (an average of maximum values of σ_1 and σ_3 for each set of element numbers were used) with different mesh generation
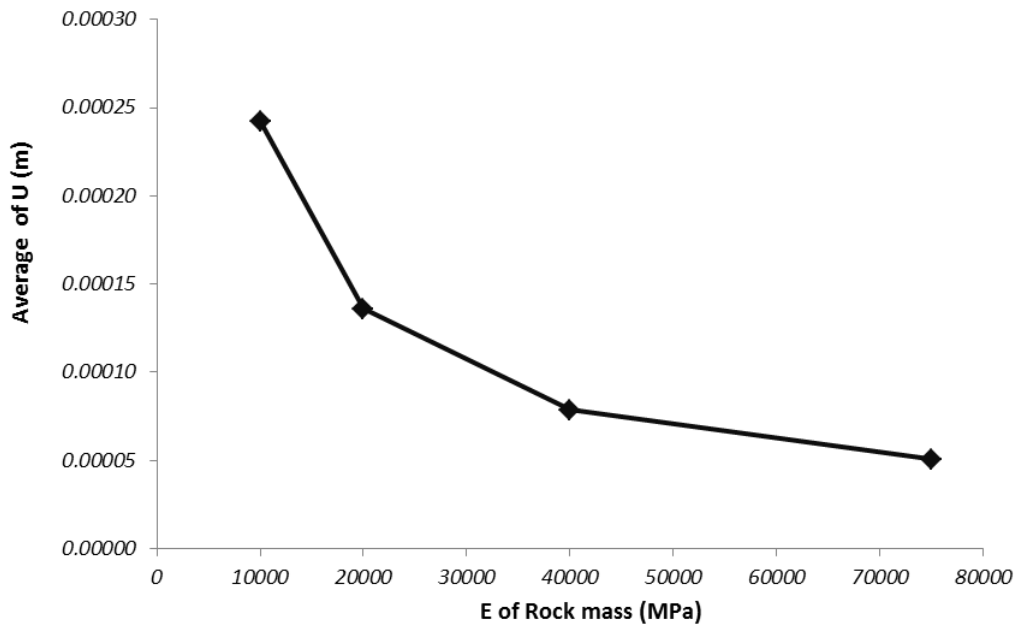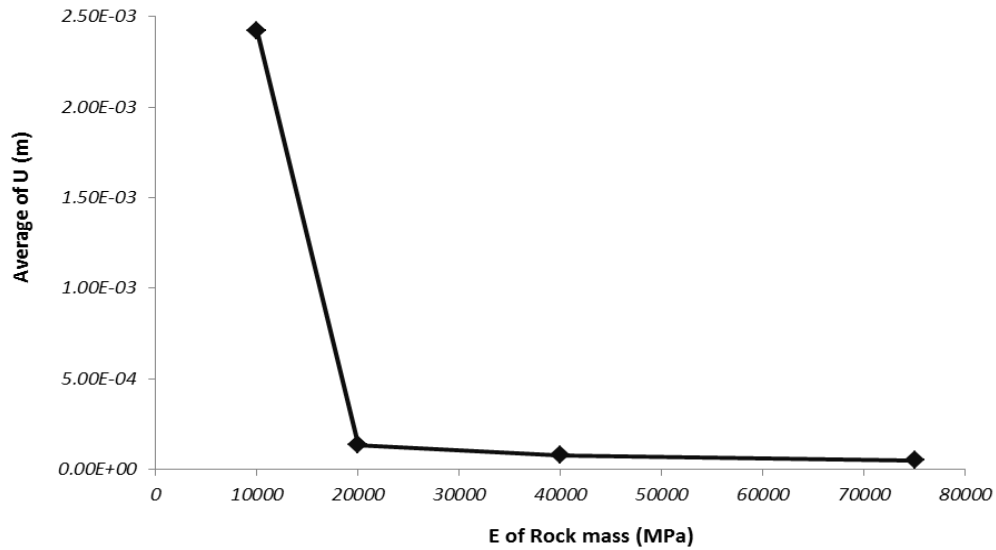

Figure 2-19 Changes in U with E_R (the average of maximum values of U for each set of element numbers were used) with different mesh generation

Figures 2-16 and 2-17 show essentially the same trend in the results as the first mesh generation method; it can be observed that as the refinement level (mesh density) or number of elements increases, σ_1 and σ_3 will show a rise and U will be constant.

Meanwhile, as the E_R/E_F increases, the difference between the two meshing methods will be more noticeable.

b) $E_F > E_R$

All the analyses were repeated when the fault zone is stiffer than the host rock mass. This time E_R was assumed to be constant and equal to 5000 MPa to make rock mass softer than the fault zone. E_F will have different values, 10000, 20000, 40000, and 75000 MPa. Other material properties such as Poisson's ratio were the same as the first model and same general settings in the analysis were used. Two different meshes were used and the results were compared; changes of σ_1, σ_3, and U were almost the same as the model with softer fault zone. As the number of elements increases maximum σ_1 and σ_3 increase as well, while U is almost constant.

For this set of analysis the effect of E on stress and displacement values was also considered. It can be concluded that as E_R/E_F decreases (E_R is constant and equal to 5000 and E_F has higher values than E_R) σ_1 shows an increase, whereas σ_3 and U decrease.

Same analyses with different meshes which was explained in previous section (section a)**,** was carried out and the results and observable trends are essentially the same as the other mesh generation method, σ_1 and σ_3 increase and U is constant. The same results as the first mesh generation method were achieved when the effect of E on principal stresses and displacement considered.

2.1.2   *E* is constant and *μ* is changing

a) $\mu_R > \mu_F$

In the second part of the investigation, the effect of Poisson's ratio on stress and displacement analysis was considered. *E* assumed to be constant and equal to 20000 MPa (not very soft and not very stiff material), also μ_R is constant and equal to 0.4 to show that rock mass consists of a ductile material. Mesh generation and sampling methods are the same as previously; two different mesh generations were applied. The results of analysis with 200 samples were considered, which, as established earlier, is the optimum.

Comparing the results of analysis for different number of elements for σ_1, σ_3, and U exhibit the same trend; the greater is the number of elements the more accurate is the analysis (accuracy is understood in the sense that as subsequent refinements are made, the results only change by a little). The smoothness of the graphs can also be achieved as the number of elements increase which is due to adequate analysis result at each sampled points.

To study the changes of stresses and displacements as a function of number of elements and Poisson's ratio, the same method as for Young's modulus was used and maximum values for σ_1, σ_3, and U were derived. The results were then plotted; Figures 2-20 and 2-21 show changes with number of elements and figures 2-22 and 2-23 illustrate changes with Poisson's ratio.

Similar to the Young's Modulus analysis, for different Poisson's ratio, as the number of elements increase, σ_1 and U increase and σ_3 is fluctuating. An increase in μ_F results in a decrease in σ_1 and U and an increase in σ_3.
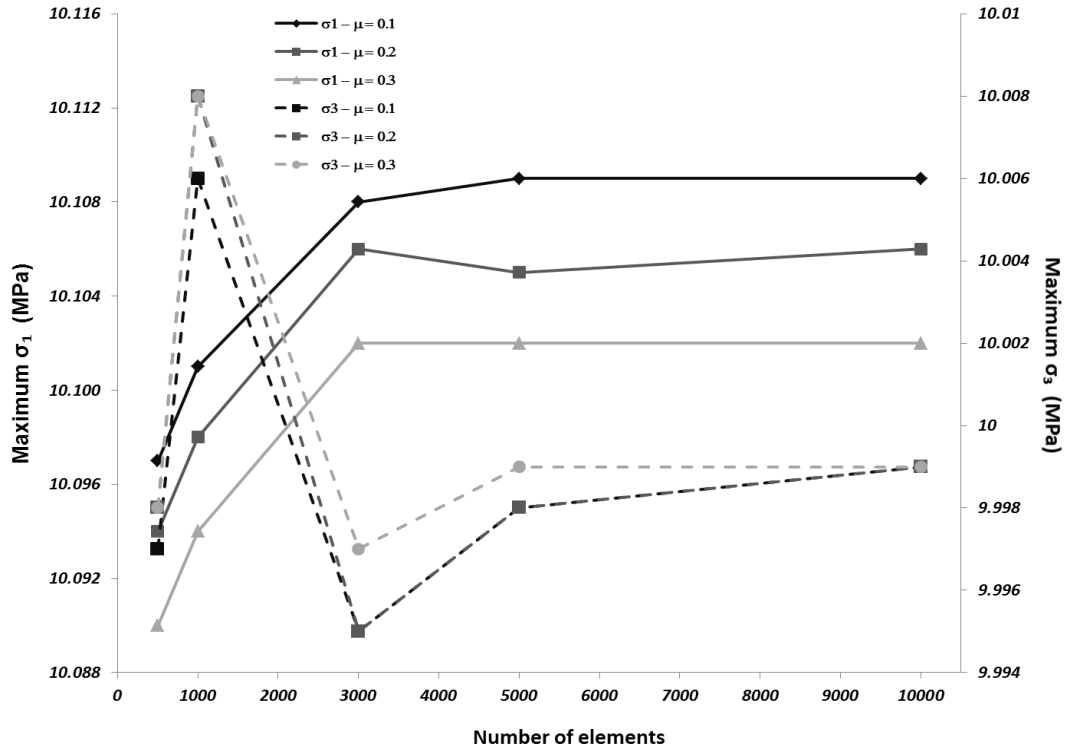
Figure 2-20 Changes of maximum σ_1 (solid lines) and σ_3 (dashed lines) with changes in number of elements for different μ_F
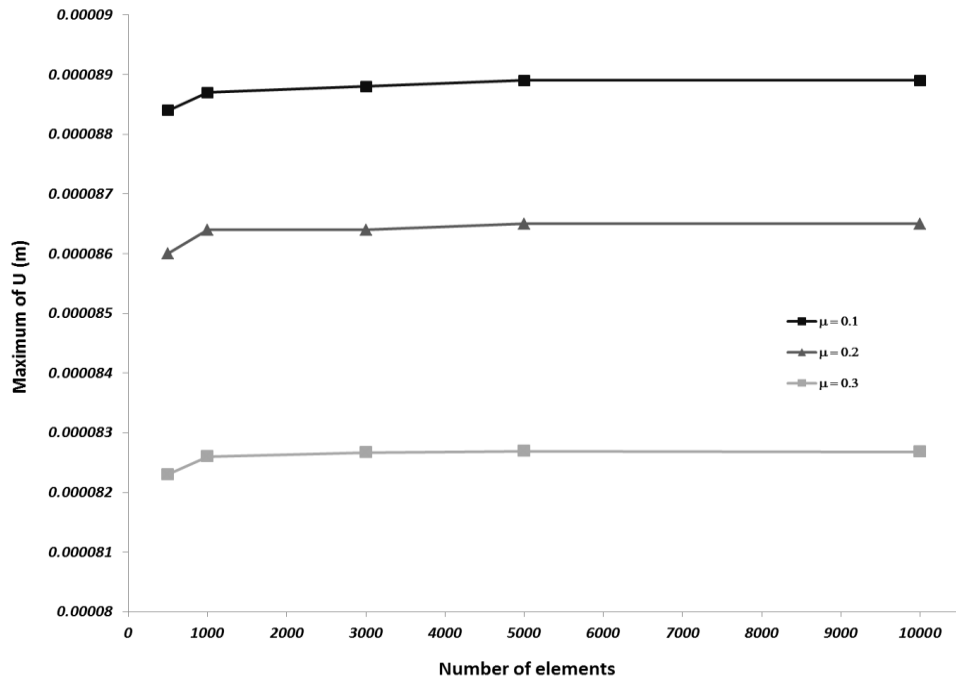
Figure 2-21 Changes of maximum U with changes in number of elements for different μ_F

53
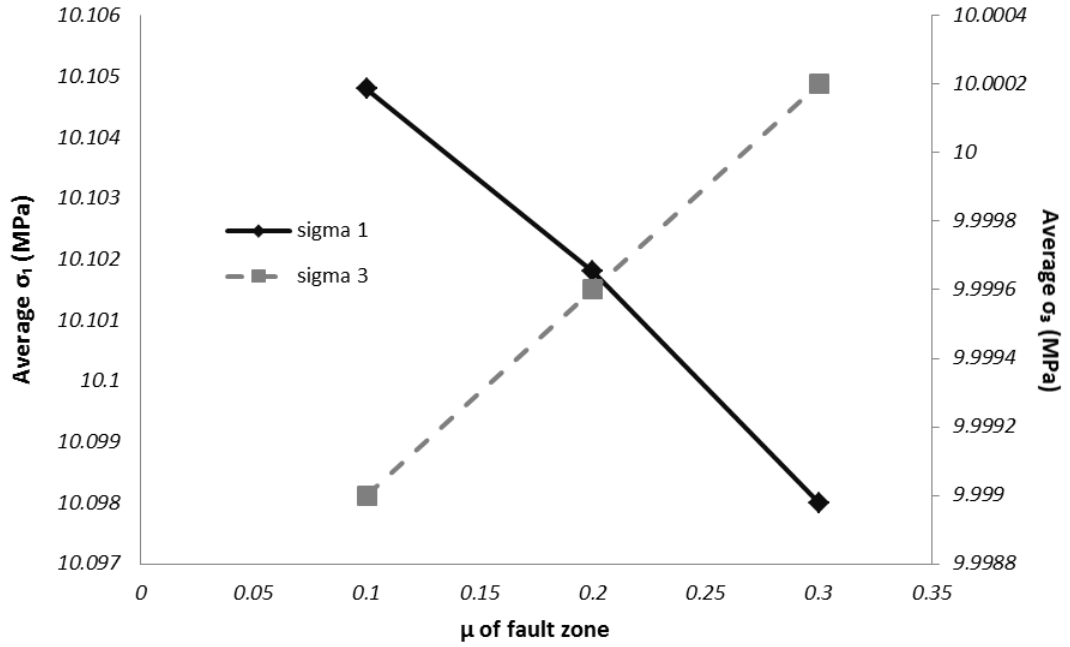
Figure 2-22 Changes in σ_1 and σ_3 with μ_F (an average of maximum values of σ_1 and σ_3 for each set of element numbers were used)
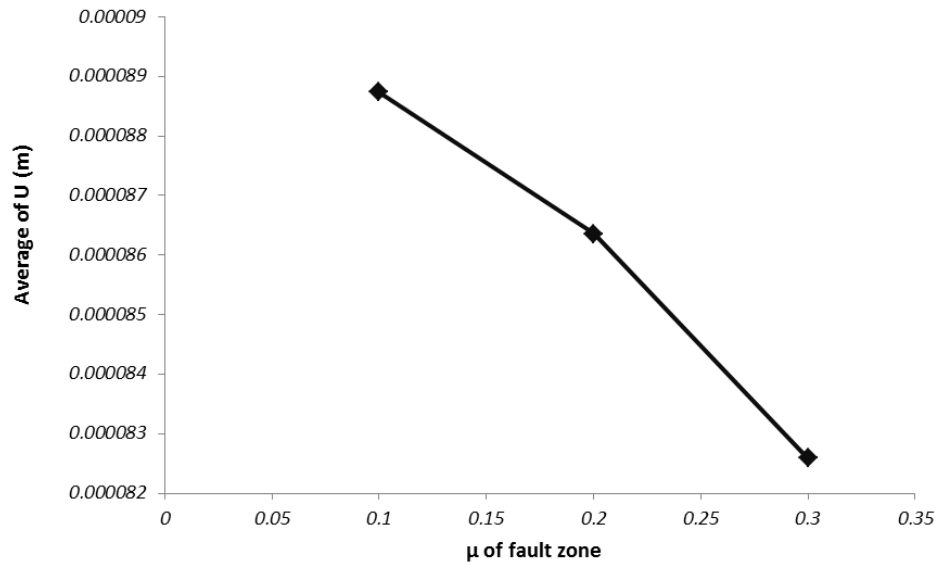
Figure 2-23 Changes in U with μ_F (an average of maximum values of U for each set of element numbers were used)

In the second round another method (mesh refinement) of mesh generations was applied for these analyses. Although only the mesh generation method is changed, as the mesh density increases σ_3 increases as well. The result of analysis for σ_1 and U was the same as the other mesh generation methods. Also, for this mesh generation method as μ_F changes, σ_1, σ_3, and U show almost the same variations as the other method.

b) $\mu_R < \mu_F$

While μ_F is constant and equal to 0.4 and E is 20000 (MPa) all the analyses were repeated twice with the two different mesh generation methods.

The first set of analysis was carried out with uniform mesh and changing the number of elements in whole model. By augmenting number of elements σ_1 and σ_3 show an increase and U was constant. The same result as the model in which $\mu_R > \mu_F$ is achieved for this set of analysis.

Then mesh refinement method was applied and results were compared to the first method of mesh generation. Changes of σ_1, σ_3, and U by increasing mesh density were as same as the first method. Also as Poisson's ratio increased σ_1, σ_3, and U followed same trend as in the first method of mesh generation.

2.2 *Model with excavation:*

The previous model is used with an excavation; the model consists of two different types of material (different E and μ) for a rock mass and fault zone, and an excavation located in a rock mass adjacent to the fault zone in the foot wall region. This scenario depicts a common approach in mining where an approach drift is excavated near an ore body. The model's geometric details are illustrated in the figure 2-24.
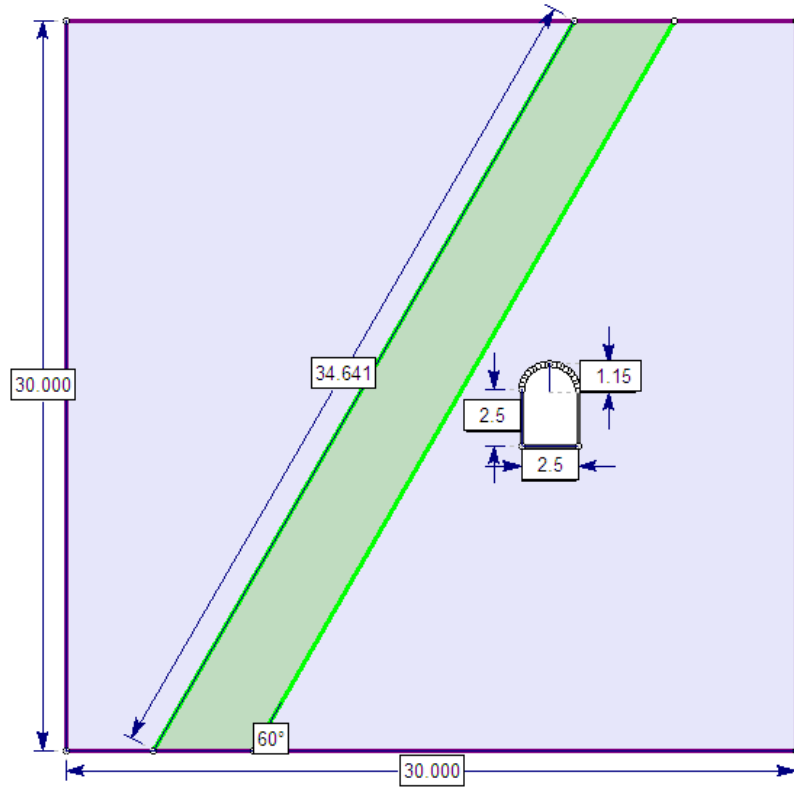
Figure 2-24 The geometry of model with an excavation (the units are meters)

The material properties are the same as the first model, which is summarized in table 2-2. Similarly the model is subjected to the same *in-situ* field stresses, Young's modulus, and Poisson's ratio as the first model along with all analysis assumptions. The only difference is that for the second model, due to the existence of an excavation, for plotting changes in stresses and displacement, two lines were selected, one longitudinal line adjacent to top of the excavation and the other one a diagonal line which covers the excavated area. The longitudinal line was located at the top of the excavation as long as the highest σ_1 values concentrates near the roof of the excavation and also this line contains the highest value of σ_3 as well, which is located in the left portion of the model. Another reason to choose a diagonal line is to show the highest variation in U. (figure 2-25)
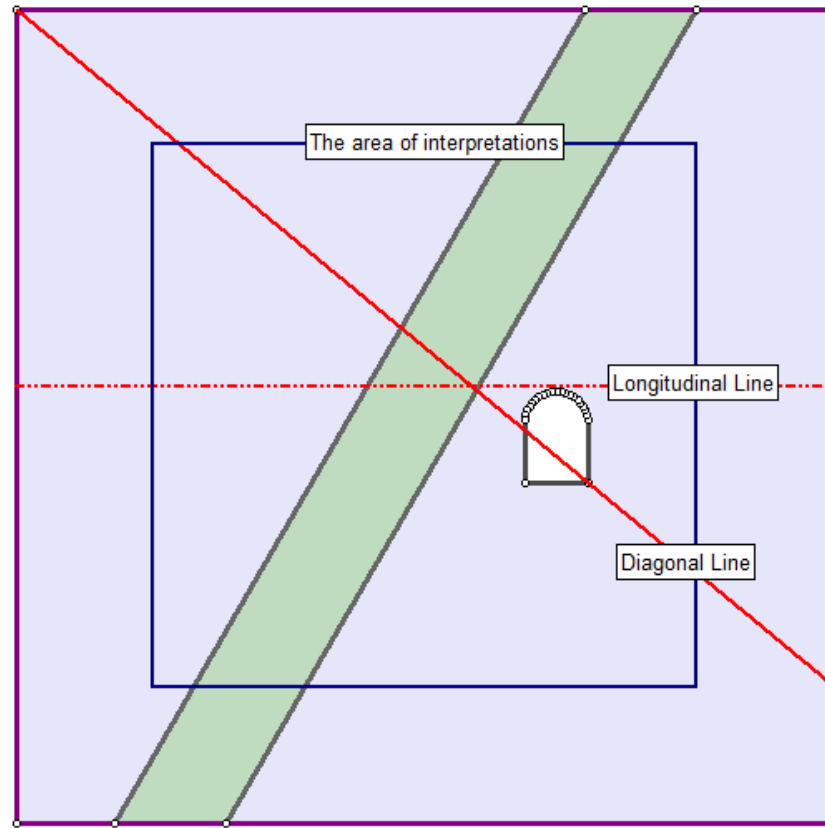
Figure 2-25 - The interpretation of analysis lines and area

Similar to the first model, analysis results were interpreted with respect to the values inside the area, which is illustrated in figure 2-25, due to having more accurate results and avoiding the errors caused by closeness of boundaries.

The same mesh generation methods were used for the model with excavation, as detailed previously.

The effect of the number of elements on the stress and displacement analysis, and the effect of the Young's modulus and Poisson's ratio where both analyzed.

2.2.1 μ is constant and E is changing

a) $E_R > E_F$

Figures 2-26 and 2-27 show that by increasing the number of elements σ_1, and U increases; however σ_3 decreases.
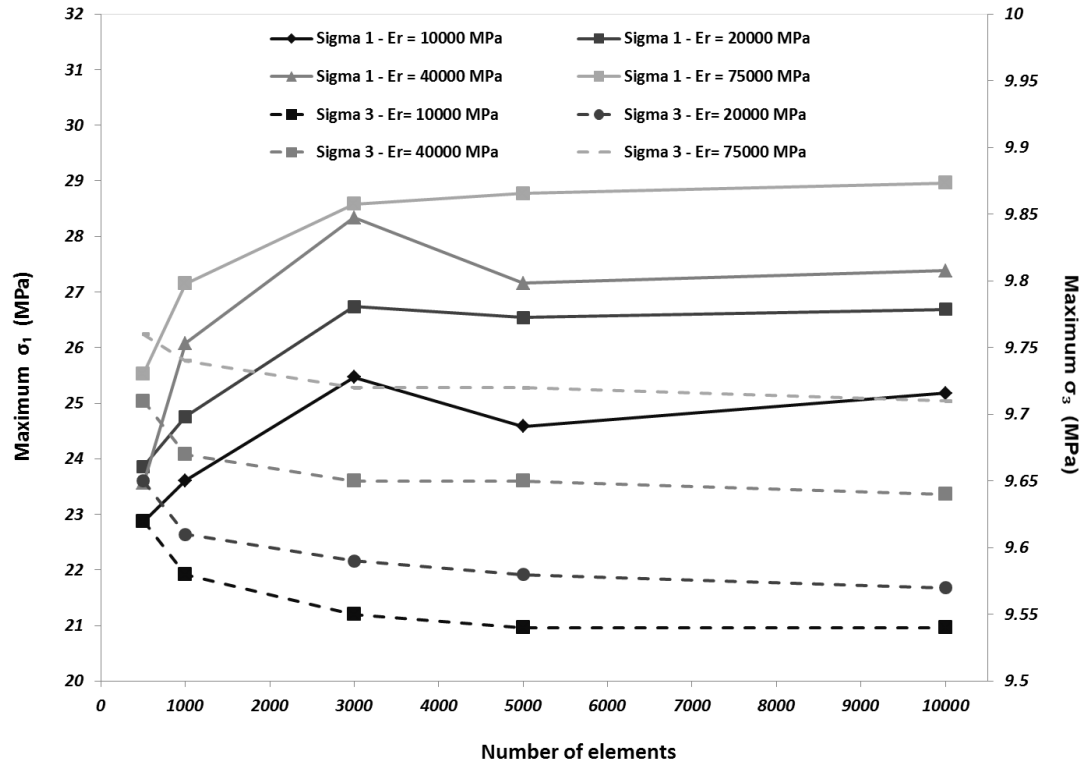
Figure 2-26 Changes of maximum σ_1 (solid lines) and maximum σ_3 (dashed lines) as the number of elements increases for different E_R

Figures 2-28 and 2-29 show that by increasing E_R/E_F , σ_1 and σ_3 both increase and U decreases. The result is as same as the first model (model without excavation).

58
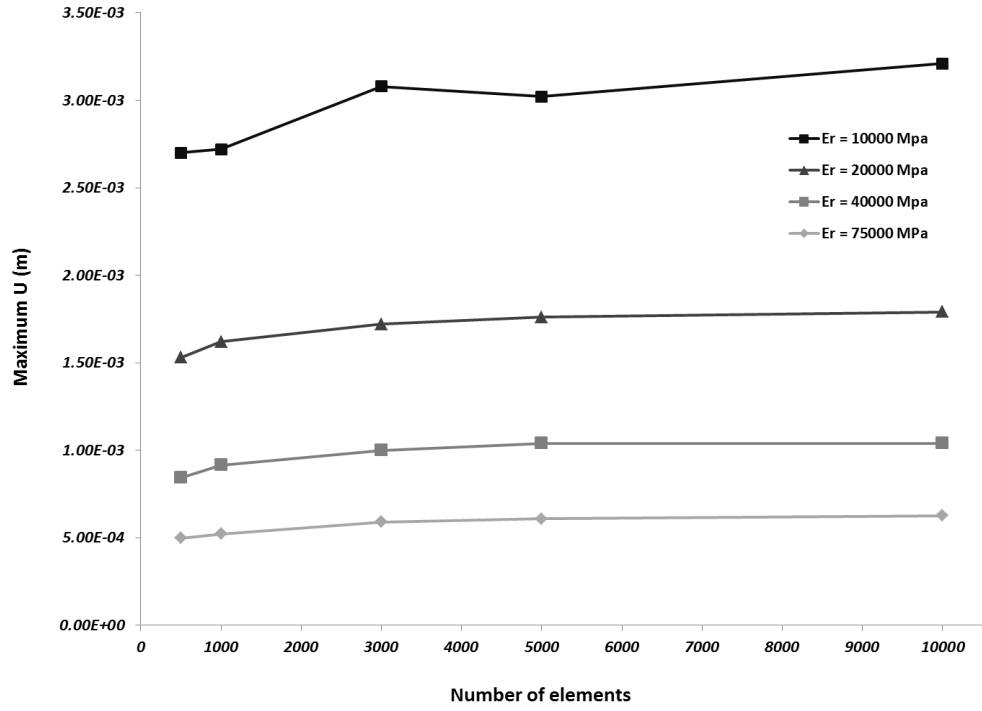
Figure 2-27 Changes of maximum U as the number of elements increases for different E_R
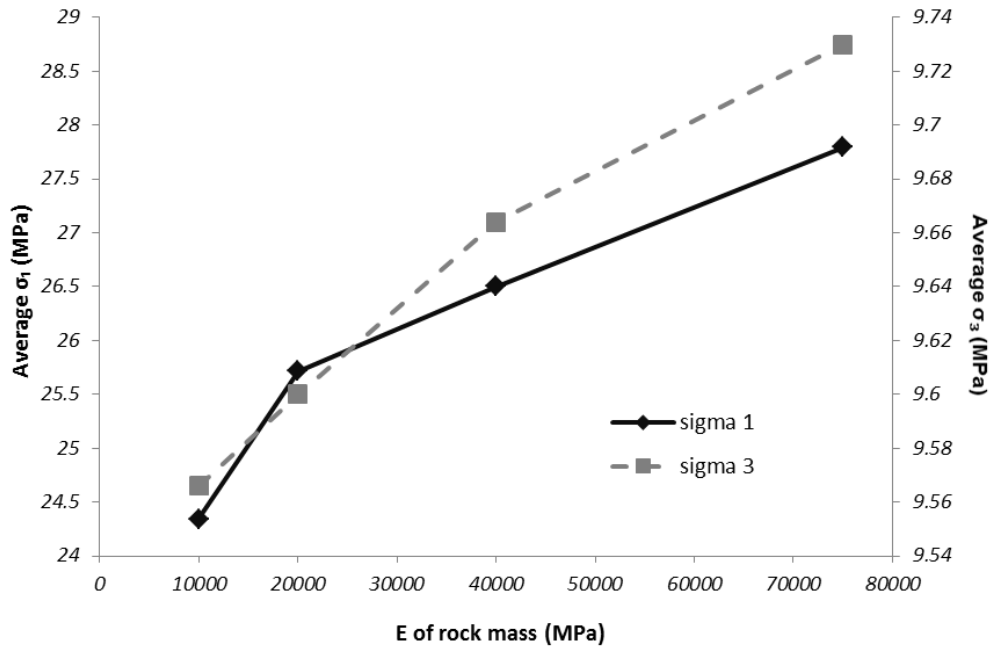
Figure 2-28 Changes in σ_1 and σ_3 with E_R (an average of maximum values of σ_1 and σ_3 for each set of element numbers were used)
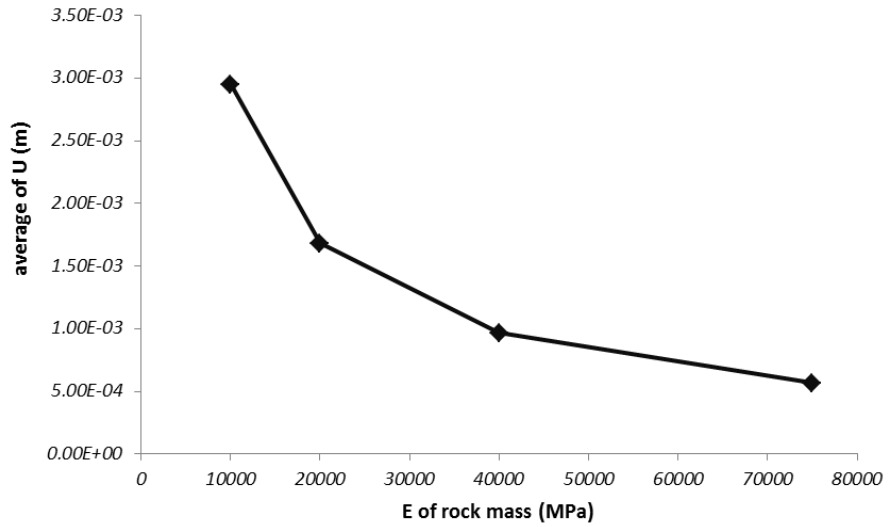
Figure 2-29 Changes in U with E_R (the average of maximum values of U for each set of element numbers were used)

For the second method of mesh generation, mesh refinement was applied in a specific area which is shown on figure 2-30. The result of the analysis, are shown in the figures2-31–2-34.
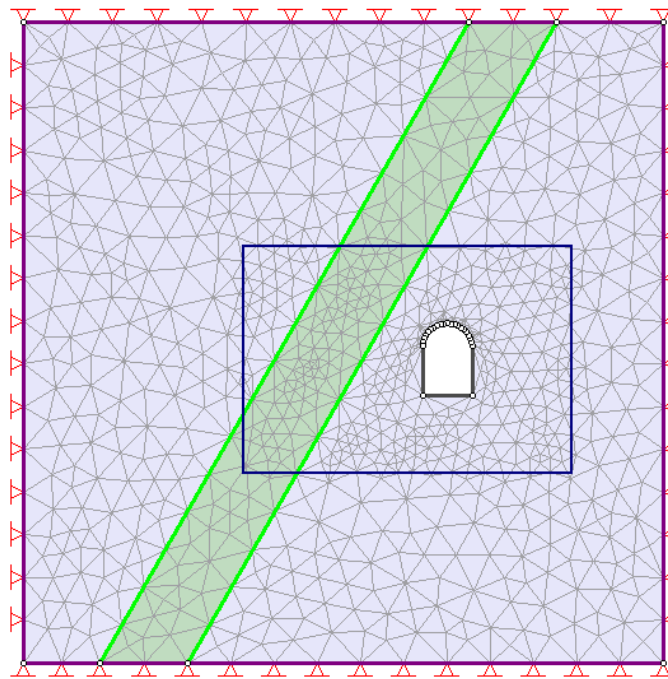
Figure 2-30 - Application of uniform coarse mesh which is refined once in a specific area around an excavation
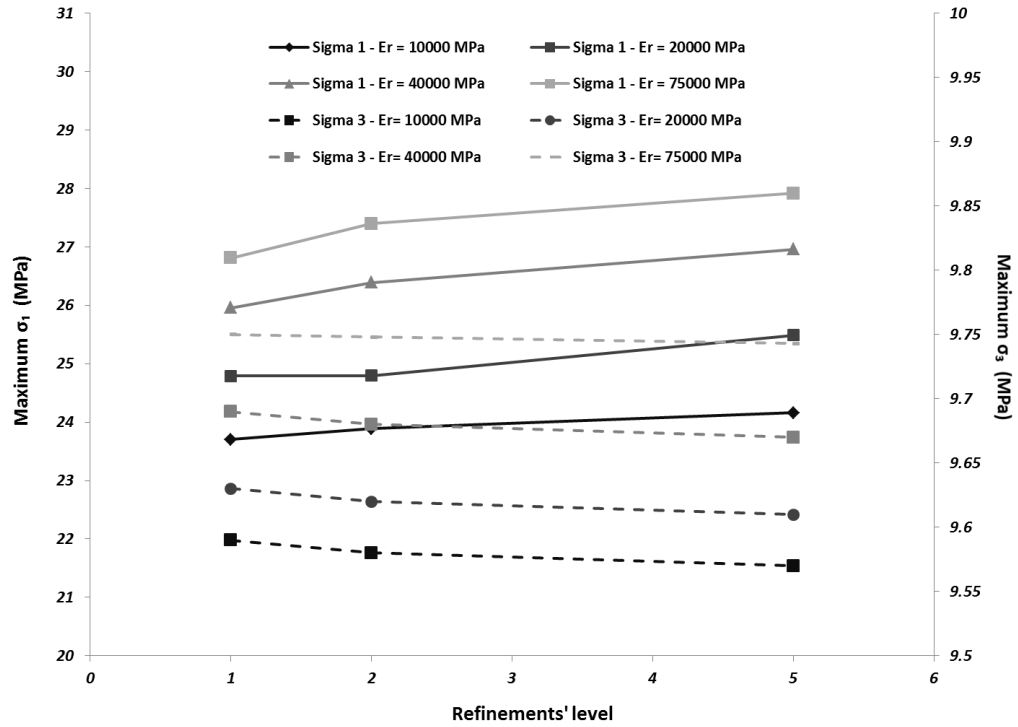
Figure 2-31 Changes of maximum σ_1 (solid lines) and maximum σ_3 (dashed lines) with refinement level for different E_R
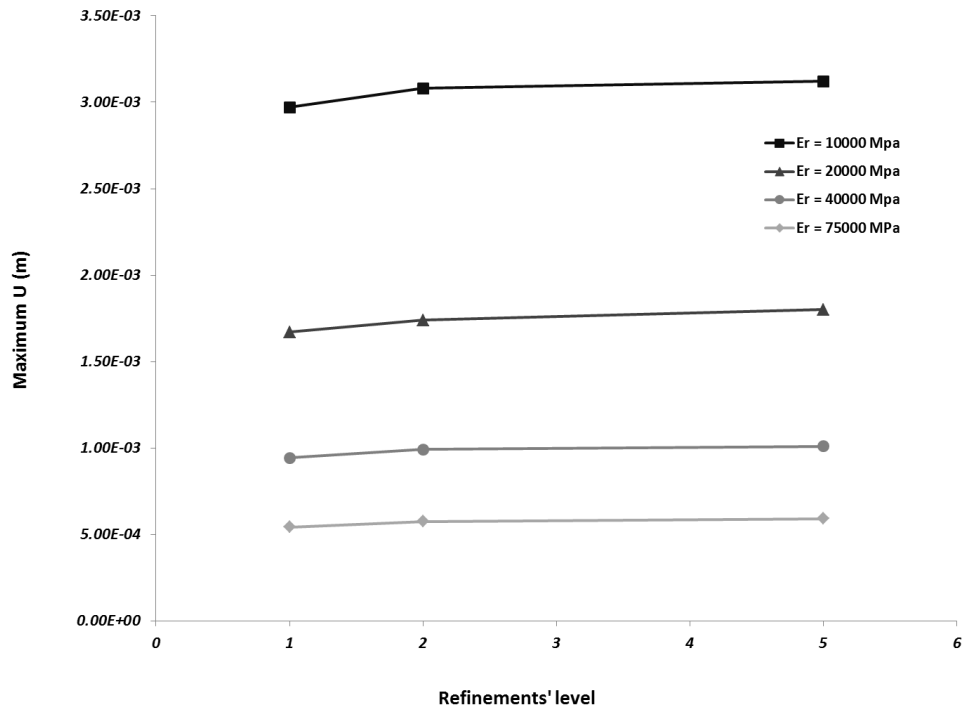
Figure 2-32 Changes of maximum displacement U with refinement level for different E_R

61
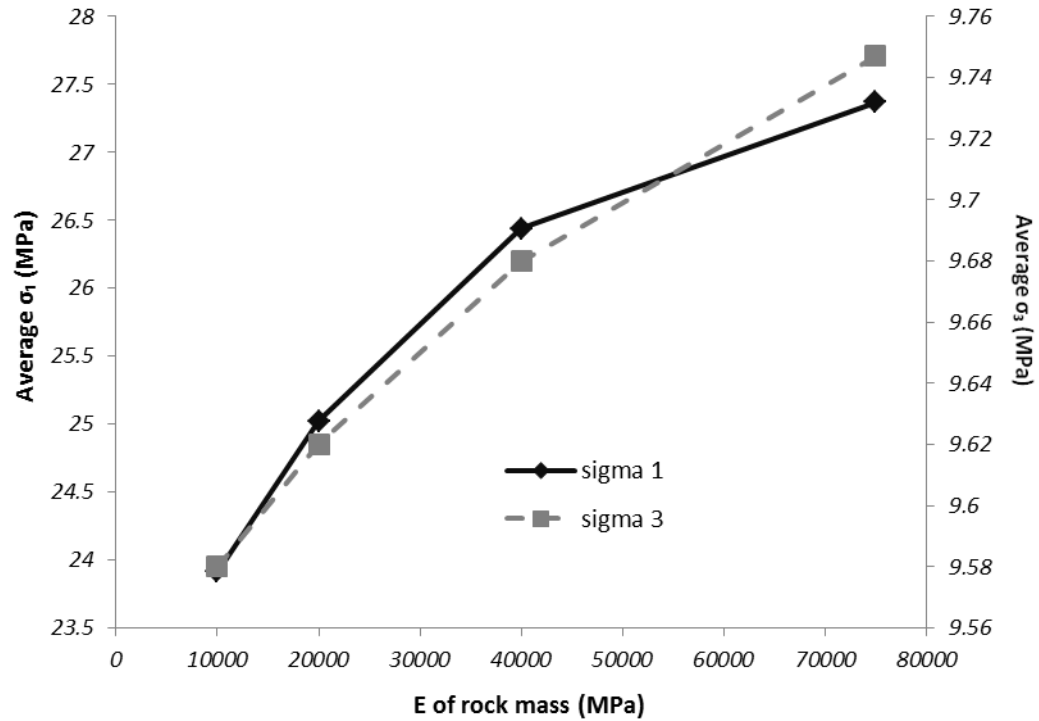
Figure 2-33 Changes in σ_1 and σ_3 with E_R (an average of maximum values of σ_1 and σ_3 for each set of element numbers were used)
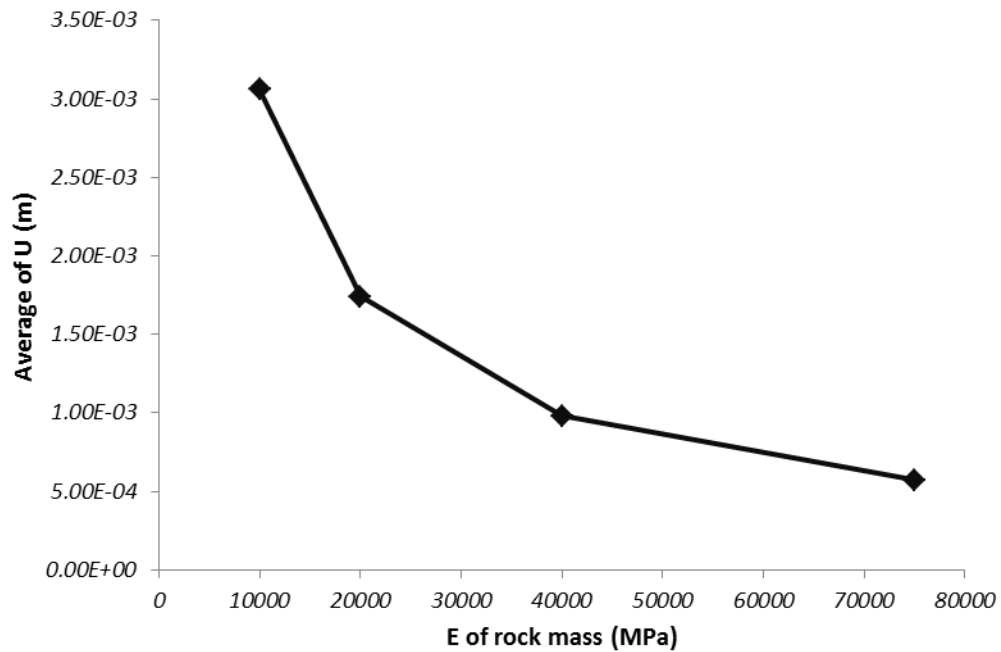
Figure 2-34 Changes in U with E_R (the average of maximum values of U for each set of element numbers were used)

The results are similar to the first method of mesh generation; σ_1 and U increase as the number of elements and the density of mesh increases in the selected area and σ_3 will decrease; however comparing with results of the first method of mesh generation, changes in stresses and displacements with number of elements are slighter.

From figures 2-33 and 2-34 it can be seen that as the young's modulus of rock mass increases σ_1 and σ_3 increase as well, while U shows a decline.

b) $E_F > E_R$

Once again as the number of elements increases, maximum σ_1 and U increase as well; however the increase occurs with a different trend. For U this trend is even different from one E_F to another one. σ_3 decreases as the number of elements increases. For this set of analysis as the ratio of E_R and E_F decline, σ_1 and U decreases; while σ_3 increases.

Stress and displacement analysis results for the second method of mesh generation were generally the same as the first one; as the refinement level increases, σ_1 and U increase and σ_3 decreases. Also changes of the maximum of σ_1 , σ_3, and U with E_F are as same as the first method.

2.2.2 E is constant and μ is changing

a) $\mu_R > \mu_F$

As like as the first model after analyzing the effect of Young's modulus, the effect of Poisson's ratio was considered. For the first set it can be concluded that σ_1 and U increase as the number of elements increases, while σ_3 decreases.

Stress and displacement changes with changes in the Poisson's ratio, was also studied. It was proved that σ_1 and U are in direct relation to μ_F, on the contrary σ_3 decreases as μ_F increases.

As the method of mesh generation changes, the result of the analysis for σ_1 changes as well. In the mesh refinement method, increasing the number of elements and density results in a decrease of σ_1. The result for σ_3 and U were the same.

Comparing the changes in σ_1, σ_3, and U with respect to μ_F, it can be concluded that σ_3 follows a different trend for this method and by increasing μ_F, increases.

b) $\mu_R < \mu_F$

The analysis result are almost the same as the situation where $\mu_R > \mu_F$; an increase in number of elements increased σ_1 and U, and decreased σ_3. Changes in Poisson's ratio have the same effect on stresses and displacement.

For this set of analysis as well two methods of mesh generation were used. The results of the second method (mesh refinement method) are substantially the same as for first one. However, the characteristics of changes in σ_1 with μ_R is different from the first method of mesh generation, in fact it is completely opposite of the first method; while changes in σ_3 and U are the same.

2.3 Discussion

All the above mentioned analysis had been carried out to determine the effect of Young's modulus and Poisson's ratio on the analysis results as the number or the density of elements is changing. In previous sections the effect of Young's modulus and Poisson's ratio has been analyzed in detail and the results of the analysis for two different methods of mesh

generations have been compared. However between Young's modulus and Poisson's ratio, one has more significant effect on stresses and displacement analysis. To compare these two rock properties, the ratio of the two different Young's modulus and Poisson's ratio for fault zone and rock mass has been considered. To clarify the comparison, for each ratio the maximum and minimum of it were compared. The ratio of E_R/E_F has its maximum value for a case that E_R is equal to 75000 MPa, and E_F is equal to 5000 MPa, and its minimum when it's on the contrary. The ratio of μ_R/μ_F is maximum when μ_R is equal to 0.4 and μ_F is equal to 0.1 and it is minimum when $\mu_R = 0.1$ and $\mu_F = 0.4$.
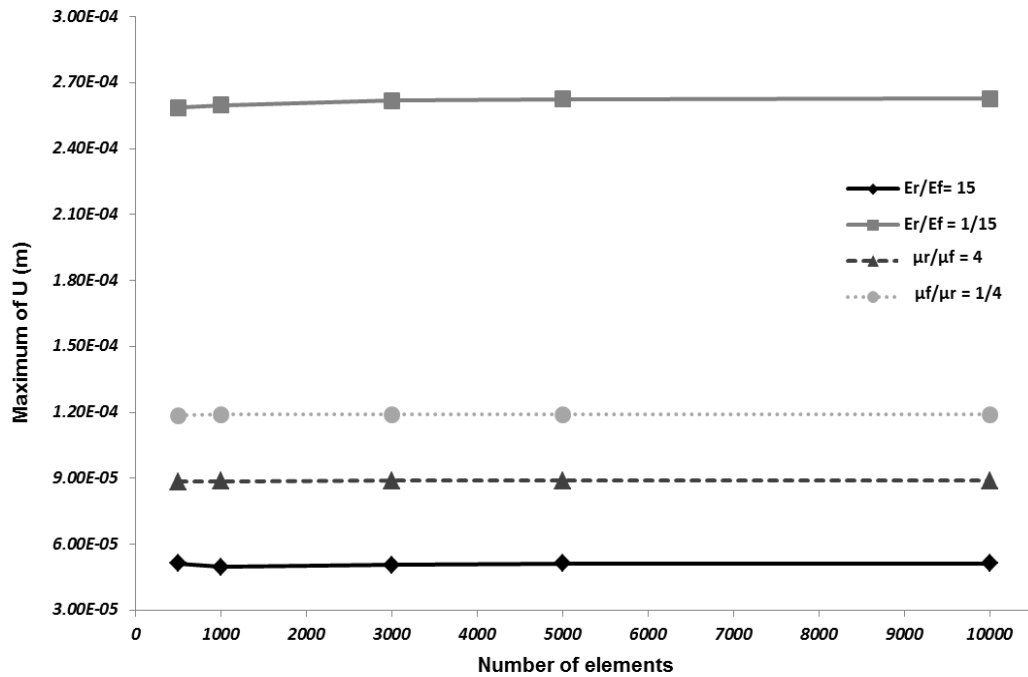
Figure 2-35 Changes of total displacement with different ratio off Young's modulus and Poisson's ratio by increasing the number of elements

Figures 2-35 and 2-36 illustrate the comparison of Young's modulus and Poisson's ratio regarding changes in total displacement and stresses, respectively.

65

From figure 2-35 it can be illustrated that as the number of elements increases changes in total displacement is almost constant; however these changes for maximum and minimum of E_R/E_F is more significant than for maximum and minimum of μ_R/μ_F.
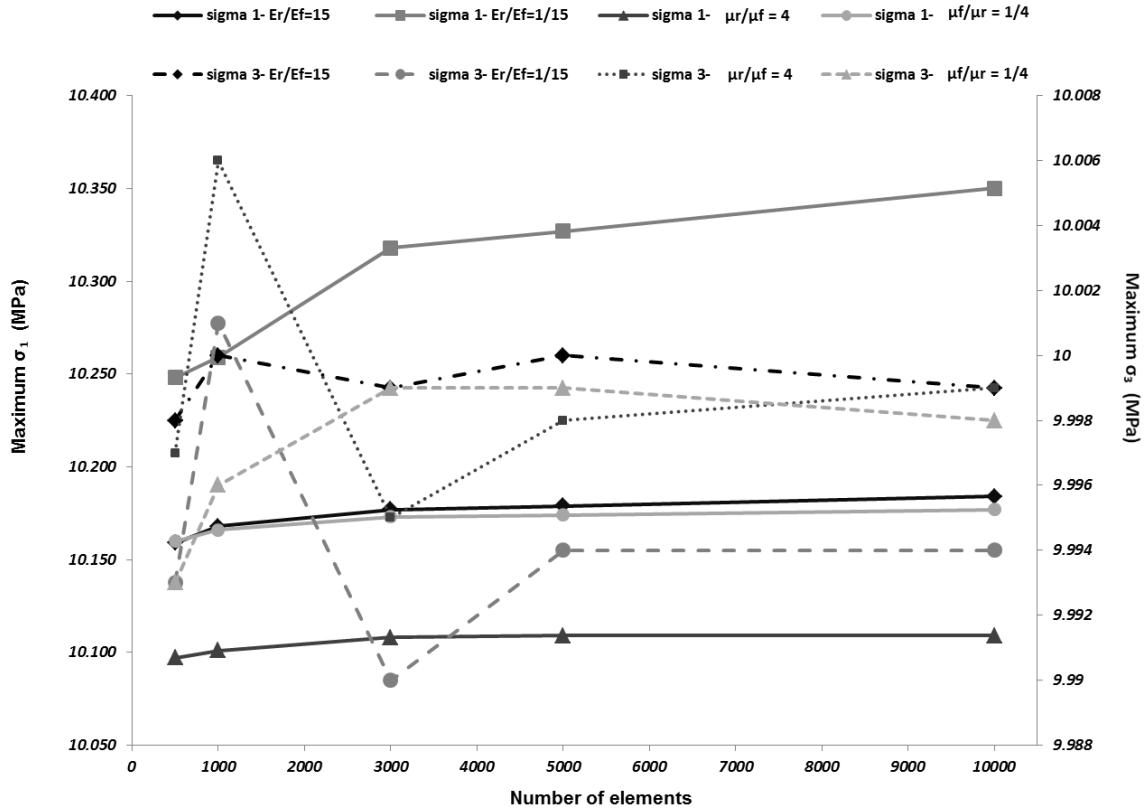
Figure 2-36 Changes of principle stresses with different ratio of Young's modulus and Poisson's ratio by increasing the number of elements

For σ_1 as like as U, changes with the ratio of Young's modulus are more noticeable than the ratio of Poisson's ratio (figure 2-36). Although, it is hard to compare the changes in σ_3 for E_R/E_F and μ_R/μ_F from figure 2-36, these changes are more obvious for changes in E_R/E_F.

To summarize all the above analysis results and discussions of results, it can be concluded that, changes in σ_1, σ_3, and U in a case that Young's modulus is changing does not

vary for the two different methods of mesh generations, and changes have a direct relation with the ratio of E_R to E_F (E_R/E_F); however stresses and displacement do not show reliable relation with Poisson's ratio. Due to the result of analysis for both Young's modulus and Poisson's ratio, the relation between the mesh generation method or mesh density and number of elements with Poisson's ratio may depend on other properties or conditions. Therefore to find out a new cost function for mesh simplification only the effect of the Young's modulus will be considered; the ratio of E_1 (higher) and E_2 (smaller).

CHAPTER THREE

3. EXPANDED COST FUNCTION AND ITS APPLICATION

3.1 Expanded cost function

The cost function and the mesh simplification operates with respect to a region of interest (ROI). This region is an area or a point at which the effect of the excavation or geological features on stresses will be studied (Zsáki & Curran, 2005). The closer the excavations or geological inclusions are, to the ROI, the more effective they are, on the stress perturbation. Regarding this concept vertices nearer to the ROI are more important for stress analysis than the ones farther away. Therefore, to apply the cost function it is essential to have an area or a point considering as ROI.

The previous cost function consists of three different costs (geometry, proximity, and visibility) multiplied by their weights, the values which indicate their level of importance in the calculations (Zsáki & Curran, 2005). The new cost function will have one more cost which is a cost based on Young's modulus.

As it has been indicated in a previous chapter, stress and displacement changes have the relation with the ratio of E_R to E_F (E_R/E_F). Likewise, the cost function of the Young's modulus is anticipated to have the same relation.

$C_{young's\ modulus}$ or C_{ym} illustrates the cost of removing a vertex due to difference between Young's modulus of the difference material existing near that vertex. Therefore, for different materials with different E, the cost function is as follow:

$$C_{ym} = 1 - \frac{E_2/E_1}{E_{max}/E_{min}} \tag{1}$$

In which:

C_{ym}= Cost of removing a vertex regarding Young's Modulus

69

E_1 = maximum E between the E's around the vertex

E_2= minimum E between the E's around the vertex

E_{max}= the maximum E of the whole area of study

E_{min}= the minimum E of the whole area of study

Therefore the new cost function is proposed:

$$C = C_g.W_g + C_P.W_P + C_V.W_V + C_{Ym}.W_{Ym} \tag{2}$$

In the first try W_g, W_P, W_V, and W_{Ym} are assumed to have the values of 1, 0.5, 0.5, and 0.5, respectively (Zsáki & Curran, 2005).

The costs of geometry, proximity, and visibility were calculated from the equations introduced by Zsaki and Curran (2005), equations (3), (4), and (5), respectively.

$$C_{geometry} = l^2/L^2 \tag{3}$$

As it can be seen in figure 3-1(a), L is a chord length between two vertices adjacent to the selected vertex, and l is distance between the chord and the vertex (Zsáki & Curran, 2005).

The cost of proximity can be calculated from equation (4):

$$C_{proximity} = \frac{d-d_{min}}{d_{max}-d_{min}} \tag{4}$$

In which d is the distance between the vertex and the ROI, and d_{max} and d_{min} are the distances between the furthest and the nearest vertices to the ROI (Zsáki & Curran, 2005) (figure 3-1(b)).

To calculate the cost of visibility equation (5) should be considered:

$$C_{visibility} = \frac{\alpha - \alpha_{min}}{\alpha_{max} - \alpha_{min}} \qquad (5)$$

Where α is the angle between averaged normal at the vertex and the vector pointing from the vertex to the ROI, α_{max} and α_{min} are the largest and the smallest angles (Zsáki & Curran, 2005). Figure 3-1 (c) illustrates the angles.
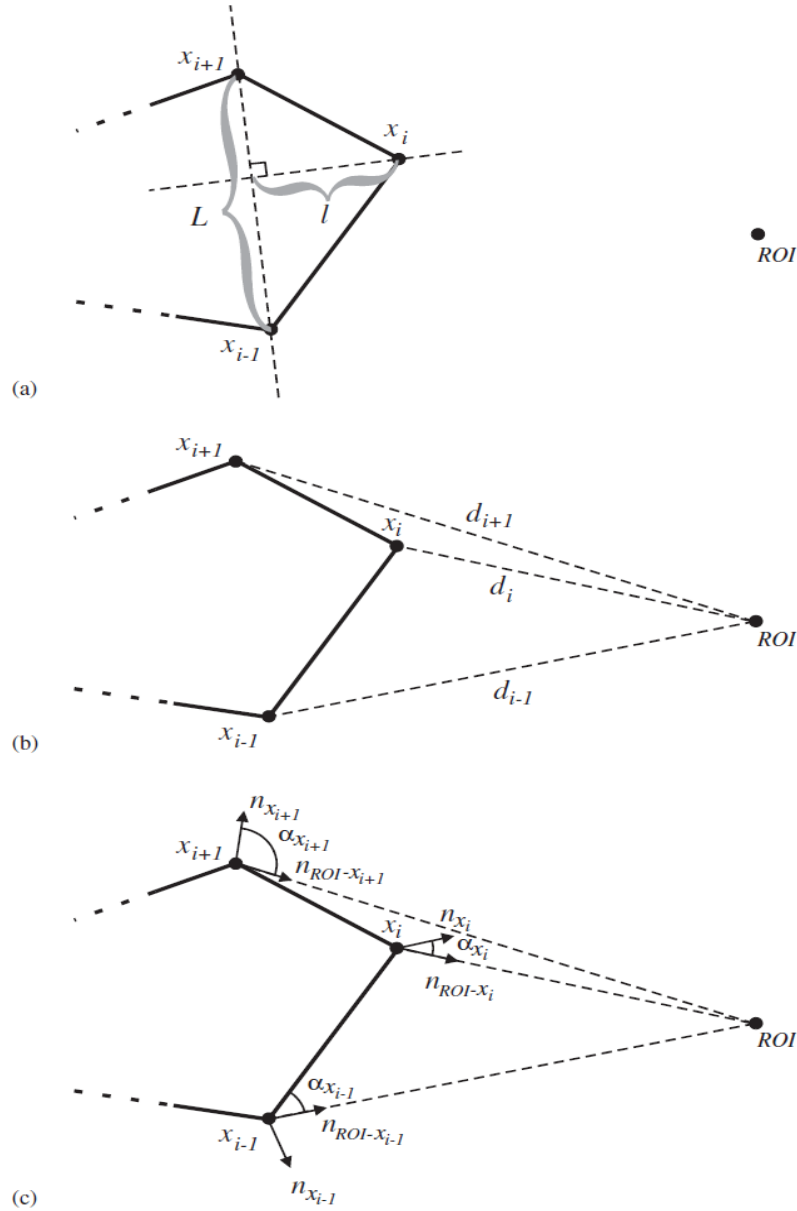
Figure 3-1 (a) geometry cost (b) proximity cost (c) visibility cost (Zsáki & Curran, 2005)

3.2 Application of the new cost function

Mesh optimization function first applied to the simplest model, a model with two different materials. E_R and E_F are 5000 MPa and 75000 MPa, respectively. The number of elements for this model is 1000, and there are 128 vertices on the boundaries, and each vertex is signified by a number which is given to the vertex by software. ROI is assumed to be a point near the fault zone with coordinates of (-0.08, -6.021) which is illustrated in figure 3-2.
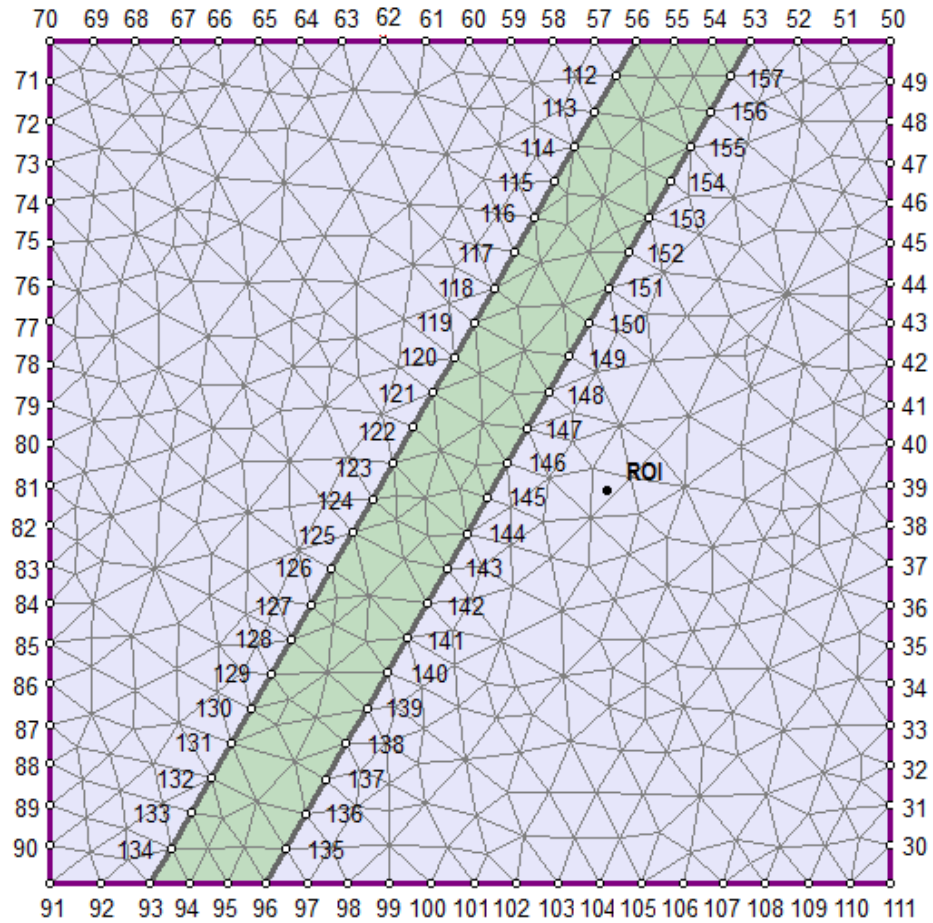
Figure 3-2 The original model which illustrates the vertices numbers and the location of the ROI

To simplify the mesh, cost function should be calculated for all of the vertices. In each round one vertex which has the least cost is removed and calculations of cost will be repeated. Figures 3-3 and 3-4, show the model after removing 20 and 40 vertices, respectively.

Figure 3-3 shows that almost all the removed vertices are located in the left boundary; however it seems that there are other vertices that have the less effect on the analysis at ROI than some of the vertices that have been removed. For instant, vertex number 69 or 92 could have the less cost than the vertex number 80 which has been removed on the third round.
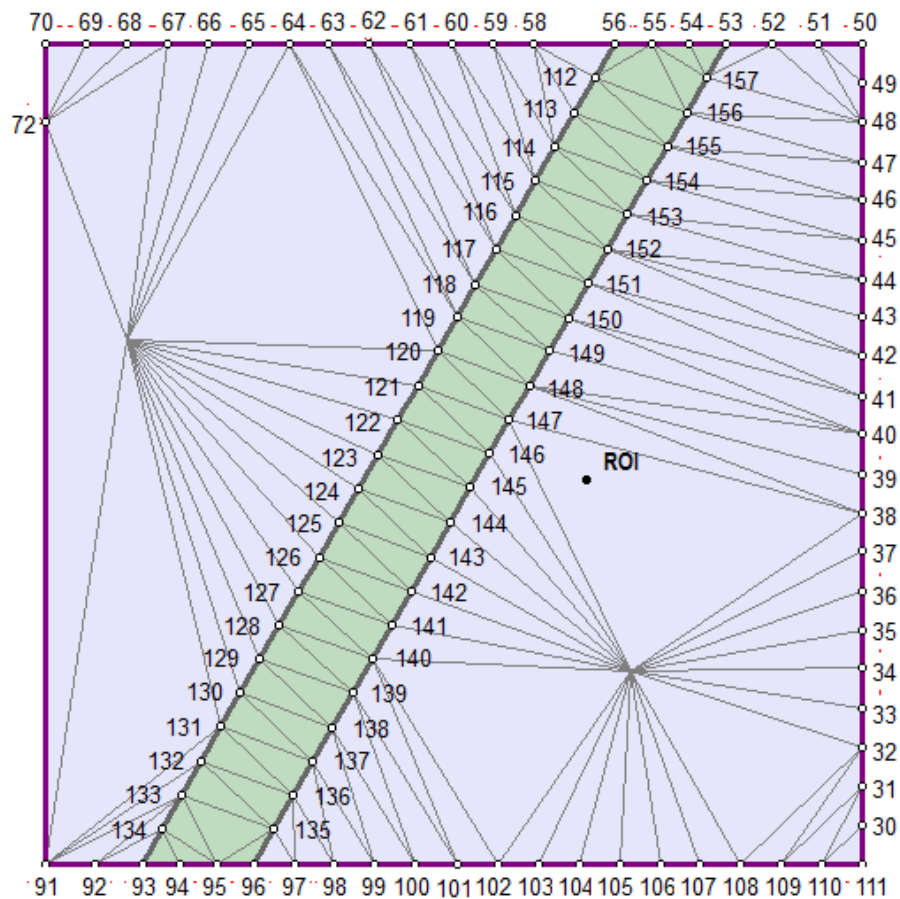
Figure 3-3 Model after removing 20 vertices

From figure 3-4 the same result can be concluded, that even after removing 20 more vertices the vertices that seems to have the less effect on the analysis still were not removed. The problem could be caused by the values that have been given to the weights related to each cost. After considering all the costs, and evaluating the model, it can be concluded that considering W_V equal to 0.5 gives more value to the visibility cost which does not seem as effective as the proximity cost for this model. Therefore to get the better result of the simplification and to have the more homogenous mesh W_V was assumed to be equal to 0.3. Calculation repeated for the new W_V value, and new results were achieved (figures 3-5).
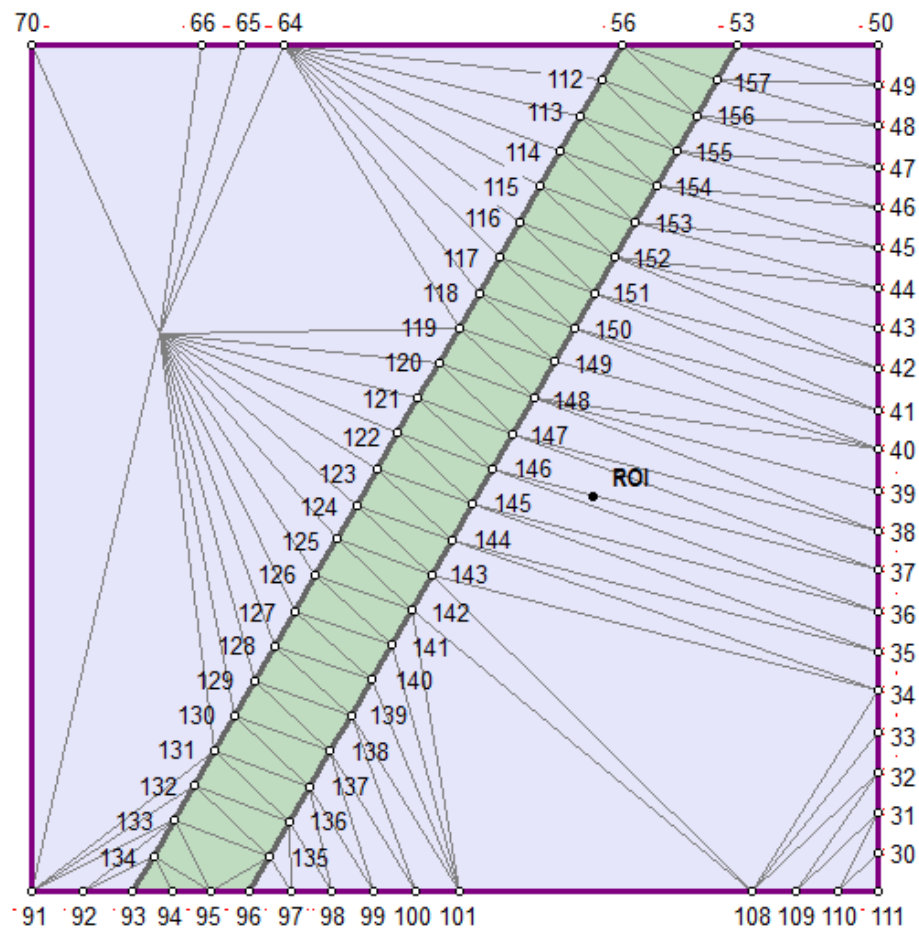
Figure 3-4 Model after removing 40 vertices

74

Although after changing W_V, vertices seems to be removed in a correct order, still the simplified model is not homogenous and uniform (figures 3-5). The length of elements in some areas is too large to give an acceptable mesh generation, for instance, the distance between vertices numbered 70 and 62 in figure 3-5. A uniform mesh is necessary to have an accurate analysis. This problem cannot be solved by changing the weight values only.
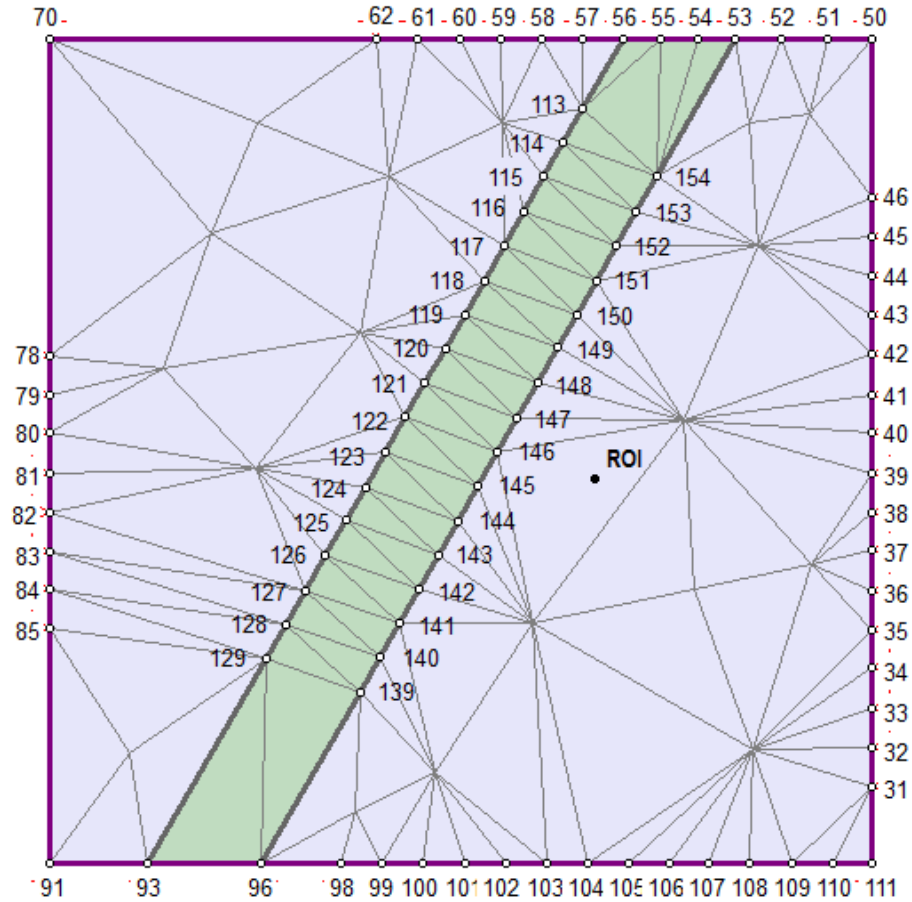
Figure 3-5 New simplified model with W_V equal to 0.3, after removing 40 vertices

To get a reasonable result from mesh optimization process, it is essential to introduce another cost. This new cost will control the distance between two adjacent vertices. This distance should not exceed a significant number. The number will be chosen, by trial and error method and it will represent the uniformity of the generated mesh after

removing each vertex. The cost as well will have a weight value which will be chosen depending on the effect of the cost on the calculation and simplification process.

The new cost will be entitled uniformity cost. As it has been said, uniformity cost depends on the distance between two consecutive vertices which should not exceed constant a (uniformity constant). Uniformity cost can be calculated from the following function:

If $D_1 > a$ or $D_2 > a$ then $C_{uniformity} = \max\left(\frac{D_1}{a}, \frac{D_2}{a}\right)$ (6)

In which D_1 and D_2 are the distances between two adjacent vertices to the vertex. The equation also shows that if neither D_1 nor D_2 were bigger than a, $C_{uniformity}$ is equal to zero.

Constant a (uniformity constant) is a coefficient of an element edge length in uniform mesh where all of elements have the same length. Practically uniform mesh has been rarely used in analysis; the common meshing method is graded mesh in which the mesh density is varies for different part of the model, therefore uniformity cost should be determined from another equation in which uniformity constant should be replaced by an equation of maximum and minimum element edge length and the distance between a vertex and ROI. For graded mesh a is variable and equal to:

$a = |d - (D_{max} - D_{\min})|$ (7)

In the above equation a is uniformity variable, d is the distance between a vertex and ROI, D_{max} and D_{min} are maximum and minimum lengths of elements, respectively. Uniformity cost for graded mesh is calculated from the same equation (6) as for uniform mesh the only difference is in the a values.

Consequently, the new cost function is:

$$C = C_g.W_g + C_P.W_P + C_V.W_V + C_{Ym}.W_{Ym} + C_U.W_U \qquad (8)$$

W_U is assumed to be equal to 0.5 for the model. Also since the uniform mesh was used for the analysis a is considered to be constant and equal to the distance between two vertices in the original model multiplied by two, which is equal to 3 (average element edge length is 1.5 for the model). The simplification result after removing 40 vertices can be found in figure 3-6.
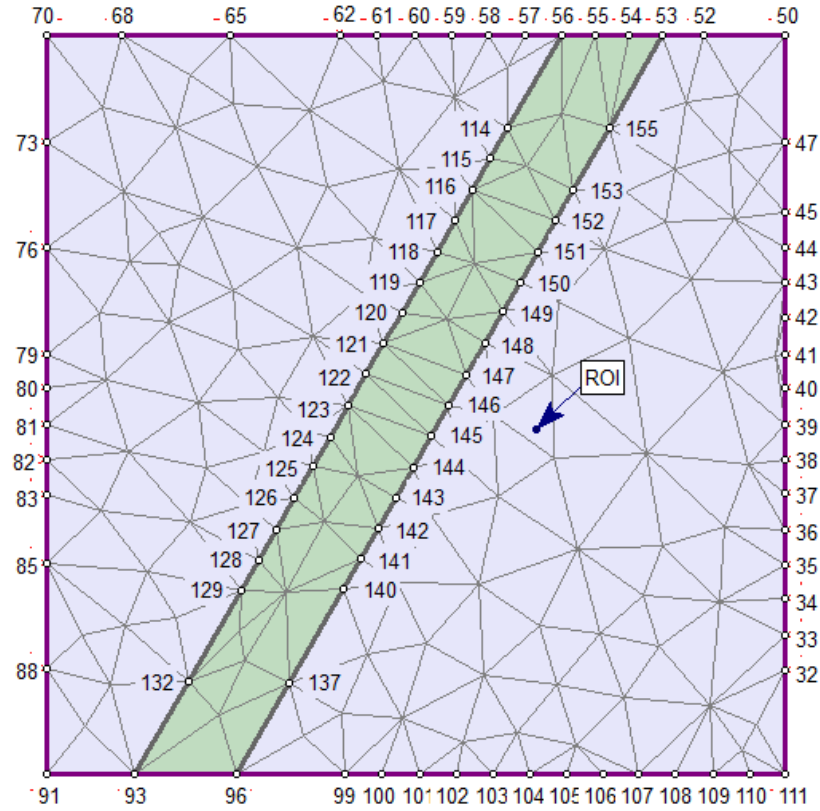
Figure 3-6 Simplified model with W_V equal to 0.3 and C_U (a = 3), after removing 40 vertices

The simplification also checked with $\boldsymbol{W_U}$ = 0.3; however results did not show a dramatic change, and it only indicated that $\boldsymbol{W_U}$ = 0.5 was an acceptable value to be chosen.

Figures 3-6 illustrates a considerable change in simplification process. It can be seen that, even after removing 40 vertices, mesh quality is acceptable.

To be certain that the value of *a* is acceptable, another value have been tried, *a*=4.5 (when *a* is equal to the element edge length multiplied by three), the result of which was as satisfactory as the first try (figure 3-7).
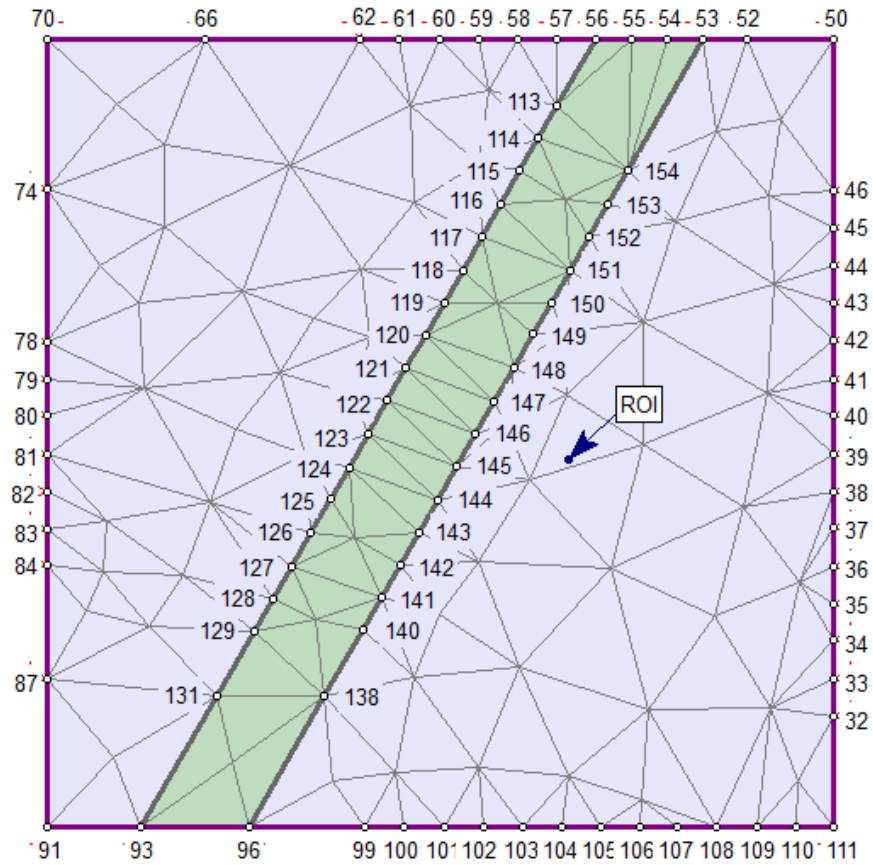
Figure 3-7 Simplified model with W_V = 0.3 and C_U (*a* = 4.5), after removing 40 vertices

As it has been discussed, figure 3-7 illustrates that the mesh generation with new *a* value (*a*=4.5) is also acceptable, and mesh generation quality is as good as the first try. The only way to choose between the two values is to compare the result of the principal stresses and displacement analysis.
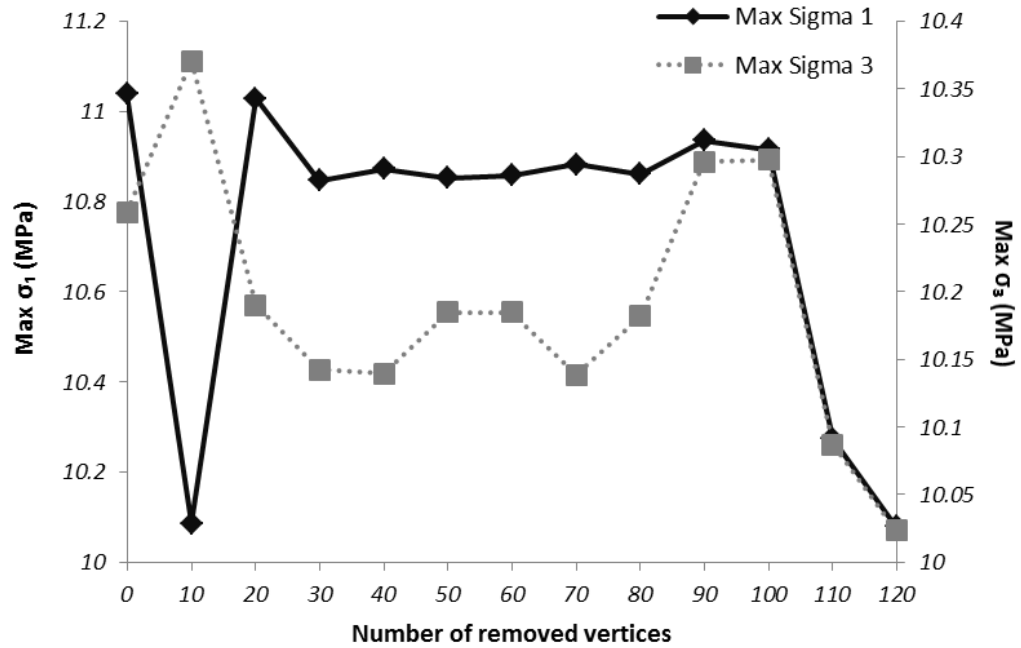
Figure 3-8 Changes in maximum σ_1 and maximum σ_3 as the number of removed vertices increases where $a=3$
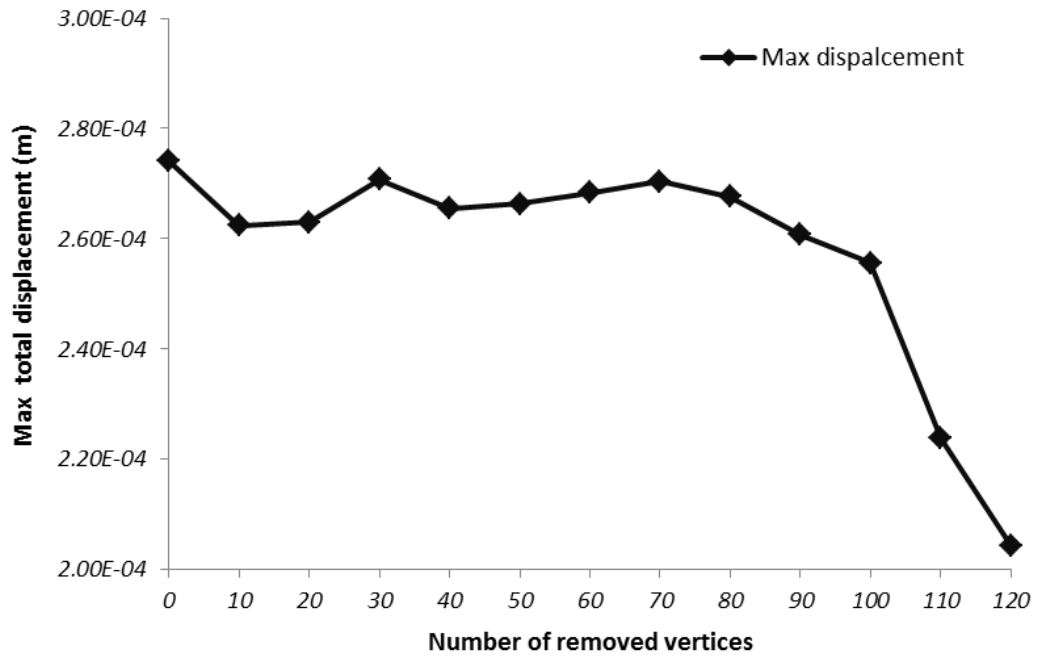
Figure 3-9 Changes in U as the number of removed vertices increases where $a=3$

To choose the best value for a the stresses and displacement results have been considered. Therefore, after removing each set of ten vertices maximum σ_1, σ_3, and U was determined. Figures 3-8 – 3-11 illustrate changes in stresses and displacements after removing 10, 20, 30, ..., and 110 vertices. Comparing figures 3-8 and 3-9 to 3-10 and 3-11, respectively, it can be concluded that $a=4.5$ is the better assumption than $a=3$. Figures 3-10 and 3-11 have less fluctuations comparing with figures 3-8 and 3-9. Therefore, vertex removal is more uniform where a is equal to 4.5.

As it has been concluded, for further calculations a will be assumed equal to 4.5 as it shows more uniform mesh during vertex removal process.
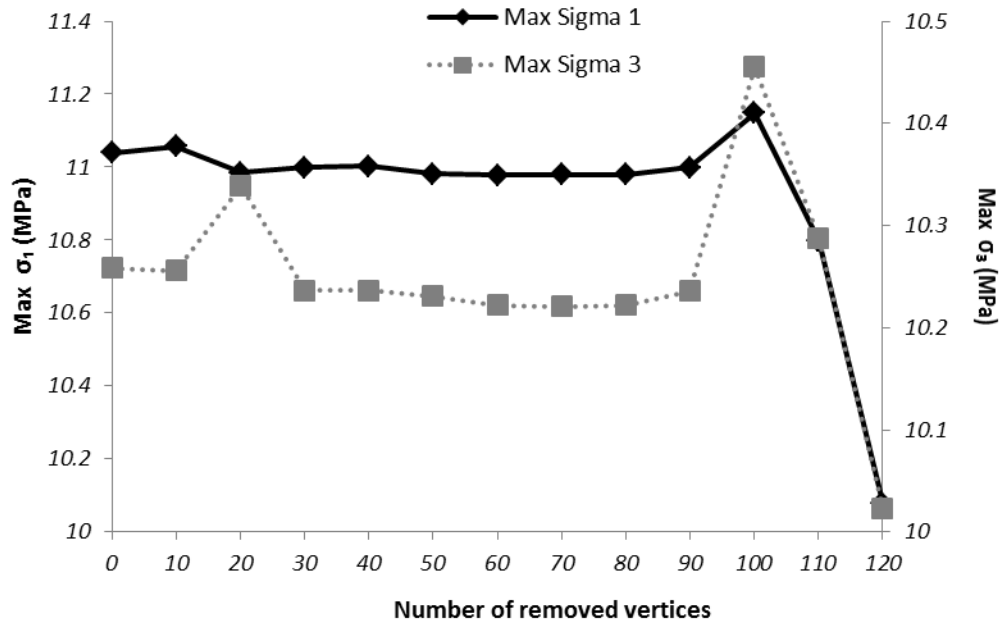
Figure 3-10 Changes in maximum σ_1 and maximum σ_3 as the number of removed vertices increases where $a=4.5$
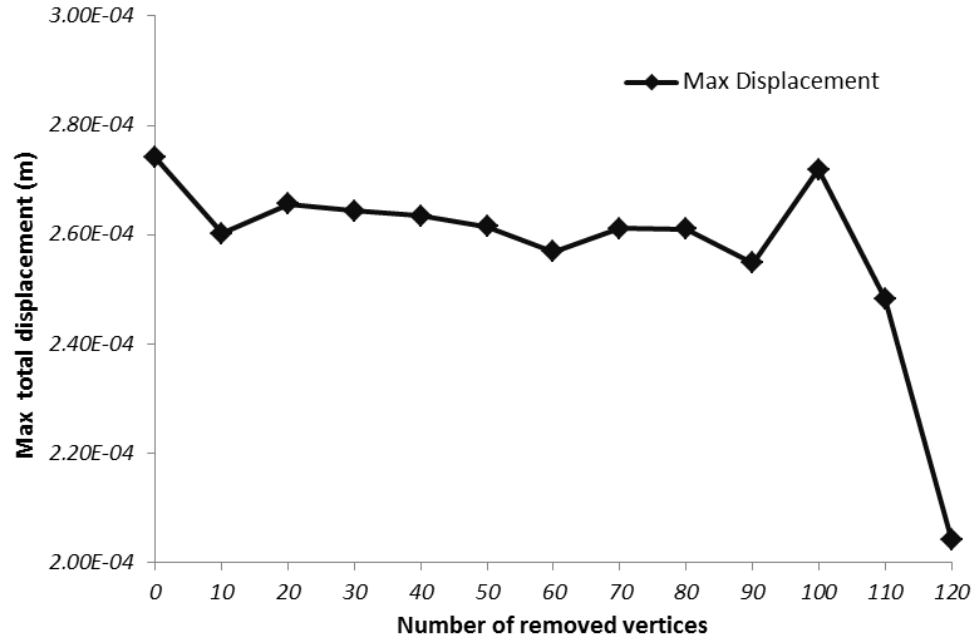
Figure 3-11 Changes in U as the number of removed vertices increases where *a=4.5*

The expanded cost function then has been applied for mesh improvement of the model with an excavation. The model is the same as the model with excavation of previous chapter, which was a model with an underground excavation at the vicinity of a fault zone.

As like as the first model, an uniform mesh was used, number of elements has 1000, Young's modulus of the rock mass is 5000 MPa, and Young's modulus of fault zone is assumed to be equal to 75000 MPa. ROI is located on the bottom right of the model with a coordinates of (3.5, -11.796). The total number of boundary vertices is 153. W_g, W_P, W_V, W_{Ym}, and W_U are equal to 1, 0.5, 0.3, 0.5, and 0.5, respectively. As it has been discussed, *a* is constant and equal to 4.5. Figures 3-12 shows the original model with excavation, and also the vertex numbers. Numbers of the vertices located on the top boundary of the excavation were removed due to overlapping; however the number of the first and the last vertices were illustrated on the figure.
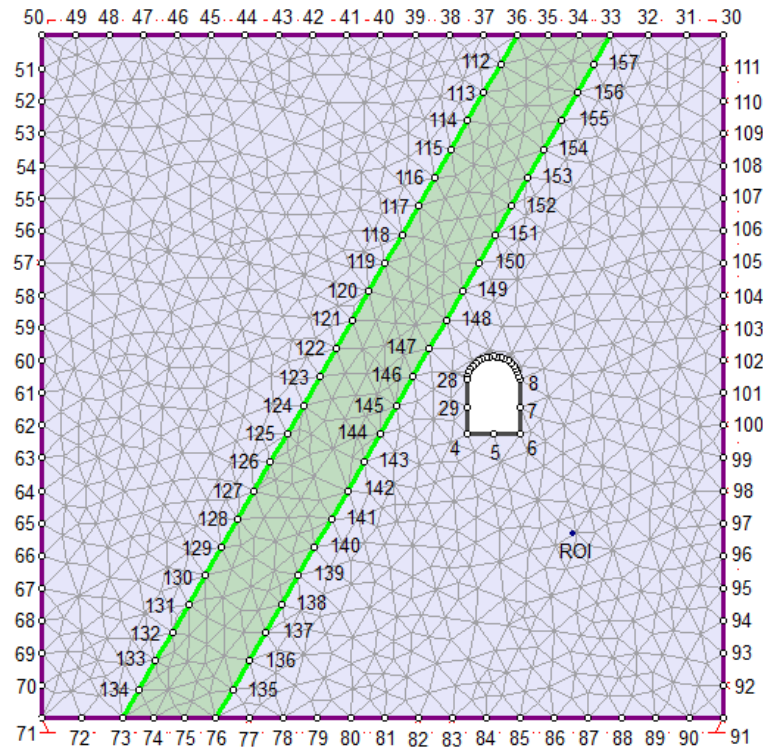
Figure 3-12 The original model with excavation
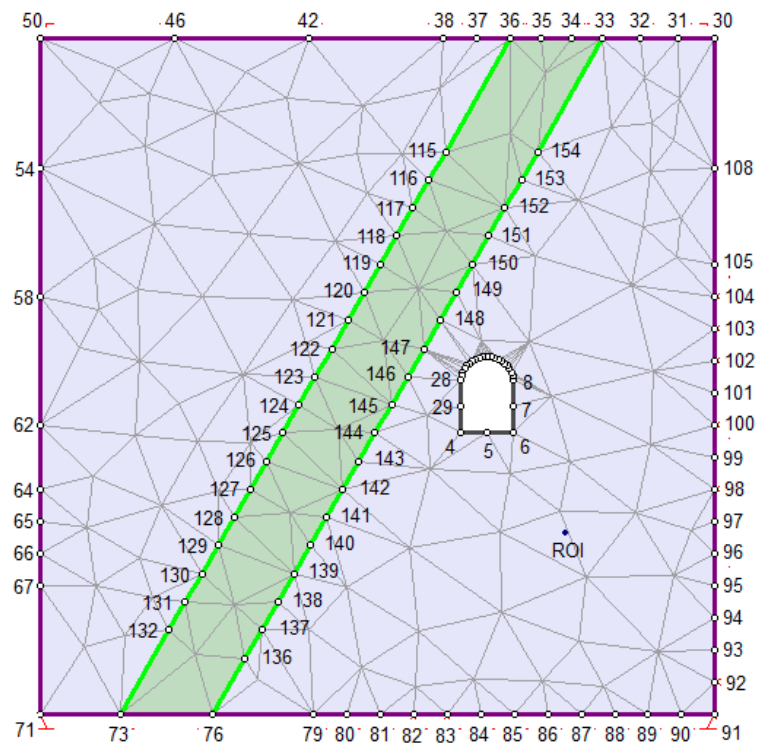
Figure 3-13 The model with excavation after removing 40 vertices

Then the cost function was applied to 153 vertices. The procedure was the same as the first model, in each round one vertex with the less cost was removed. Figure 3-13 illustrates the model after removing 40 vertices. As it has been expected despite of removing 40 vertices, mesh is still uniform. From the figure also it can be seen that the vertices removed from the areas far from the ROI.
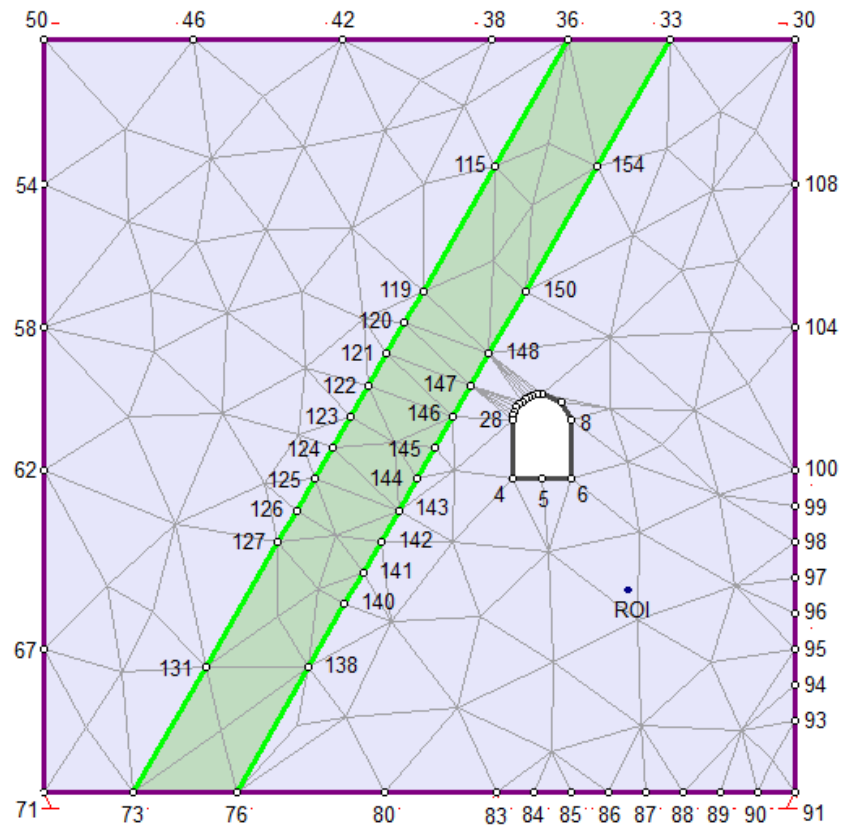
Figure 3-14 Model after removing 80 vertices

Figure 3-14 illustrates the model with 80 removed vertices. Since the vertices removed from the top of the excavation are not defined in the figure 3-14, figure 3-15 focused on the excavation area, and shows the vertex number and the removed vertices from the excavation.
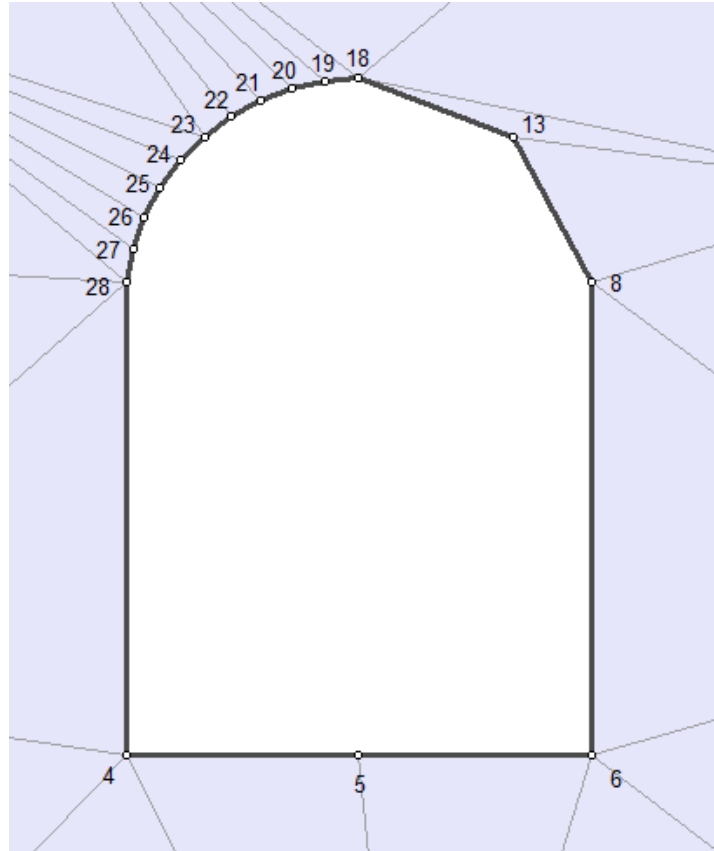
Figure 3-15 The excavation boundary after removing 80 vertices from the whole model

Vertex removal continued until all the vertices have been removed, then the stress and displacement analysis after removing each set (10 vertices) were determined and the mesh quality were examined, to decide how many vertices should be removed which completely depends on the accuracy of the analysis and the quality of the mesh.

Table 3-1 compares mesh quality for the original model and after removing vertices. As listed in   table 3-1 mesh quality is acceptable for up to 90 removed vertices.

Furthermore, figures 3-16 and 3-17 illustrate that principal stresses and total displacement analysis has the same result as the original model when less than 90 vertices

has been removed, after which as shown in the figures 3-16 and 3-17 the results were not as accurate as they had to be.

Table 3-1 Mesh quality for each 10 removed vertices (153 vertices)

Removed vertices	Elements with side length ratio greater than 30	Elements with internal angle less than 2	Elements with internal angle greater than 175	Number of inverted elements	Total bad elements
0	0	0	0	0	0/2054
10	0	0	0	0	0/392
20	0	0	0	0	0/385
30	0	0	0	0	0/373
40	0	0	0	0	0/350
50	0	0	0	0	0/283
60	0	0	0	0	0/265
70	0	0	0	0	0/259
80	0	0	0	0	0/244
90	0	0	0	0	0/229
100	0	2	0	0	2/206
110	0	0	0	0	0/176
120	0	0	0	0	0/94
130	0	0	0	0	0/44
138	0	1	0	0	1/28

Since the number of vertices that should been removed depends on stresses and displacement analysis, and as it has been concluded the best results achieved when less than 90 vertices have been removed, it can be concluded that the procedure should be terminated after removing 60% of vertices. This number differs from model to model and for each model stresses and displacement analysis should be done and mesh quality should be checked for each set of removed vertices to determine the appropriate number of vertices that can be removed while the results are still as accurate as possible.
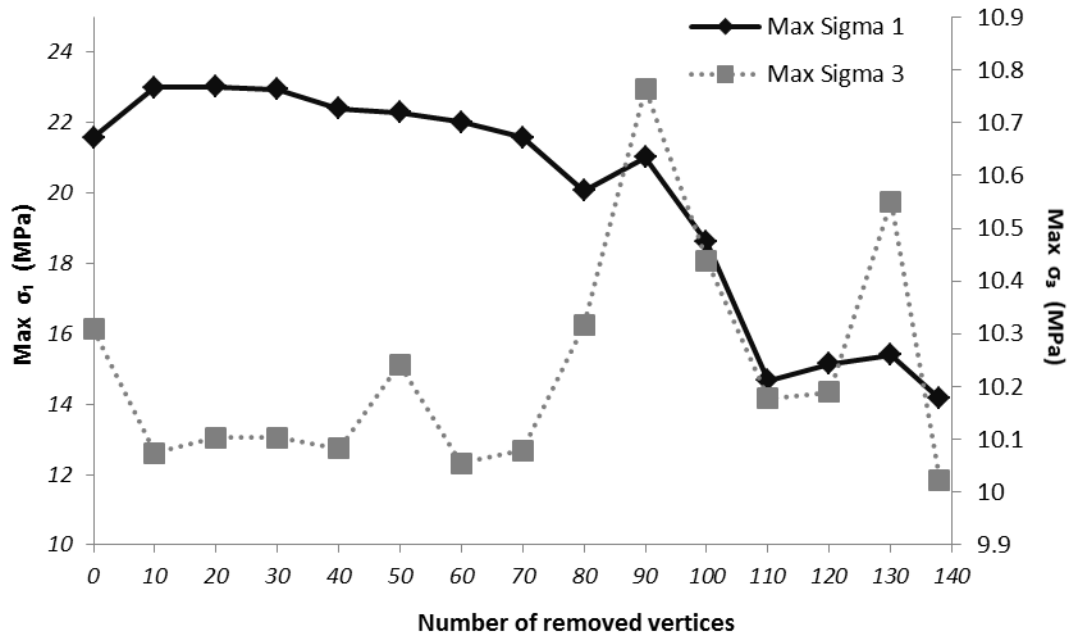
Figure 3-16 Changes in maximum principal stresses as vertices being removed
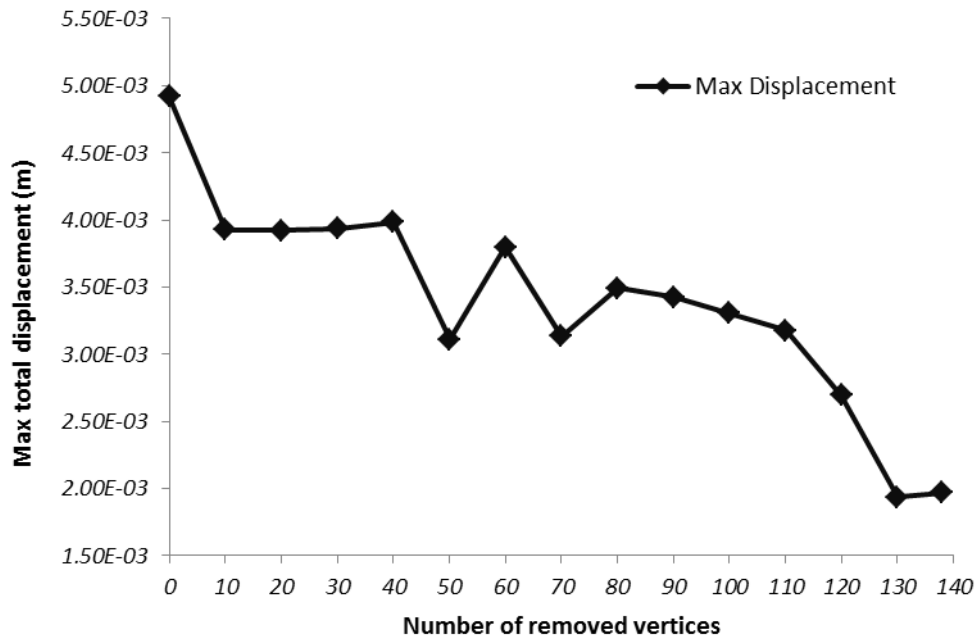
Figure 3-17 Changes in maximum displacement as vertices being removed

86

3.3 Case Study

To properly check the effect of the new cost function, the new equation has been applied on a real case with multiple excavations and different materials. Figure 3-18 shows the studied model. Model consists of 12 excavations and three different materials. ROI located in the host rock and at center of the model close to excavations and the hard rock material boundary.
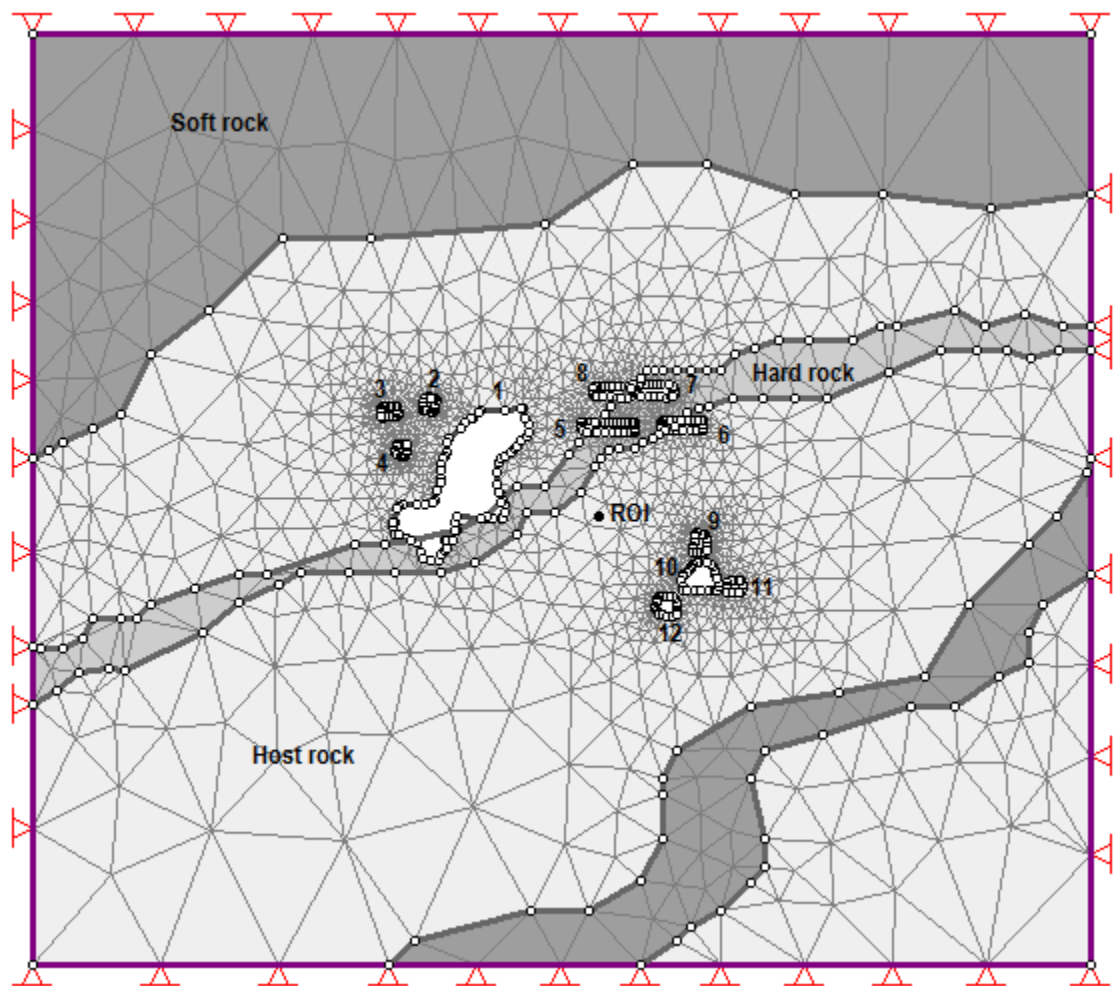
Figure 3-18 A case study with multiple excavations and different material

Table 3-2 illustrates material properties for three different materials in the model. As it can be seen Young's modulus is different from one material to another; however Poisson's ratio, cohesion, and other properties are assumed to be the same for all materials.

Table 3-2 Material properties (case study)

Material Name	Color	Initial Element Loading	Elastic Type	Young's Modulus (MPa)	Poisson's Ratio	Failure Criterion	Material Type	Tensile Strength (MPa)	Friction Angle (peak) (deg)	Cohesion (peak) (MPa)	Piezo Line	Ru
Host rock		Field Stress Only	Isotropic	20000	0.3	Mohr Coulomb	Elastic	0	35	10.5	None	0
Soft rock		Field Stress Only	Isotropic	5000	0.3	Mohr Coulomb	Elastic	0	35	10.5	None	0
Hard rock		Field Stress Only	Isotropic	60000	0.3	Mohr Coulomb	Elastic	0	35	10.5	None	0

As it has been illustrated in figure 3-18 graded mesh was used for this model, therefore uniformity cost should have a uniformity variable instead of uniformity constant. To calculate the uniformity variable, the equation number (7) should be used. All the costs were determined from the same equations as the previous two models (equations number 1, 3, 4, 5, and 6). Then the new cost function (8) was applied to the model. The calculations were repeated for 490 vertices.

Figure 3-19 shows the model after removing 100 vertices. As it has been expected, vertices had been removed from the areas far from the ROI, mostly from the exterior boundaries, and the material boundaries with the highest Young's modulus ratio.
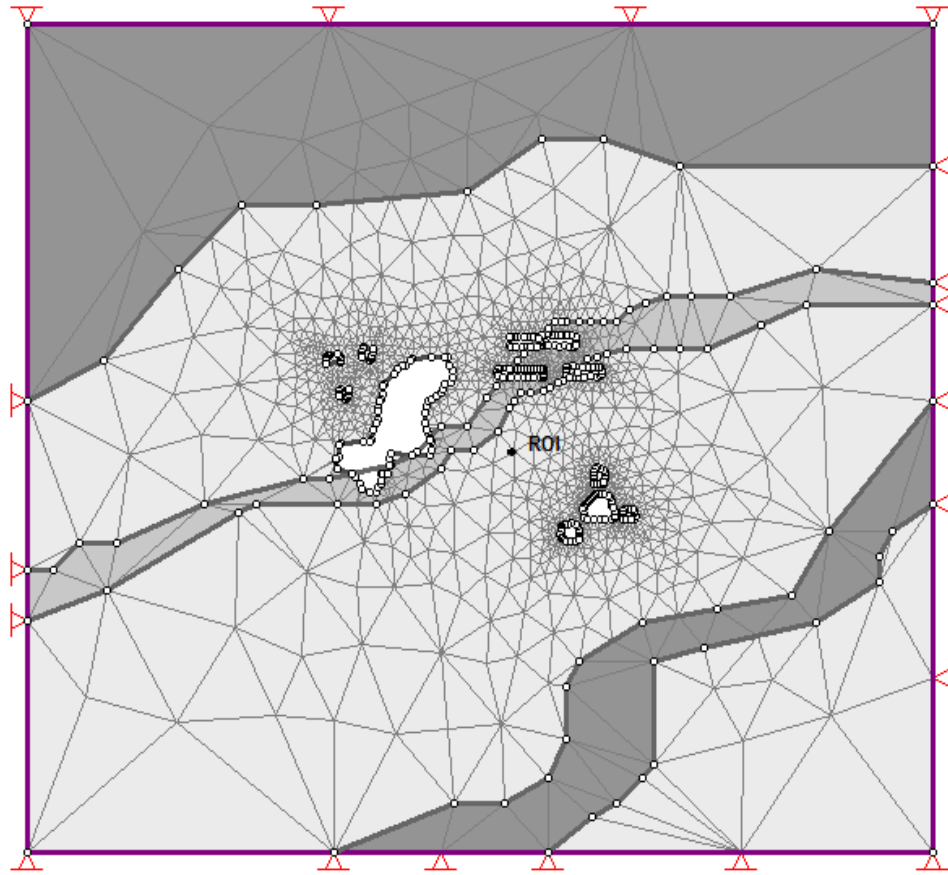
Figure 3-19 The Model after removing 100 vertices
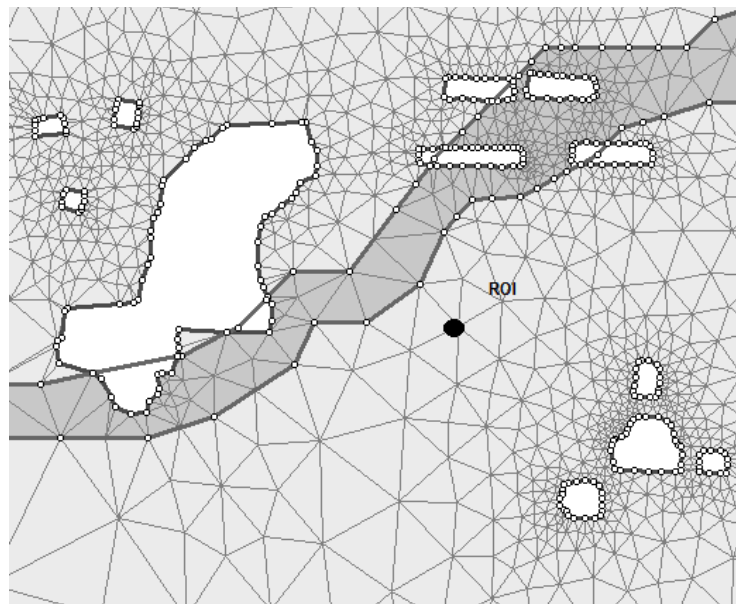
Figure 3-20 A close up of excavations after removing 100 vertices.

Figure 3-20 shows a close up of excavations, which once more confirms the previous argument about the vertex removal expectations. The excavation and material boundaries closer to the ROI are almost untouched after removing 20% of the vertices. Vertices have been removed from excavations number 2,3, and 4 mostly.

Table 3-3 Mesh quality for each set of 20 removed vertices and the original model (490 vertices)

Removed vertices	Elements with side length ratio greater than 30	Elements with internal angle less than 2 degrees	Elements with internal angle greater than 175 degrees	Number of inverted elements	Total bad elements
0	0	0	0	0	0/3688
20	0	0	0	0	0/3565
40	0	0	0	0	0/3511
60	0	0	0	0	0/3174
80	0	0	0	0	0/3005
100	0	0	0	0	0/2827
120	0	0	0	0	0/2724
140	0	0	0	0	0/2534
160	0	0	0	0	0/2336
180	0	0	0	0	0/2104
200	0	0	0	0	0/1910
220	0	0	0	0	0/1754
240	0	1	1	0	1/1546
260	1	3	1	0	3/1348
280	1	3	1	0	3/1214
300	1	3	0	0	3/1110
320	1	3	0	0	3/1004
340	1	2	0	0	2/774
360	1	2	0	0	2/633
380	1	2	0	0	2/506

As like as previous models mesh quality and stresses and displacements analysis were determined. Mesh quality checked for each set of 20 removed vertices; results are available in table 3-3. Mesh quality changed after removing 240 vertices, before which total bad elements number are zero (table 3-3).
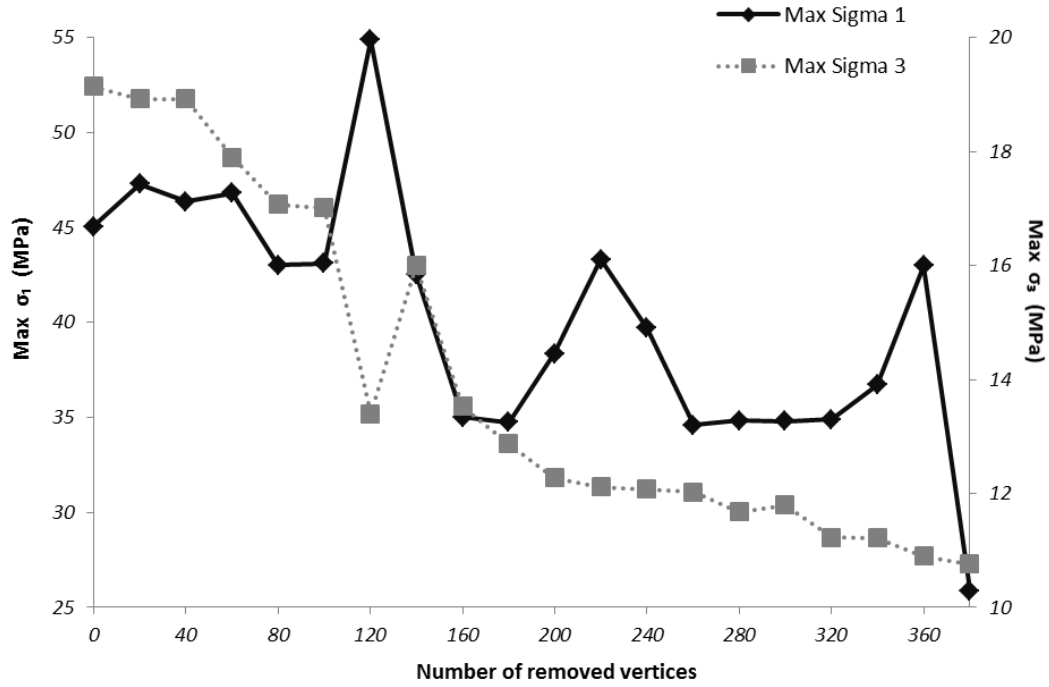
Figure 3-21 Changes in principal stresses for each set of 20 removed vertices

As it has been discussed, to find the limit for vertex removal, stresses and displacement analysis results for each set of 20 removed vertices and the original model were compared (figured 3-21 and 3-22). Results for stresses and displacement analysis illustrate that as the vertices have been removed principal stresses and total displacement decrease steadily which were predictable; however a sudden changes can be found in σ_1, σ_3 after removing 120 vertices which are perhaps due to a bad element that then after removing 20 more vertices improved. Considering both mesh quality and stresses and displacement analysis it can be concluded that vertex removal should be continued until mesh quality changes and the number of total bad elements increases. For the studied model vertex removal process should be terminated when less than 50% (240 vertices) of vertices were removed, to achieve both a simpler model and accurate results.

91
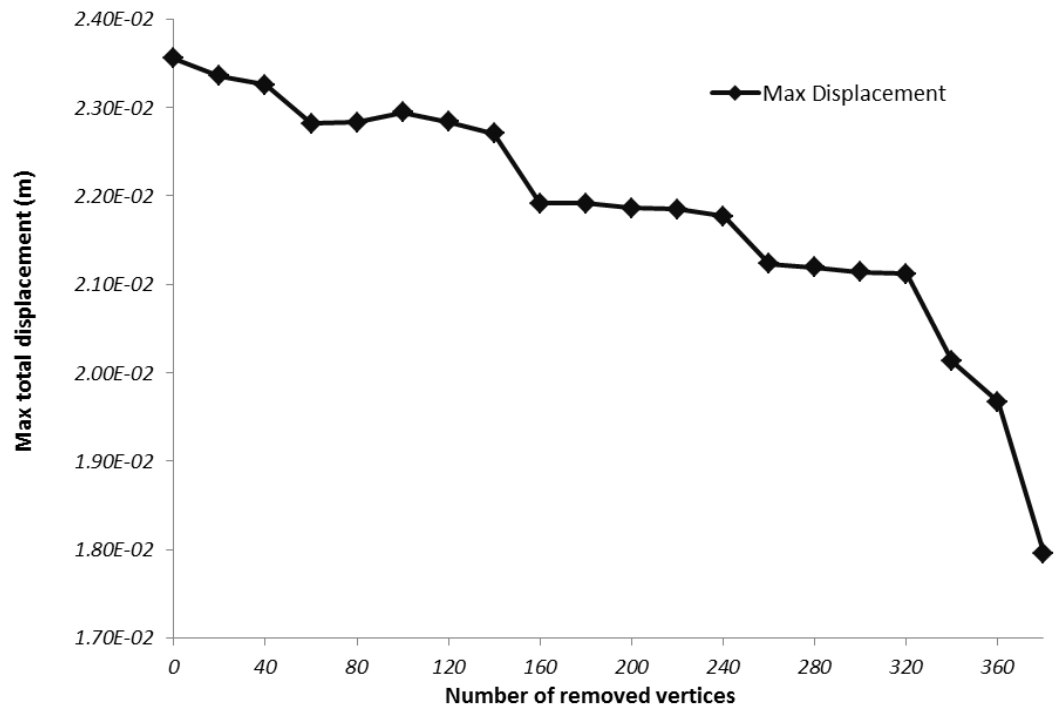
Figure 3-22 Changes in total displacement for each set of 20 removed vertices

CONCLUSION

Underground excavation simulations and analysis is a complex problem solving process. The existence of geological heterogeneity around an excavation makes the stress and displacement analysis even more complicated. Numerical modeling methods such as finite element method are intended to determine the stress analysis with the best accuracy at the less time and by less computer memory consumption. Despite the purpose of its existence, finite element method is not as efficient as it should be. Considerable efforts were done to improve the quality of the method. This thesis as well aims to improve the analysis process and results by considering both material properties and excavations' situation and geometry.

To fulfill the purpose of the research, a model with an excavation and different materials was considered. The effects of materials were studied considering Young's modulus and Poisson's ratio among varieties of material properties. The results of 670 analyses show that Young's modulus has more significant effect on stress and displacement analysis comparing to Poisson's ratio; however considering other material properties it cannot be said that Poisson's ratio has no effect on stress and displacement analysis, it can only be concluded that for this model, and in the same situation as assumed for these models, the Poisson's ratio did not affect the analysis result significantly.

To improve the finite element analysis results considering material properties, only Young's modulus was taken into account. The cost of removing a vertex depending on the material properties that the vertex is situated in, then was formulated and added to the existing cost function. The new cost function has then applied to two models, one with two different materials and another with different materials and an excavation. Process then

encountered a problem, when the mesh was not as uniform as it should be after removing vertices. To overcome the problem another cost was introduced which is called Uniformity Cost. The new cost improved the process and the expected results were achieved.

The results of the original model and the model after removing vertices for different set of removed vertices were compared. The analysis accuracy was acceptable. Then a real case with the same assumption as the previous models and with multiple excavations and materials was chosen. The cost function was applied for almost 500 vertices and the results after and before vertex removal were compared which once again approved the accuracy of the proposed functions.

Despite all the effort the cost function still is not complete. For further studies other material properties (tensile strength, cohesion, etc.) should be taken into account; and their effect on stress analysis and their relation to mesh density should be studied whether separately or together with another rock property. In addition, the proposed simplification method can be generalized for the 3D finite element analysis as well; however changes should be done to make this method compatible with the 3D environment.

REFERENCES

Bern, M., & Eppstein, D. (1992). Mesh generation and optimal triangulation. In F. H. Ding-Zhu Du (Ed.), *Computing in euclidean geometry* (pp. 23-90) World Scientific Pub Co Inc. Retrieved from http://www.ics.uci.edu/~eppstein/pubs/BerEpp-CEG-95.pdf

Cai, M. (2008). Influence of stress path on tunnel excavation response – numerical tool selection and modeling strategy. *Tunnelling and Underground Space Technology, 23*(6), 618-628. doi:DOI: 10.1016/j.tust.2007.11.005

Cai, M., Kaiser, P. K., Tasaka, Y., Maejima, T., Morioka, H., & Minami, M. (2004). Generalized crack initiation and crack damage stress thresholds of brittle rock masses near underground excavations. *International Journal of Rock Mechanics and Mining Sciences, 41*(5), 833-847. doi:DOI: 10.1016/j.ijrmms.2004.02.001

Cavendish, J. C., Field, D. A., & Frey, W. H. (1985). An approach to three-dimensional finite element mesh generation. *International Journal for Numerical Methods in Engineering, 21*(2), 329-347. doi:10.1002/nme.1620210210

Choi, C. K., & Kwak, H. G. (1990). The effect of finite element mesh size in nonlinear analysis of reinforced concrete structures. *Computers & Structures, 36*(5), 807-815. doi:DOI: 10.1016/0045-7949(90)90151-Q

De Bresser, J. H. P. (1996). Steady state dislocation densities in experimentally deformed calcite materials: Single crystals versus polycrystals. *J.Geophys.Res., 101*, 22189-22201. doi:10.1029/96JB01759

De Cougny, H. L., & Shephard, M. S. (1999). Parallel refinement and coarsening of tetrahedral meshes. *International Journal for Numerical Methods in Engineering, 46*(7), 1101-1125. doi:10.1002/(SICI)1097-0207(19991110)46:7<1101::AID-NME741>3.0.CO;2-E

Denayer, A. (1978). Automatic generation of finite element meshes. *Computers & Structures, 9*(4), 359-364. doi:DOI: 10.1016/0045-7949(78)90121-9

Eberhardt, E. (2001). Numerical modelling of three-dimension stress rotation ahead of an advancing tunnel face. *International Journal of Rock Mechanics and Mining Sciences, 38*(4), 499-518. doi:DOI: 10.1016/S1365-1609(01)00017-X

Everitt, R. A., & Lajtai, E. Z. (2004). The influence of rock fabric on excavation damage in the lac du bonnett granite. *International Journal of Rock Mechanics and Mining Sciences, 41*(8), 1277-1303. doi:DOI: 10.1016/j.ijrmms.2004.09.013

Fairhurst, C. (2003). Stress estimation in rock: A brief history and review. *International Journal of Rock Mechanics and Mining Sciences, 40*(7-8), 957-973. doi:DOI: 10.1016/j.ijrmms.2003.07.002

Fotoohi, K., & Mitri, H. S. (1996). Non-linear fault behavior near underground excavation - a boundary element approach. *International Journal for Numerical and Analytical Methods in Geomechanics, 20*(3), 173-190. doi:10.1002/(SICI)1096-9853(199603)20:3<173::AID-NAG814>3.0.CO;2-H

Fuchs, K., & Müller, B. (2001). World stress map of the earth: A key to tectonic processes and technological applications. *Naturwissenschaften, 88*(9), 357-371. doi:10.1007/s001140100253

Gercek, H. (2007). Poisson's ratio values for rocks. *International Journal of Rock Mechanics and Mining Sciences, 44*(1), 1-13. doi:DOI: 10.1016/j.ijrmms.2006.04.011

Golshani, A., Oda, M., Okui, Y., Takemura, T., & Munkhtogoo, E. (2007). Numerical simulation of the excavation damaged zone around an opening in brittle rock. *International Journal of Rock Mechanics and Mining Sciences, 44*(6), 835-845. doi:DOI: 10.1016/j.ijrmms.2006.12.005

Hao, Y. H., & Azzam, R. (2005). The plastic zones and displacements around underground openings in rock masses containing a fault. *Tunnelling and Underground Space Technology, 20*(1), 49-61. doi:DOI: 10.1016/j.tust.2004.05.003

Hart, R. (2003). Enhancing rock stress understanding through numerical analysis. *International Journal of Rock Mechanics and Mining Sciences, 40*(7-8), 1089-1097. doi:DOI: 10.1016/S1365-1609(03)00116-3

Hattangady, N. V. (1999a). Coarsening of mesh models for representation of rigid objects in finite element analysis. *International Journal for Numerical Methods in Engineering, 44*(3), 313-326. doi:10.1002/(SICI)1097-0207(19990130)44:3<313::AID-NME502>3.0.CO;2-V

Hattangady, N. V. (1999b). Faster analysis of forming problems through use of coarse mesh models for dies. *Finite Elements in Analysis and Design, 32*(1), 21-35. doi:DOI: 10.1016/S0168-874X(98)00073-0

Hoek, E., & Brown, E. T. (1994). *Underground excavation in rock* Taylor & Francis.

Ho-Le, K. (1988). Finite element mesh generation methods: A review and classification. *Computer-Aided Design, 20*(1), 27-38. doi:DOI: 10.1016/0010-4485(88)90138-8

Itasca International Inc. (1998). *3DEC (three dimensional distinct element code)*. Minneapolis: Retrieved from http://www.itascacg.com/3dec/index.php

Itasca International Inc. (2000). *UDEC (universal distinct element code)*. Minneapolis: Retrieved from http://www.itascacg.com/udec/index.php

Itsaca International Inc. (2000). *FLAC (fast lagrangian analysis of continua)*. Minneapolis: Retrieved from http://www.itascacg.com/flac/index.php

Jiang, Y., Li, B., & Yamashita, Y. (2009). Simulation of cracking near a large underground cavern in a discontinuous rock mass using the expanded distinct element method. *International Journal of Rock Mechanics and Mining Sciences, 46*(1), 97-106. doi:DOI: 10.1016/j.ijrmms.2008.05.004

Kenkmann, T., & Dresen, G. (1998). Stress gradients around porphyroclasts: Palaeopiezometric estimates and numerical modelling. *Journal of Structural Geology, 20*(2-3), 163-173. doi:DOI: 10.1016/S0191-8141(97)00074-6

Lee, H. J., & Song, J. H. (2005). Finite-element analysis of fatigue crack closure under plane strain conditions: Stabilization behavior and mesh size effect. *Fatigue & Fracture of Engineering Materials & Structures, 28*(3), 333-342. doi:10.1111/j.1460-2695.2005.00881.x

Lei, X. Y., Swoboda, G., & Zenz, G. (1995). Application of contact-friction interface element to tunnel excavation in faulted rock. *Computers and Geotechnics, 17*(3), 349-370. doi:DOI: 10.1016/0266-352X(95)99217-F

Li, Z., Liu, H., Dai, R., & Su, X. (2005). Application of numerical analysis principles and key technology for high fidelity simulation to 3-D physical model tests for underground caverns. *Tunnelling and Underground Space Technology, 20*(4), 390-399. doi:DOI: 10.1016/j.tust.2005.01.004

Martin, C. D., & Chandler, N. A. (1993). Stress heterogeneity and geological structures. *International Journal of Rock Mechanics and Mining Sciences & Geomechanics Abstracts, 30*(7), 993-999. doi:DOI: 10.1016/0148-9062(93)90059-M

Martin, C. D., Kaiser, P. K., & Christiansson, R. (2003). Stress, instability and design of underground excavations. *International Journal of Rock Mechanics and Mining Sciences, 40*(7-8), 1027-1047. doi:DOI: 10.1016/S1365-1609(03)00110-2

Martino, J. B., & Chandler, N. A. (2004). Excavation-induced damage studies at the underground research laboratory. *International Journal of Rock Mechanics and Mining Sciences, 41*(8), 1413-1426. doi:DOI: 10.1016/j.ijrmms.2004.09.010

McKinnon, S. D., & Garrido de la Barra, I. (2003). Stress field analysis at the el teniente mine: Evidence for N–S compression in the modern andes. *Journal of Structural Geology, 25*(12), 2125-2139. doi:DOI: 10.1016/S0191-8141(03)00068-3

Miller, G. L., Talmor, D., & Teng, S. H. (1999). Optimal coarsening of unstructured meshes. *Journal of Algorithms, 31*(1), 29-65. doi:DOI: 10.1006/jagm.1998.0990

Owen, S. (1998). A survey of unstructured mesh generation technology. Paper presented at the *7th International Meshing Roundtable,* Dearborn, Michigan, USA. *, 3*(6) 239-267. Retrieved from http://citeseer.ist.psu.edu/owen98survey.html

Palmström, A., & Singh, R. (2001). The deformation modulus of rock masses — comparisons between in situ tests and indirect estimates. *Tunnelling and Underground Space Technology, 16*(2), 115-131. doi:DOI: 10.1016/S0886-7798(01)00038-4

Park, S. J., Earmme, Y. Y., & Song, J. H. (1997). Determination of the most appropriate mesh size for a 2-D finite element analysis of fatigue crack closure behavior. *Fatigue & Fracture of Engineering Materials & Structures, 20*(4), 533-545. doi:10.1111/j.1460-2695.1997.tb00285.x

Rebaï, S., Philip, H., & Taboada, A. (1992). Modern tectonic stress field in the mediterranean region: Evidence for variation in stress directions at different scales. *Geophysical Journal International, 110*(1), 106-140. doi:10.1111/j.1365-246X.1992.tb00717.x

Rocscience Inc. (2008). *Phase2*. Toronto: Retrieved from http://www.rocscience.com/products/3/Phase2

Sato, T., Kikuchi, T., & Sugihara, K. (2000). In-situ experiments on an excavation disturbed zone induced by mechanical excavation in neogene sedimentary rock at tono mine, central japan. *Engineering Geology, 56*(1-2), 97-108. doi:DOI: 10.1016/S0013-7952(99)00136-2

Siebrits, E., & Crouch, S. L. (1993). Geotechnical applications of a two-dimensional elastodynamic displacement discontinuity method. *International Journal of Rock Mechanics and Mining Sciences & Geomechanics Abstracts, 30*(7), 1387-1393. doi:DOI: 10.1016/0148-9062(93)90126-X

Singh, K. B., Singh, T. N., Singh, D. P., & Jethwa, J. L. (1994). Effect of discontinuities on strata-movement problems in collieries: A review. *Geotechnical and Geological Engineering, 12*(1), 43-62. doi:10.1007/BF00425936

Soni, B. K. (2000). Grid generation: Past, present, and future. *Applied Numerical Mathematics, 32*(4), 361-369. doi:DOI: 10.1016/S0168-9274(99)00057-4

Soni, B. K., Shih, A. M., & Ito, Y. (2010). Grid generation techniques. In R. Blockley, & W. Shyy (Eds.), *Encyclopedia of aerospace engineering* () doi:10.1002/9780470686652.eae051

Suorineni, F. T., Tannant, D. D., & Kaiser, P. K. (1999). Determination of fault-related sloughage in open stopes. *International Journal of Rock Mechanics and Mining Sciences, 36*(7), 891-906. doi:DOI: 10.1016/S0148-9062(99)00055-8

van Kreveld, M., Löffler, M., & Silveira, R. I. (2010). Optimization for first order delaunay triangulations. *Computational Geometry, 43*(4), 377-394. doi:DOI: 10.1016/j.comgeo.2009.01.010

Wiles, T. D. (2006). Reliability of numerical modelling predictions. *International Journal of Rock Mechanics and Mining Sciences, 43*(3), 454-472. doi:DOI: 10.1016/j.ijrmms.2005.08.001

Zhang, Y. Z., Dusseault, M. B., & Yassir, N. A. (1994). Effects of rock anisotropy and heterogeneity on stress distributions at selected sites in north america. *Engineering Geology, 37*(3-4), 181-197. doi:DOI: 10.1016/0013-7952(94)90055-8

Zhu, W. C., & Bruhns, O. T. (2008). Simulating excavation damaged zone around a circular opening under hydromechanical conditions. *International Journal of Rock Mechanics and Mining Sciences, 45*(5), 815-830. doi:DOI: 10.1016/j.ijrmms.2007.09.007

Zoback, M. L., & Magee, M. (1991). Stress magnitudes in the crust: Constraints from stress orientation and relative magnitude data. *Philosophical Transactions: Physical Sciences and Engineering, 337*, 181-194.

Zsáki, A. M., & Curran, J. H. (2005). A continuum mechanics-based framework for boundary and finite element mesh optimization in two dimensions for application in excavation analysis. *International Journal for Numerical and Analytical Methods in Geomechanics, 29*(4), 369-393. doi:10.1002/nag.418